Stabilization and Tracking Control of Pan-Tilt Platforms Using Novel Estimators and Acceleration Based Robust Control Techniques

by

Sanem EVREN HAN

Submitted to the Graduate School of Sabancı University
in partial fulfillment of the requirements for the degree of
Doctor of Philosophy

Sabanci University

July 2017

PhD DISSERTATION

APPROVED BY:

Prof. Dr. Mustafa Ünel (Thesis Supervisor) .....

Asst. Prof. Dr. Meltem Elitaş .....

Assoc. Prof. Dr. Şeref Naci Engin .....

Prof. Dr. Ali Koşar .....

Asst. Prof. Dr. Ertuğrul Çetinsoy .....

DATE OF APPROVAL: 18/08/2017

To my most beloved family

Stabilization and Tracking of Pan-Tilt Platforms Using Novel Estimators and Acceleration Based Robust Control Techniques

Sanem Evren Han
ME, PhD Dissertation, 2017
Thesis Supervisor: Prof. Dr. Mustafa Ünel

Keywords: Stabilization, Acceleration Feedback, Adaptive Control, Learning Control, Sensor Fusion, Master-Slave Kalman Filter, High Gain Observer

Abstract

High precision stabilization is one of the fundamental problems in the control of robotic manipulators. It is generally regarded as a special case of the trajectory tracking problem in the control literature. This thesis focuses on the development of various robust control algorithms for robotic systems to achieve and maintain high precision stabilization against periodic/aperiodic parameter uncertainties and unknown external disturbances due to terrain changes, high frequency vibrations and sudden shocks, wind and other environmental factors.

Robust stabilization problem is first tackled by employing angular acceleration feedback in an inner loop acceleration controller. To this end, a novel master-slave type Kalman filter algorithm is proposed where an extended Kalman filter (EKF) and an inverse phi-algorithm are combined in a master-slave configuration to estimate reliable angular acceleration signals by fusing 3-axis gyroscope, 3-axis accelerometer and 3-axis magnetometer data. Performance of the proposed estimator is evaluated through a high fidelity simulation model where estimated accelerations are used as feedback signals in the stabilization control of a pan-tilt platform subject to external disturbances. When the acceleration feedback is incorporated into the control loop, higher precision stabilization is achieved. The performance of the proposed estimator is compared to Newton predictor enhanced Kalman filter (NPEKF) and the error state Kalman filter (ErKF). The master-slave Kalman filter outperforms NPEKF and provides comparable results with ErKF.

A polytopic quasi-LPV model of the pan-tilt system is developed and an LMI based optimal LQR controller that utilizes acceleration feedback is then synthesized based on this LPV model. Since the parameter vector is 4 dimensional, the desired LQR controller is synthesized by interpolating LMIs at 16 vertices of the polytope. A cascaded nonlinear high gain observer is designed to obtain reliable estimates of position, velocity and acceleration signals from noisy encoder measurements. Simulation results show that the proposed LMI based optimal LQR controller outperforms the classical LQR controller.

This thesis also tackles the robust periodic trajectory tracking problem of robot manipulators. A hybrid learning based adaptive control approach using acceleration feedback is developed for robot manipulators subject to parameter uncertainties and unknown periodic dynamics with a known period. Learning and adaptive feedforward terms are designed to compensate for periodic and aperiodic disturbances. The acceleration feedback is incorporated into both learning and adaptive controllers to provide higher stiffness to the system against unknown periodic disturbances and robustness to parameter uncertainties. A closed-loop stability proof is provided where it is shown that all system signals remain bounded and the proposed hybrid controller achieves global asymptotic position tracking. Results obtained from a high fidelity simulation model demonstrates the validity and effectiveness of the developed hybrid controller.

Özgün Kestiriciler ve İvme Tabanlı Gürbüz Kontrol Teknikleri
Kullanılarak Pan-Tilt Platformların Stabilizasyon ve İzleme Kontrolü

Sanem EVREN HAN
ME, PhD Sunumu, 2017
Tez Danışmanı: Prof. Dr. Mustafa Ünel

Anahtar Kelimeler: Stabilizasyon, İvme Geri Beslemesi, Uyarlamalı Kontrol, Öğrenmeli Kontrol, Sensör Füzyonu, Usta-Yamak Kalman Filtresi, Yüksek Kazanç Gözlemleyicisi

Özet

Yüksek stabilizasyon hassasiyeti, robotik manipülatörlerinin kontrol edilmesinde karşılaşılan temel problemlerden biridir. Kontrol teorisi literatüründe, stabilizasyon genellikle bir yörünge izleme probleminin özel bir hali olarak düşünülmektedir. Dolayısıyla bu tez, robotik sistemler için sistemdeki periyodik/aperiyodik parametre belirsizliklerine ve arazi değişiklikleri, yüksek-frekanslı titreşimler, rüzgar ve diğer çevresel faktörlerden kaynaklanan bilinmeyen dış bozucu etkilere karşı yüksek hassasiyetli stabilizasyon sağlamak ve bunu korumak için çeşitli gürbüz kontrol tasarımlarının geliştirilmesi üzerine odaklanmaktadır.

Gürbüz stabilizasyon probleminin üstesinden ilk kez açısal ivme geri beslemesinin iç döngü ivme kontrolünde kullanılmasıyla gelinmektedir. 3-eksenli jiroskop, 3-eksenli ivmeölçer ve 3-eksenli manyetometre ölçümlerinin birleşiminden güvenilir ivme bilgisinin kestirimi için, genişletilmiş bir Kalman filtresi (GKF) ve ters-ϕ algoritmasının bir usta-yamak biçiminde bütünleştirildiği özgün bir usta-yamak Kalman filtresi önerilmiştir. Önerilen usta-yamak sensör füzyonu algoritmasının performansı, bir yüksek sadakatli benzetim modeli üzerinde, kestirilen ivme bilgisini, dış bozucu etkilere maruz kalan 2-serbestlik dereceli pan-tilt platformun stabilizasyon kontrolünde geri besleme sinyali olarak kullanılmasıyla değerlendirilmiştir. İvme geri beslemesi kontrol döngüsünde kullanıldığı zaman yüksek stabilizasyon hassasiyeti sağlanmıştır. Önerilen füzyon algoritmasının performansı, Kalman filtresi ile geliştirilmiş Newton kestiricisi ve hata durum Kalman filtresi ile karşılaştırılmıştır. Önerilen usta-yamak filtresi, Kalman filtresi ile geliştirilmiş Newton kestiricisinden üstün gelirken, önerilen algoritma ve hata durum Kalman filtresi ile elde edilen sonuçlar benzerlik göstermektedir.

Pan-tilt sisteminin bir politopik sözde doğrusal parametre değişim modeli geliştirilmiş ve ivme geri beslemesini kullanan doğrusal matris eşitsizliği tabanlı doğrusal bir ikinci dereceden regülatör kontrolcüsü, bu model üzerinden sentezlenmiştir. Parametre vektörü, 4 boyutlu olduğu için istenilen doğrusal ikinci dereceden regülatör kontrolcüsü, doğrusal matris eşitsizliklerini 16 köşede interpole ederek sentezlenmektedir. Bir iç içe geçmiş yüksek kazançlı gözlemci yapısı, gürültülü enkoder ölçümlerinden güvenilir pozisyon, hız ve ivme sinyallerinin tahminlerini elde

edebilmek için tasarlanmıştır. Benzetim sonuçlarına göre önerilen doğrusal matris eşitsizliği tabanlı doğrusal parametre değişim kontrolcüsünün klasik doğrusal ikinci dereceden regülatör kontrolcüsünden üstün gelmektedir.

Bu tez çalışmasında ayrıca bir robotik platformun gürbüz periyodik yörünge izleme problemi çözülmeye çalışılmıştır. İvme geri besleme sinyalini kullanan yeni bir hibrit öğrenme tabanlı uyarlamalı kontrol yaklaşımı, parametre belirsizliklerine ve periyodu bilinen ama kendisi bilinmeyen, zamanla değişen periyodik dinamiklere maruz kalan robotik sistemler için geliştirilmiştir. Öğrenme ve uyarlamalı ileri besleme terimleri periyodik ve periyodik olmayan bozucu etkileri gidermektedir. İvme geri beslemesi hem öğrenme hem de uyarlamalı kontrolcüsüne dahil edilerek bilinmeyen periyodik bozuculara ve parametre belirsizliklere karşı sisteme yüksek sertlik ve gürbüzlük sağlamaktadır. Bütün sistem sinyallerinin sınırlı kaldığını ve önerilen kontrolcünün global asimptotik pozisyon izleme başarımını gösteren kapalı-çevrim kararlılık analizi verilmiştir. Bir yüksek sadakatli benzetim modeli ile elde edilen sonuçlar, önerilen hibrit kontrol yönteminin geçerliliğini ve verimliliğini göstermektedir.

Acknowledgements

It is a great pleasure to extend my gratitude to my thesis advisor Prof. Dr. Mustafa Ünel for his precious guidance, constructive suggestions and support in overcoming numerous obstacles I have been facing through my research. I am greatly indebted to him for his supervision, patience, motivation, and immense knowledge. I would like to thank him for encouraging my research and for allowing me to grow as a research scientist. His advice on both research as well as on my career have been priceless.

I would gratefully thank Asst. Prof. Dr. Meltem Elitaş, Assoc. Prof. Dr. Şeref Naci Engin, Prof. Dr. Ali Koşar, Ass. Prof. Dr. Ertuğrul Çetinsoy for spending their valuable time to serve as my jurors. I would like to show my greatest appreciation to the jury committee for their insightful comments, feedbacks and suggestions.

I would like to offer my special thanks to all the members of Control, Vision and Robotics (CVR) research group, Gökhan Alcan, Ekin Yağış, Hammad Zaki and Diyar Khalis for their pleasant team-work, feedback, cooperation and friendship. I am also grateful to all of the other members of the Mechatronics Laboratory, especially to Yusuf Mert Şentürk, and Wisdom Chukwunwike Agboh. It was fantastic and unforgettable to work with all them in the same laboratory.

Finally, a special thanks to my family. I would like to express the deepest appreciation to my beloved husband Hakan Han who was always there cheering me up and stood by me through the good times and bad. I would like to thank my parents, for giving birth to me at the first place and supporting me spiritually throughout my life. I am also thankful to my brother for his love and support.

Contents

List of Figures

List of Tables

Chapter 1

1 Introduction

A typical motion control problem consists of generating and following a desired trajectory when the system is exposed to noises and uncertainties. Some of the examples include autonomous vehicles, mobile robots performing tasks on rough surfaces, and marine underactuated vehicles [1]-[3]. All those nonlinear systems need highly accurate tracking performance. In the last two decades, a lot of industrial applications require robots to perform repetitive tasks such as assembly, manufacturing systems and satellite formation with consistent precision and accuracy [4]-[5]. This type of control problem is referred as periodic trajectory tracking problem.

Stabilization is regarded as special case of a general tracking problem in the control theory literature although they are usually considered as two different control problems. Stabilization is becoming increasingly popular in different application areas such as target identification, security and defense, gun-turret control, search and rescue, entertainment and environmental monitoring [6]-[9]. The objective of stabilization is to maintain the desired orientation of the platform relative to earth frame and at the same time reject all external disturbances. Gyro-stabilized inertially stabilized platforms (ISP) and 2 DOF pan-tilt mechanisms are mostly used for the need of pointing a camera, a laser range finder or a radar on a given target while the mounted platform is moving. Examples of military and commercial applications are given in Figure 1. All of these applications require very accurate stabilization in the order of micro-radians because small angular displacements may lead to large position errors if the target is kilometers away.

Figure 1: Stabilization with pan-tilt platforms

Motivated by the aforementioned applications, both periodic trajectory tracking and stabilization are important tasks in the control of robotic manipulators. Various control methods such as PID control, adaptive control, neural network control, and fuzzy control [10]-[12] are used to improve the dynamic response of the system. Due to unknown disturbances and parameter uncertainties during actual system operation, it is not always possible to achieve desired tracking and stabilization performances with traditional control approaches. Robust control algorithms are required to cope with unknown disturbances and parameter uncertainties.

1.1 Motivation

Robust control algorithms are needed to achieve sufficiently small tracking and stabilization errors. It is known that the use of acceleration feedback is effective for the disturbance rejection in industrial applications such as servo control machines and robot arms which continuously interact with the environment and work under different loads. Although acceleration feedback is used in several applications, the role of acceleration feedback has not been fully explored in the tracking and stabilization problems. The main objective of this thesis is to develop robust tracking and stabilization control algorithms based on acceleration feedback. However, the success of acceleration control techniques largely depends on reliable acceleration

feedback. Therefore, novel observers and sensor/data fusion algorithms will be developed for estimating reliable acceleration information.

Angular positions are generally provided by encoders or Inertial Measurement Units (IMU). Typical inertial sensors that are used in IMU are 3-axis gyroscopes, 3-axis linear accelerometers, and 3-axis magnetometers. While a 3-axis gyroscope measures angular velocities about 3 axes, a 3-axis linear accelerometer measures specific forces about 3 axes and a 3-axis magnetometer measures earth's magnetic field in 3 axes, respectively. Sometimes, a 3-axis inclinometer, which is also an accelerometer that provides higher precision data, is also used in IMU to measure roll and pitch angles. Euler angles are generally estimated by fusing the raw sensor data using an appropriate sensor/data fusion algorithm such as Kalman filter [13]. Although the estimation of Euler angles is a well-known problem, accurate and efficient estimation of Euler velocities and accelerations is still an active research area. In the context of this thesis, we will extend the well-known estimation problem to include estimation of Euler velocities and accelerations as well.

A new sensor fusion method for reliable angular acceleration estimation using a master-slave Kalman filter is presented. The proposed filter estimates the angular acceleration by extending the state vector of the AHRS (Attitude and Heading Reference System) to include both Euler rates and accelerations in addition to Euler angles and gyro biases. It employs both an extended Kalman filter (EKF) and an inverse Φ-algorithm in a master-slave configuration. While the master estimator (EKF) feeds the slave estimator (inverse Φ) with the estimated gyro biases, the slave estimator (inverse Φ) estimates bias compensated angular velocity, acceleration and jerk signals in the body frame and sends them to the master. The proposed Kalman filter is developed in a master-slave configuration due to the following reasons:

- The master filter estimates the augmented state vector which includes gyro biases as well.
- The process dynamics of the new estimation problem needs the computation of body frame angular accelerations and jerks; so a slave filter is required to estimate these accelerations and jerks.
- The process dynamics of the new estimation problem requires the use of smooth and unbiased angular velocities to provide reliable Euler angle, velocity and acceleration information; so a slave filter that utilizes the unbiased gyroscope measurements is developed to obtain smooth and unbiased estimates of angular velocities.
- In the slave filter, unbiased gyroscope velocities are used as measurements

where biases estimated by the master filter are subtracted from the gyroscope measurements.

The master-slave filter is used to obtain reliable estimates which are employed as feedback signals in the stabilization control of a 2-DOF pan-tilt platform. The performance of the stabilization control largely depends on the reliable feedback information. The stabilization control is designed by using an inner loop acceleration approach. When the pan-tilt platform is subject to external disturbances, use of reliable acceleration feedback improves the robustness of the system against the disturbances. Results obtained from a high fidelity simulation model which consists of the nonlinear dynamical model of the pan-tilt system subject to external disturbances and models of the inertial sensors (gyroscopes, accelerometers and magnetometers), demonstrate better performance of the PI controller enhanced with acceleration feedback over the conventional PI controller which does not utilize such feedback.

Nowadays linear optimal robust controllers are used for the stabilization of nonlinear systems represented by linear parameter varying (LPV) models. The key feature of LPV models is to provide the use of linear optimal control methods for the control of nonlinear MIMO dynamic systems. Such controllers are obtained by optimizing a cost function. It is known that disturbances manifest themselves first as acceleration signals; so better disturbance rejection can be achieved by acceleration feedback. This motivated us to design a new cost function that includes acceleration errors.

In literature, learning based controllers are considered for robotic manipulators that perform the same task repeatedly. This type of controllers improve system performance by utilizing previous error signals into the control input. However, the standard learning controller cannot reject aperiodic disturbances. This motivates the design of a new hybrid learning based adaptive controller using the acceleration feedback to achieve global position tracking for robotic manipulators despite the parameter uncertainties and unknown periodic dynamics.

The proposed hybrid controller utilizes learning based feedforward terms to compensate for periodic disturbances, and adaptive based feedforward terms to reject aperiodic disturbances. Since it is well-known that the effects of disturbances manifest themselves in the acceleration signals first, acceleration feedback is incorporated into the learning control and this should improve the robustness of the system against unknown periodic dynamics. The performance of the controller largely depends on reliable position, velocity and acceleration signals. However, obtaining velocity and acceleration signals from encoder position data is challenging due to the encoder quantization errors. In literature, different methods [14]-[16] exist to provide useful velocity and acceleration estimates from noisy encoder

measurements for the control purposes. In this thesis, a cascaded high gain observer (HGO) structure is developed to estimate position, velocity and acceleration signals. Estimated position, velocity and acceleration signals are then used in the proposed hybrid controller. The hybrid controller is developed on an n-rigid link robotic manipulator. A closed-loop stability proof where the filtered error is modified by including the integral of the position tracking error is provided to show that all system signals are bounded and global asymptotic position tracking is ensured. The performance of the proposed hybrid learning based adaptive controller is evaluated on a 2-DOF pan-tilt platform.

1.2 Contributions of the Thesis

This thesis makes the following contributions:

- A new estimation problem is stated by extending the state vector of AHRS to include both Euler rates and accelerations in addition to Euler angles and gyro biases. Thus, the state dimension of AHRS problem is increased from 6 to 12. A master-slave Kalman filter is proposed to solve this new estimation problem by fusing noisy IMU measurements.

- A cascaded high gain observer (CHGO) is developed to estimate reliable velocity and acceleration signals from noisy encoder measurements.

- A polytopic quasi-LPV model of a pan-tilt system is obtained and an acceleration based LQR controller is synthesized based on the developed LPV model for the stabilization of the pan-tilt system.

- A new linear parametrization property is proposed for robotic manipulators. The well-known linear parametrization property is modified such that the regressor matrix depends on link accelerations besides link velocities, and the unknown parameter vector includes both actuator moment of inertia and friction parameters. By using this new linear parametrization property, acceleration feedback is incorporated into the adaptive controller to improve the robustness of the system against unknown aperiodic disturbances.

- A new learning controller that utilizes acceleration feedback is developed for a general error system to successfully reject periodic disturbances. The standard learning controller developed by [17] is modified by including acceleration signals in the filtered error variable. Reliable accelerations are estimated by the CHGO. The same learning controller is then modified for rejecting periodic disturbances acting on the robot dynamics by including

both acceleration error and the integral of the position tracking error in the filtered error variable.

- A hybrid learning based adaptive control algorithm has been developed by integrating acceleration based adaptive and learning controllers. The hybrid controller increases the robustness of the system against aperiodic and periodic disturbances.

- Closed-loop stability proofs of all nonlinear controllers are provided to show that all system signals remain bounded and global asymptotic position tracking is ensured.

1.3 Outline of the Thesis

Chapter 2 presents the literature survey and theoretical background for the sensor fusion algorithms, high gain observers, acceleration feedback, LPV modeling approaches, and hybrid nonlinear learning/adaptive controllers. Chapter 3 details development of the proposed master-slave Kalman filter, and a cascaded high gain observer structure. Chapter 4 presents stabilization control using inner loop acceleration control. Chapter 5 derives a polytopic quasi-LPV model of the pan-tilt system, and synthesizes an acceleration based LMI-LQR controller based on the proposed LPV model for pan-tilt stabilization. In Chapter 6, the proposed hybrid learning/adaptive controllers are designed and the closed loop stability proofs of all nonlinear controllers are provided. Chapter 7 presents simulation results. Finally, Chapter 8 concludes the thesis with several remarks.

1.4 Publications

1.4.1 *Journal Articles*

- High Precision Stabilization of Pan-Tilt Systems Using Reliable Angular Acceleration Feedback from a Master-Slave Kalman Filter, **S. Evren**, and M. Unel, *Journal of Intelligent and Robotic Systems*, DOI: 10.1007/s10846-017-0522-9, 2017 (Published Online).

- Planar Formation Control of Swarm Robots Using Dynamical Elliptic Fourier Descriptors, **S. Evren**, and M. Unel, *Transactions of the Institute of Measurement and Control*, Vol. 37, No. 5, pp. 661–671, May, 2015.

- A Hybrid Acceleration Based Learning and Adaptive Controller for Periodic Trajectory Tracking of Robot Manipulators, **S. Evren**, and M. Unel (To be submitted).

1.4.2 *Conference Proceedings*

- Stabilization of a Pan-Tilt System Using a Polytopic Quasi-LPV Model and LQR Control, **S. Evren**, and M. Unel, *42nd Annual Conference of the IEEE Industrial Electronics Society (IECON 2016)*, Florence, Italy, October, 23–27, 2016.

- A New Learning Controller for Periodic Disturbance Rejection, **S. Evren**, and M. Unel, *Asian Control Conference (ASCC)*, 2017 (Under Review).

- Stabilization of Pan-Tilt Systems Using Acceleration Based LMI-LQR Controller, **S. Evren**, and M. Unel, *Asian Control Conference (ASCC)*, 2017 (Under Review).

Chapter 2

2 Literature Survey and Background

This chapter reviews recent developments in sensor fusion algorithms, nonlinear high gain observers, acceleration feedback, learning controller, adaptive controller, hybrid learning based adaptive controllers, and highlights the drawbacks and suggests possible improvements.

2.1 Sensor Fusion

Sensor fusion is combining data measured by homogeneous and/or heterogeneous sensors such that the fused information has less uncertainty (more accurate) than when these sources were used individually. Today, the most widely used sensor fusion algorithms are Kalman filter and its variations such as Extended Kalman filter (EKF), Unscented Kalman filter (UKF) and Adaptive Kalman filter (AKF). The subsequent sections present the principles of Kalman filter and Extended Kalman filter. Readers are referred to [13] for detailed information. Alternatively, an indirect Kalman filter approach (error state Kalman filter) has emerged to estimate the error in the state vector rather than the state itself [18]-[19].

2.1.1 Kalman Filter

Kalman filter [20] has been developed by Rudolf E. Kalman around 1960s. Since then, it is a popular sensor fusion technique that combines a linear system model with statistical methods to accurately estimate the state of the system. Kalman filter can be used in different application areas such as guidance, navigation and control for aircrafts and spacecrafts, time series analysis in signal processing, motion planning and control for robotic manipulators.

Kalman filter involves a two step process; prediction and update stages. In the prediction stage, it estimates state variables along with their uncertainties by using a linear process model. In the second stage, those estimates are updated by using a weighted average when the noisy measurement is obtained. Less weight is given to estimates with higher uncertainties. KF is a recursive linear algorithm where it

utilizes current measurements, and a priori predicted states, not the past information. Kalman filter guarantees optimal estimates when process and measurement errors are white Gaussian noises with zero means (time uncorrelated noises), and noise covariance matrices are precisely known. Due to difficulty of getting better estimates of noise covariance matrices, it is not easy to implement KF in practice. Those matrices can be estimated by trial and error based on a priori knowledge or using a well-known autocovariance least squares (ALS) technique [21] in which the time-lagged autocovariances of routine operating data is utilized for covariance matrix estimation.

A classical Kalman filter considers a discrete time linear dynamic system model in a state space form:

$$x_k = F_k x_{k-1} + B_k u_k + \omega_k \tag{2.1}$$

where F_k is the state transition matrix which is applied to the previous state, x_{k-1}, B_k is the control input matrix applied on the control input vector, u_k, and ω_k is the white Gaussian process noise with zero mean, $\omega_k \sim \mathcal{N}(0, Q_k)$ with the process noise covariance matrix, Q_k. Measurement model is as follows:

$$z_k = H_k x_k + v_k \tag{2.2}$$

where z_k is the measurement at time k, H_k is the observation matrix, and v_k is the white Gaussian measurement noise with zero mean, $v_k \sim \mathcal{N}(0, R_k)$ with the measurement noise covariance matrix, R_k. The state of the KF can be represented by a posteriori state estimate at time k given observations up to and including at time k, $\hat{x}_{k/k}$, and a posteriori error covariance matrix, $P_{k/k}$. Kalman filter is implemented based on the prediction and update equations given by (2.3)-(2.9).

Prediction Stage

Predicted a priori state estimate, $\hat{x}_{k/k-1}$, and a priori estimate covariance, $P_{k/k-1}$, are as follows:

$$\hat{x}_{k/k-1} = F_k \hat{x}_{k-1/k-1} + B_k u_k \tag{2.3}$$

$$P_{k/k-1} = F_k P_{k-1/k-1} F_k^T + Q_k \tag{2.4}$$

where $\hat{x}_{k-1/k-1}$ and $P_{k-1/k-1}$ are the a posteriori state and covariance at time $k-1$ given observations up to and including at time $k-1$, respectively. Initial values, $\hat{x}_{0/0}$ and $\hat{P}_{0/0}$, are randomly selected.

Update Stage

State estimates are updated based on the following innovation or measurement residual:

$$\tilde{y}_k = z_k - H_k \hat{x}_{k/k-1} \tag{2.5}$$

with z_k provided in (2.2). Similarly, residual covariance is given as:

$$S_k = R_k + H_k P_{k/k-1} H_k^T \tag{2.6}$$

and an optimal Kalman gain is defined as:

$$K_k = P_{k/k-1} H_k^T S_k^{-1} \tag{2.7}$$

A posteriori state estimate, $\hat{x}_{k/k}$, and a posteriori covariance, $P_{k/k}$, are updated using Kalman gain and a priori estimates:

$$\hat{x}_{k/k} = \hat{x}_{k/k-1} + K_k \tilde{y}_k \tag{2.8}$$

$$P_{k/k} = (I - K_k H_k) P_{k/k-1} \tag{2.9}$$

where I denotes identity matrix.

2.1.2 Extended Kalman Filter

Kalman filter provides optimal estimates for linear system models with additive white Gaussian noise. However, most of the practical systems are nonlinear. This motivates the development of the extended Kalman filter (EKF) to employ Kalman filter for nonlinear models. EKF is the nonlinear version of the Kalman filter which is based on the linearization of process and measurement models about an estimate of the current mean and covariance. Process and measurement models do not have to be linear functions of the state. However, they need to be differentiable functions. Nonlinear process and measurement models are defined as follows:

$$x_k = f_k(x_{k-1}, u_{k-1}) + \omega_k \tag{2.10}$$

$$z_k = h_k(x_k) + v_k \tag{2.11}$$

where f and h are nonlinear state dynamics and measurement model, $\omega_k \sim \mathcal{N}(0, Q_k)$ and $v_k \sim \mathcal{N}(0, R_k)$ are zero mean multivariate Gaussian process and measurement noises with covariances Q_k and R_k. Functions f and h cannot be applied directly. A matrix of partial derivatives, called *Jacobian matrix*, is computed for each function, f and h, at each time step with the current predicted states. Extended Kalman filter is designed based on the prediction and update equations given by (2.12)-(2.20).

Prediction Stage

Predicted a priori state estimate, $\hat{x}_{k/k-1}$, and a priori covariance, $P_{k/k-1}$, are defined as follows:

$$\hat{x}_{k/k-1} = f(\hat{x}_{k-1/k-1}, u_k) \tag{2.12}$$

$$P_{k/k-1} = F_{k-1} P_{k-1/k-1} F_{k-1}^T + Q_{k-1} \tag{2.13}$$

and the state transition matrix is defined by the following Jacobian matrix:

$$F_{k-1} = \left. \frac{\partial f}{\partial x} \right|_{\hat{x}_{k-1/k-1}, u_{k-1}} \tag{2.14}$$

where $\hat{x}_{k-1/k-1}$ and $P_{k-1/k-1}$ are the a posteriori state and covariance at time $k-1$ given observations up to and including at time $k-1$, respectively. Initial values, $\hat{x}_{0/0}$ and $\hat{P}_{0/0}$, are randomly selected.

Update Stage

The following innovation or measurement residual is used to update state estimates:

$$\tilde{y}_k = z_k - h\hat{x}_{k/k-1} \tag{2.15}$$

and the measurement z_k at time k is given in (2.11). Residual covariance is as follows:

$$S_k = R_k + H_k P_{k/k-1} H_k^T \tag{2.16}$$

where

$$H_k = \left. \frac{\partial h}{\partial x} \right|_{\hat{x}_{k/k-1}} \tag{2.17}$$

and *a near-optimal* Kalman gain is obtained as:

$$K_k = P_{k/k-1} H_k^T S_k^{-1} \tag{2.18}$$

which updates the following a posteriori state estimate, $\hat{x}_{k/k}$, and a posteriori covariance, $P_{k/k}$:

$$\hat{x}_{k/k} = \hat{x}_{k/k-1} + K_k \tilde{y}_k \tag{2.19}$$

$$P_{k/k} = (I - K_k H_k) P_{k/k-1} \tag{2.20}$$

where I denotes identity matrix.

2.2 IMU and Attitude Estimation with Sensor Fusion

This section describes typical inertial sensors used in an inertial measurement unit (IMU), and well-known attitude estimation techniques that use IMU together with a digital signal processor (DSP) to provide reliable attitude estimates.

2.2.1 Inertial Measurement Unit

Reliable attitude (orientation) information is essential in the control of robotic platforms. Traditionally, joint angles are sensed by high resolution encoders or resolvers. In recent years, advances in the development of micro-electromechanical systems (MEMS) have significantly improved the cost-performance ratio of inertial sensors such as a 3-axis gyroscope, a 3-axis accelerometer and a 3-axis magnetometer [22]-[23]. While a 3-axis gyroscope measures angular velocities about 3 axes, a 3-axis linear accelerometer measures specific forces about 3 axes and a 3-axis magnetometer measures earth's magnetic field in 3 axes, respectively. Those inertial sensors form an inertial measurement unit as depicted in Figure 2.

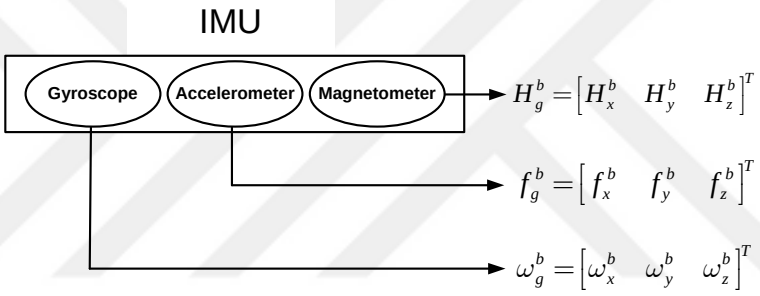

Figure 2: Inertial Measurement Unit

IMU together with a digital signal processor provides angle information by fusing measured data from typical inertial sensors. Sometimes, a 3-axis inclinometer is also used in IMU to measure roll and pitch angles. The inclinometer is an accelerometer and provides higher precision data. In the subsequent sections, inertial sensors used in IMU are briefly described. However, the detailed mathematical models of these sensors are presented in Chapter 3.

2.2.2 Attitude Estimation with Sensor Fusion

The individual use of MEMS inertial sensors is not sufficient to determine attitude angles. Gyroscopes have high bandwidth and thus operate in a fast manner. However, they suffer from drift problems due to integration of gyro biases. On the other hand, accelerometers have low bandwidth and therefore they provide relatively accurate roll and pitch angles from the components of the gravity vector in a slow manner. Similarly, determining yaw angle from the components of the earth's magnetic field using a magnetometer is a drift-free but slow process. To obtain fast and accurate attitude angles, outputs of inertial sensors must be fused, i.e. sensor/data fusion.

Today, modern attitude and heading reference systems (AHRS) consist of an inertial measurement unit (IMU) and an onboard processor. As mentioned previously, a typical IMU is formed by a 3-axis gyroscope, a 3-axis accelerometer and a 3-axis magnetometer. A sensor fusion algorithm is employed in AHRS to combine individual sensor measurements to obtain more reliable attitude estimates. Sensor fusion algorithms eliminate disadvantages of inertial sensors and provide a complementary behavior where estimates mimic gyroscope measurements in the short term and accelerometer outputs in the long term. The extended Kalman filter [24]-[25], adaptive Kalman filter [26], unscented Kalman filter [27] to fuse signals from a low cost IMU to estimate the orientation. On the other hand, the signals measured by the same sensors can be fused to estimate the position, velocity and acceleration information [28]-[30].

Deterministic (the bias, scale factor and misalignment errors) and stochastic (angular white noise (AWN), angular random walk (ARW), rate random walk (RRW), quantization noise and bias instability) errors in the gyroscope lead to drift problems in the long-run. Therefore, the researchers have focused on modeling the gyroscope accurately and analyzed its errors [31]-[33]. Bayard et al. [31] designed a virtual gyroscope by integrating 4 low-cost MEMS gyroscope with Kalman Filter. The accuracy of the virtual gyroscope is increased by minimizing the variance of stochastic error. Chang et al. [32] developed an integrated MEMS gyroscope array method composed of two levels of optimal filtering to improve gyroscope accuracy. In the first level filtering, several homogeneous gyroscopes are combined through Kalman filtering into a single effective device that outperforms any individual sensor. In the second level filtering, the accuracy of the gyroscope is improved by fusing the heterogeneous sensor data observed by the gyroscope, accelerometer and magnetometer. Experiments show that three gyroscopes with a bias drift of 35 degree per hour could be combined into a virtual gyroscope with a drift of 1.07 degree per hour through the first-level filter, and the bias drift was reduced to 0.53 degree per hour after the second-level filtering . Similar to work in [31], Lam et al. [33] designed a virtual gyroscope by fusing the data observed from the homogeneous gyroscopes. However, they estimate both the deterministic errors (scale factor and misalignment errors) and stochastic errors (RRW and ARW).

Diao et al. [34] analyzed the gyro error characteristics with the help of Allan variance and built the gyroscope random drift by autoregressive (AR) and autoregressive moving-average (ARMA) models. Kalman filter is used to effectively restrain the gyro drift and improve the gyro precision. Ruan and Yu [35] similarly analyzed MEMS gyro based on the AR model. Improved Sage-Husa adaptive Kalman filter which has a fading factor of Strong Tracking Filter (STF) is used to filter out gyro drift.

GPS is widely used in navigation. However, the position obtained from GPS

is often degraded due to obstruction and multipath effect caused by buildings, city infrastructure and vegetation. IMU and a processor (e.g. DSP) with suitable fusion algorithms form an inertial navigation system (INS). Inertial navigation systems have also bottlenecks; they suffer from the large inertial sensor errors. Therefore, integrated GPS/INS systems are becoming increasingly popular because of their complementary characteristics [35]-[36]. GPS/INS systems provide high accuracy position and orientation information in all environments, especially those where satellite availability is restricted.

Bikonis and Demkowicz [36] proposed an EKF to integrate GPS and INS systems for pedestrians location in urban environment. Obtained results show that EKF algorithm can overcome the problem of huge INS drifts and GPS outages. Thus, the proposed EKF is more accurate and robust than algorithms using data from GPS and INS systems separately. Rios and White [37] designed a low cost solid state GPS/IMU navigation unit that integrates measurements from a GPS, gyroscopes, accelerometers and magnetometers by an EKF algorithm to provide a complete navigation solution at a high output rate. The results show that the attitude and heading errors are less than 0.1 degrees under static conditions and they are less than 0.5 degrees under dynamic flight tests when compared to a high accuracy INS system.

Zhang et al. [38] developed an autonomous vehicle navigation method by integrating the measurements of IMU, GPS and digital compass. This method is composed of two steps to overcome the low precision of the sensors. The first step is to establish sophisticated dynamic models which consider Earth self rotations, measurement biases and system noises. In the second step, the system estimation is implemented by using an Unscented Kalman filter which has higher calculation accuracy compared to an EKF. Nebot et al. [39] presented a strap-down INS/GPS integrated system where the gyroscopes and the accelerometers are physically strapped to the vehicle. The strap-down systems are commonly used today for reducing the costs, eliminating the gimbal rock and removing the need for some calibrations.

Caron et al. [40] proposed a GPS/IMU Multisensor Kalman filter algorithm and introduced the contextual variables to define the fuzzy validity domains of each sensor. They detect and reject the bad data delivered by GPS sensor using contextual information. Thus the algorithm increases the reliability of the position information. Also, GPS/INS integration is not satisfactory due to INS drifts and unreliable GPS data. To solve this problem, the authors propose to feed the fusion process based on a multisensor Kalman filter directly with the acceleration information provided by IMU.

2.3 Nonlinear Observers

Some researchers focused on the design and analysis of nonlinear observers [41]-[43] to have good estimates from low cost inertial sensors due to the convergence problems in Kalman filtering. Mahony et al. [41] proposed three nonlinear observers posed directly on the special orthogonal group (SO(3)) driven by reconstructed attitude and angular velocity measurements. Because of the similarity of the architecture to those of linear complementary filters, proposed observers are termed as direct complementary filter, passive complementary filter and explicit complementary filter. Both direct and passive filters can be extended to estimate gyro biases online. The performance of the observers are demonstrated with a set of experiments performed on a robotic test bed and a radio controlled unmanned aerial vehicle. Bachman et al. [42] presented a quaternion-based complementary filter algorithm for processing the output data from 9-axis MARG (Magnetic field, Angular Rate, and Gravity) sensor unit containing three orthogonally mounted angular rate sensors, three orthogonal linear accelerometers and three orthogonal magnetometers. Madgwick [43] introduced a new orientation estimation algorithm that is applicable to both IMU and MARG systems. The algorithm employs a quaternion based representation of orientation to describe the coupled nature of orientations in three dimensions and is not subject to the problematic singularities associated with an Euler angle representation.

High gain observers (HGOs) have been also utilized to get reliable position estimates. Estimates provided by HGOs have been used in nonlinear feedback control since 1980s [44]-[46]. The works presented in [47]-[49] applied HGOs to nonlinear systems and obtained global results under global Lipschitz conditions. Esfandiari and Khalil [50] mentioned that HGOs could destabilize the closed loop system when the observer gains are designed as sufficiently high in the lack of global Lipschitz conditions. The authors showed that peaking phenomenon which was introduced by [51] causes finite escape time for nonlinear systems. The work in [50] solved this problem by saturating the control input during the peaking period. This can be achieved by designing the control input as a globally bounded function of the state estimates.

It is known that asymptotic stability can be recovered through the separation principle in linear control theory. However, this principle does not consider the recovery of region of attraction and state trajectories. Many of the works [52]-[54] related to HGOs that extend the separation principle to nonlinear systems have been also focused on the recovery of asymptotic stability. Actual performance of the nonlinear systems has been recovered by high gain observers. Atassi and Khalil [55] show that HGO recovers also region of attraction and state trajectories of the state feedback controller as the observer gains are sufficiently high. This is ob-

served because of the combination of fast observer with control saturation. Since then, many researchers [56]-[58] have used high gain observers to get reliable estimates which are provided as feedback to nonlinear controllers to solve stabilization and tracking problems.

2.4 Acceleration Feedback

Acceleration feedback control focuses on designing closed-loop control using acceleration feedback to enhance robustness against external disturbances. The acceleration feedback signal contains the effects of unknown disturbances. Therefore, acceleration control responds faster and rejects the disturbances successfully.

Schmidt and Lorenz [59] demonstrated the principles, design methodologies and implementation of acceleration feedback to substantially improve the performance of DC servo drives. They showed that acceleration feedback acts as an electronic inertia to provide higher stiffness to the system. The success of acceleration control techniques in literature depends on the accurate and continuous acceleration feedback. Robust angular accelerations which are estimated by the sensor fusion algorithms mentioned above are incorporated as feedback signals into the following control techniques: the inner loop acceleration control [60]-[61], disturbance observer based control [62]-[65], dynamic compensation [66]-[67], fuzzy control [68], loop shaping [69], feedforward compensation [70]-[71] and contact transition control [72]. Early studies reject the disturbances by using acceleration signals as feedback to proportional-integral (PI) controller, proportional-derivative (PD) controller and proportional-integral-derivative (PID) controller [60], [61], [63].

Deur and Peric [60] extended PI speed controller with an inner loop acceleration control. The proposed method provides 50% smaller response time than PI speed controller. Han et al. [61] introduced the acceleration feedback to enhance the independent PD control performance of multi-DOF mechatronic system.

Disturbance observers provide the estimates of the disturbances (total mechanical load torque and parameter uncertainties) using the acceleration signal. Hori [62] is one of the first researchers who presented theoretical analysis and experimental results of disturbance observer based control with acceleration feedback. Jeong et al. [63] proposed an acceleration based disturbance observer (AbDOB) to improve the attitude control performance of a quad-rotor system under the unknown disturbances. Acceleration signals are used to estimate the control input torque. Then, the disturbance is estimated by the difference between the nominal control input torque and the estimated control input torque. That difference cancels out the disturbance. The proposed method performs better than the PD control.

Kobayashi et al. [64] analyzed the disturbance observers to identify the pa-

rameter variations of the haptic motion platforms. Authors showed that the cut-off frequency of the low-pass filter used in the disturbance observer where the robustness is assured depends on the parameter variations. Haptic motion platforms require much wider bandwidth to interact with unknown environments. The conventional disturbance observer attains the acceleration information by the second order derivative of a position response so the bandwidth is limited due to the derivative noise. To enlarge the bandwidth of a disturbance observer, Katsura et al. [65] proposed a position-acceleration integrated disturbance observer (PAIDO). Since an acceleration sensor is implemented in it, the control performance of the PAIDO is superior to the conventional one.

Mizochi et al. [66] showed higher significance of the sampling period of an output than that of an input in acceleration control. The authors proposed the multirate sampling method for the acceleration control. Based on the experimental results, a shorter output sampling period has better performance than a longer input sampling period. Shang and Cong [67] developed a dynamic acceleration control (DAF) by introducing acceleration feedback into the robust dynamics compensation to restrain the trajectory disturbances on the planar parallel manipulator. DAF can eliminate the trajectory disturbances due to sudden acceleration and deceleration.

Rubaai et al. [68] implemented an embedded hybrid H_∞ adaptive fuzzy control structure for trajectory tracking control of a brushless servo drive system. The control structure employs a fuzzy logic controller incorporating a H_∞ tracking controller with an acceleration feedback signal. The fuzzy logic controller is integrated with an adaptive law based on Lyapunov synthesis approach to compensate for system uncertainty and random changes in the external load acting on the drive system. The experiments show that the proposed method provides better performance than the traditional H_∞ controller.

Torsional resonance limits the velocity controller bandwidth in most industrial drives. Acceleration feedback is a general solution for low-frequency resonance but it has practical limitations such as dead time. Makkapati et al. [69] proposed an extended acceleration feedback to overcome those limitations. In this method, acceleration feedback is combined with loop shaping techniques. The results present an improvement in the bandwidth of the velocity control loop. This technique can be used for other mechanical systems suffering from mechanical resonance.

The angular acceleration information is generally used to increase the stabilization and trajectory tracking performance of the inertially stabilized platforms (ISP). Rezac and Hurak [70] designed accelerometer based feedforward vibration rejection for inertially stabilized 2 DOF gimbal platform. Experiments prove that significant vibration rejection is achieved with this feedforward compensation scheme. Bai and Zhang [71] added accelerometer based feedforward compensation to PID

control system to reject the disturbances in 3 DOF gimbal platform. The proposed method improves the accuracy of ISP more than 10% compared to the traditional PID controller without feedforward compensation. Joint acceleration and velocity feedbacks are incorporated into a classical internal force control of a robot in contact with the environment. This is intended to achieve a robust contact transition and force tracking performance for varying unknown environments, without any need of adjusting the controller parameters. Xu et al. [72] proposed a unified control structure for free motion, contact transition, and constrained motion. The authors discussed the influence of the acceleration and velocity feedbacks on the force tracking performance during the postcontact period.

2.5 LPV Modeling Approaches

Linear parameter varying (LPV) models are linear state space systems whose matrices depend on a time varying external parameter vector [73]. The entries of the parameter vector are the scheduling variables that represent the varying operating conditions of the system. LPV models are called as quasi-LPV when the scheduling variables contain the measurable system inputs, outputs or states instead of only exogenous signals.

Linear time-invariant (LTI) models are not sufficient when the nonlinear robotic systems are used in large workspaces [74]. Shamma and Athans [75] first developed LPV models for gain-scheduled controllers. Since then LPV models have attracted more researchers.

In literature, different LPV modelling approaches exist [76]. Jacobian linearization [77] is the simplest approach to obtain LPV models. This method is based on the first order linear approximations with respect to a set of equilibrium points. State transformation [78] is also a popular technique to derive a LPV model. The goal is to eliminate all nonlinear terms in the scheduling parameters. This method performs a coordinate change in the nonlinear equations of the system and provides quasi-LPV model of the system.

Marcos and Balas [79] developed a novel approach for the derivation of quasi-LPV models. This approach is called as function substitution because it is based on the substitution of a decomposition function by (scheduling parameter-dependent) functions linear in the scheduling vector. The decomposition function is the combination of all the terms of the nonlinear system that are not affine with respect to the nonscheduling states and control inputs. These terms are not function of the scheduling vector alone.

Today, well-known linear optimal controllers [80] are applied to nonlinear systems represented by LPV models. Therefore, the key feature of LPV models is to provide the use of linear optimal control methods to nonlinear MIMO dynamic

systems. LPV models can be used to synthesize linear optimal robust controllers such as the linear quadratic regulator (LQR). This controller deals with the optimization of a cost function or performance index [81]. The states and the control inputs are weighted based on their importance to seek for appropriate transient and steady state behaviours. The LQR controller has been generally derived by solving an algebraic Riccati equation. When a set of Lyapunov inequalities is solved, it is difficult to find a common Lyapunov matrix analytically. This can be solved numerically by convex programming algorithms involving LMIs [82]. While the algebraic solution can only be applied to one plant, the numerical procedure can take into account multiple plants. Thus, the LQR deals with uncertain systems at different operation points.

Several H_∞ control techniques have been also synthesized on LPV models. Siqueira et al. [83] developed procedures based on H_∞ techniques to achieve position control of underactuated manipulators. In the deterministic approach, two nonlinear control techniques are compared in order to verify the differences in structure and robustness of controllers based on quasi-linear parameter varying representation and game theory. Experimental results have shown that the quasi-LPV technique has presented better robustness in comparison with the game theory technique. Yu et al. [84] combined the gain scheduling theory with H_∞ controller for the LPV model of the robotic manipulator. A control performance comparison between the proposed controller and the single H_∞ LTI controller is made by experiments. Hilhorst et al. [85] designed reduced order multi objective H_2/H_∞ controllers for discrete time LPV systems. Experimental validations on a lab-scale overhead crane with varying cable length illustrate the practical viability of the approach.

Many researchers synthesize the LPV controller for the stabilization purposes. Seghal and Tiwari [86] designed the LQR controller to maintain the triple inverted pendulum on a cart around its unstable equilibrium position using single control input. Similarly, Kumar and Jerome [87] described the method for stabilizing and trajectory tracking of Self Erecting Single Inverted Pendulum (SESIP) using the LQR. Castiello et al. [88] presented a stabilization nonlinear control algorithm for a mini rotorcraft with four rotors and compared the results with LQR controller.

2.6 Hybrid Learning Based Adaptive Controllers

Robotic applications usually involve repetitive tasks such as assembling, packaging, manufacturing, construction, and mine clearing. This motivates researchers to focus on the development of learning control methods that compensate the unknown nonlinear periodic robot dynamics with a known period to improve link position tracking performance. However, unknown robot dynamics can also be

aperiodic. Hybrid control algorithms are usually required to compensate for unknown disturbances with periodic and aperiodic components. The subsequent sections present the state of the art learning controller algorithms, and hybrid learning based adaptive controller algorithms.

2.6.1 Learning Controllers

The aim of a learning control is to achieve desired system performance by updating the control input from past errors either repeatedly over a fixed finite time interval, or repetitively (cyclically) over an infinite time interval. Typical learning control strategies are generally categorized into iterative learning control (ILC) and repetitive control (RC). ILC method achieves perfect tracking of the system output to a desired trajectory repeatedly on a fixed time (pre-specified) interval whereas RC handles the problem of the periodic reference tracking and periodic disturbance rejection. ILC requires to reset the system to the initial condition at the beginning of each cycle to perform the repetitive tasks, i.e. achieving same desired trajectory. Repetitive control, on the other hand, needs no initial repositioning and the system operates continuously. ILC scheme was proposed by Arimoto et al. [89] in 1984, and Lyapunov-like based designs of iterative learning control [90]-[92] have been developed. ILC methods have been designed for both nonlinear and linear uncertain systems with the global Lipschitz conditions [93]-[95].

In parallel to the developments in those controllers, repetitive learning controllers have gained remarkable interest to solve similar tracking problems without the requirement for initial repositioning. Earlier works of the repetitive controllers have been developed by [96] for linear time-invariant systems. The stability analysis was conducted for linear processes that repeat continuously in [97]. Similar to ILC, repetitive control has been applied on nonlinear systems [98]-[102]. Messner et al. [98] identified and compensated a nonlinear disturbance function where it is represented as an integral of a predefined kernel function multiplied by an unknown influence function. Using the past information of the plant, the learning rule was utilized to indirectly estimate the disturbance function by updating the influence function estimate. This controller achieves asymptotic disturbance cancellation. Dixon et al. [99]-[101] proposed a repetitive learning control for nonlinear systems with an exogenous periodic disturbance that satisfies the matching condition. The works in [98]-[100] needs parameterizable plants and their goal is to achieve asymptotic convergence along the time horizon. Cao et al. [101] designed a repetitive variable structure control (RVSC) for nonlinear systems without the need of parametrization. This method incorporates repetitive control into VSC. The robustness to the uncertain system is ensured by the VSC, and the modeling uncertainties are relaxed to be locally Lipschitz instead of being globally Lipschitz. State infor-

mation may not be available in many applications for the controller design. Xu et al. [102] developed a new observer based learning controller approach for a class of nonlinear systems with time varying parameter uncertanities. Those uncertanities are assumed to be periodic and the only prior knowledge is the periodicity. This approaches considers two classes of system nonlinearities. The first class of nonlinearity is the global Lipschitz continuous functions of the unknown state variables, whereas the second class is the local Lipschitz continuous functions of the accessible output variables. The Lyapunov-like energy function is employed to facilitate the learning control design, for the incorporation of any available system knowledge.

2.6.2 Hybrid Learning Based Adaptive Controllers

Dixon et al. [99]-[100] proposed a hybrid adaptive/learning control scheme to achieve global asymptotic link position tracking despite unknown robot dynamics with periodic and aperiodic components. The authors applied the saturation function to the standard learning control law and solved the boundedness problem by showing that the proposed learning feedforward term is bounded for all times. Ouyang and Zhang [103] developed a new control method called adaptive learning PD (AL-PD) control. While PD control acts as a basic feedback control part, learning feedforward control is an iteratively updated term to cope with the unknown robot dynamics. When the number of iterations increase, AL-PD control guarantees the tracking errors converge arbitrarily close to zero. Ngo et al. [104] also designed an adaptive iterative learning control (AILC) of uncertain robot manipulators in task space for trajectory tracking. The hybrid controllers developed in [100]-[104] need infinite memory due to iterative control structure and exponential convergence is not guaranteed. Vecchio et al. [105] proposed a hybrid adaptive learning control scheme to solve the periodic tracking problem for single-input, single-output uncertain feedback linearizable systems with maximal relative degree and matching unstructured uncertainties, i.e. no parametrization is available for uncertain nonlinearities. The authors have developed in Fourier series expansion the unknown periodic reference input signal with a known period. The proposed controller learns the reference control signal and identifies the Fourier-coefficients of any truncated approximation. Liuzzo and Tomei [106] developed the input reference signals as Fourier series expansion and designed AL-PD control that learns the input reference signals by identifying their Fourier coefficients. When the Fourier series expansion of each input reference signal is finite, global asymptotic tracking and local exponential tracking of both the input and the output reference signals is obtained. Delibasi et al. [107] proposed a self tuning, desired compensation adaptation law (DCAL) [108] based adaptive controller with

disturbance estimation based on Fourier Series Expansion. The proposed hybrid controller guarantees global asymptotic link tracking.

Wang et al. [109] designed a backstepping adaptive iterative learning control (AILC) where the backstepping like procedure is used to design the main structure of the AILC. The developed controller has two parts; a fuzzy neural network (FNN) is utilized to approximate unknown certainty equivalent controller, and a robust learning term is used to compensate for uncertainty from the network approximation error. Thus, the boundedness of internal signals is guaranteed. Tracking error asymptotically converges to zero. Benosman [110] concentrated on the use of well-known extremum seeking (ES) theory [111] in the learning based adaptive control structure. The local integral input-to-state stability (iISS) feedback controller with a model-free ES algorithm is combined to obtain a learning-based adaptive controller. Wang and Chien [112] developed an observer-based adaptive iterative learning control using a filtered fuzzy neural network. A state tracking error observer is introduced to design the iterative learning controller using only the measurement of joint position. An observation error model is derived based on the state tracking error observer. Then, by introducing some auxiliary signals, the iterative learning controller is proposed based on the use of an averaging filter.

Chapter 3

3 Sensors and Proposed Estimation Algorithms

Modeling of MEMS inertial sensors and the proposed estimation algorithms are presented in this chapter.

3.1 Sensor Modeling

MEMS inertial sensors (gyroscopes, accelerometers and magnetometers) and encoders are modeled by corrupting the true sensor measurements with sensor errors.

3.1.1 Gyroscope

Gyroscopes measure angular rates in the body frame. The gyroscope output can be modeled as:

$$\omega_g^b = \omega_0^b + b_g + \eta_g \tag{3.1}$$

where $\omega_0^b = \begin{bmatrix} \omega_{x_0}^b & \omega_{y_0}^b & \omega_{z_0}^b \end{bmatrix}^T$ defines the true rotation rates in the body frame, b_g and η_g represent the gyro biases and noises.

3.1.2 Accelerometer

Accelerometers measure specific forces in the body frame. These forces are the total accelerations relative to free-fall and represented by f_a. It is assumed that IMU is attached to the body center and earth rotation effects are neglected. Then, the true specific forces are computed in the inertial frame as follows:

$$f_0^n = \dot{V}^n + g, \qquad g = \begin{bmatrix} 0 \\ 0 \\ -9.81 \end{bmatrix} \tag{3.2}$$

where $\dot{V}^n$ denotes a vector of the translational accelerations of the body and g is the acceleration due to gravity. Since accelerometers measure the specific forces

in the body frame, f_0^n is multiplied by the rotation matrix, R_n^b, to transform from inertial to body frame as shown in (3.3).

$$f_0^b = R_n^b f_0^n = R_n^b \dot{V}^n + R_n^b g \tag{3.3}$$

The rotation matrix from the inertial frame to the body frame, R_n^b, is computed using XYZ convention of the Euler angles. Specifically, the first rotation is about X axis by a roll angle ϕ, which is denoted as $R_x(\phi)$. The second rotation, $R_y(\theta)$, is about Y axis by a pitch angle θ. Finally, the third rotation, $R_z(\psi)$, is about Z axis by a yaw angle ψ. Then the rotation matrix is computed by the product of these transformation matrices as follows:

$$\begin{aligned} R_n^b &= R_x(\phi)R_y(\theta)R_z(\psi) \\ &= \left[\begin{array}{c|c|c} c_\psi c_\theta & c_\theta s_\psi & -s_\theta \\ \hline c_\psi s_\phi s_\theta - c_\phi s_\psi & c_\phi c_\psi + s_\phi s_\psi s_\theta & c_\theta s_\phi \\ \hline s_\phi s_\psi + c_\phi c_\psi s_\theta & c_\phi s_\psi s_\theta - c_\psi s_\phi & c_\psi c_\theta \end{array}\right] \end{aligned} \tag{3.4}$$

where

$$R_x(\phi) = \begin{bmatrix} 1 & 0 & 0 \\ 0 & c_\phi & s_\phi \\ 0 & -s_\phi & c_\phi \end{bmatrix}, \quad R_y(\theta) = \begin{bmatrix} c_\theta & 0 & -s_\theta \\ 0 & 1 & 0 \\ s_\theta & 0 & c_\theta \end{bmatrix}, \quad R_z(\psi) = \begin{bmatrix} c_\psi & s_\psi & 0 \\ -s_\psi & c_\psi & 0 \\ 0 & 0 & 1 \end{bmatrix}$$

with $c_\Delta \triangleq \cos\Delta$ and $s_\Delta \triangleq \sin\Delta$. Usually V^n is assumed to be constant and therefore $\dot{V}^n = 0$. Then, (3.3) is expressed as:

$$f_0^b = R_n^b g = \begin{bmatrix} -g s_\theta \\ g c_\theta s_\phi \\ g c_\phi c_\theta \end{bmatrix} \tag{3.5}$$

where ϕ and θ are the roll and pitch angles. The output of the accelerometer is modeled as:

$$f_a^b = f_0^b + b_a + \eta_a \tag{3.6}$$

where b_a and η_a define the accelerometer biases and noises.

3.1.3 Magnetometer

Magnetometers measure the strength of the magnetic fields in the body frame. The magnetometer output is modeled as:

$$H_m^b = H_0^b + b_m + \eta_m \tag{3.7}$$

where H_0^b defines the true magnetometer measurements in the body frame, b_m and η_m represent the magnetometer biases and noises.

3.1.4 Encoder

Encoder measures joint angles in control applications. q_m is the measured encoder data defined as follows:

$$q_m = q_0 + b_e + \eta_e \tag{3.8}$$

where q_m is the measured encoder data, q_0 is the true encoder measurement, and b_e and η_e represent the encoder biases and noises, respectively.

3.2 Sensor Fusion by a Master-Slave Kalman Filter

Conventional sensor fusion methods based on Kalman filter estimate Euler angles and the gyroscope biases [113]-[114]. The state vector is defined as follows [115]:

$$x_s = \begin{bmatrix} \phi & \theta & \psi & b_{g_x} & b_{g_y} & b_{g_z} \end{bmatrix}^T = \begin{bmatrix} \Theta^T & b_g^T \end{bmatrix}^T \tag{3.9}$$

where $\Theta \equiv \begin{bmatrix} \phi & \theta & \psi \end{bmatrix}^T$ represent Euler angles (roll, pitch and yaw) and the gyroscope biases are denoted by $b_g \equiv \begin{bmatrix} b_{g_x} & b_{g_y} & b_{g_z} \end{bmatrix}^T$. The nonlinear process dynamics is described by the following kinematic relationship between the Euler rates $\Omega = \begin{bmatrix} \dot{\phi} & \dot{\theta} & \dot{\psi} \end{bmatrix}^T$ and the angular velocity vector $\omega = \begin{bmatrix} \omega_x & \omega_y & \omega_z \end{bmatrix}^T$ [116] :

$$\Omega = \mathbb{B}\omega \tag{3.10}$$

where $\mathbb{B}$ is the velocity transformation matrix defined as:

$$\mathbb{B} = \begin{bmatrix} 1 & \sin\phi \tan\theta & \cos\phi \tan\theta \\ 0 & \cos\theta & -\sin\phi \\ 0 & \sin\phi \sec\theta & \cos\phi \sec\theta \end{bmatrix} \tag{3.11}$$

The velocity transformation matrix, $\mathbb{B}$, given by (3.11) becomes singular when $\theta = \pi/2$ because $\tan\theta = \infty$ or $\sec\theta = \infty$ at $\theta = \pi/2$. In this work, the tilt axis is constrained to be in the range $[0, \pi/2)$, and therefore there is no gimbal lock problem. It should be remarked that the choice of Euler angles or quaternions is a matter of preference, and due to its simplicity Euler angles are preferred. The state vector in (3.9) is extended to include angular velocities and accelerations; i.e.

$$X = \begin{bmatrix} \phi & \theta & \psi & \dot{\phi} & \dot{\theta} & \dot{\psi} & \ddot{\phi} & \ddot{\theta} & \ddot{\psi} & b_{g_x} & b_{g_y} & b_{g_z} \end{bmatrix}^T \tag{3.12}$$

$$= \begin{bmatrix} \Theta^T & \Omega^T & \Gamma^T & b^T \end{bmatrix}^T \tag{3.13}$$

where $\Gamma \equiv \begin{bmatrix} \ddot{\phi} & \ddot{\theta} & \ddot{\psi} \end{bmatrix}^T$ defines Euler accelerations.

In accordance with the new state vector (3.13), the following continuous-time process dynamics is obtained by differentiating the nonlinear dynamics in (3.10):

$$\frac{d}{dt}X = \begin{bmatrix} \dot{\Theta} \\ \dot{\Omega} \\ \dot{\Gamma} \\ \dot{b}_g \end{bmatrix} = \begin{bmatrix} \mathbb{B}\omega \\ \dot{\mathbb{B}}\omega + \mathbb{B}\alpha \\ \ddot{\mathbb{B}}\omega + 2\dot{\mathbb{B}}\alpha + \mathbb{B}\gamma \\ 0_{3\times 1} \end{bmatrix} + W \tag{3.14}$$

where angular accelerations and jerks are denoted by $\dot{\omega} \equiv \alpha = \begin{bmatrix} \alpha_x & \alpha_y & \alpha_z \end{bmatrix}^T$ and $\dot{\alpha} \equiv \gamma = \begin{bmatrix} \gamma_x & \gamma_y & \gamma_z \end{bmatrix}^T$ in the body coordinate frame. Non-deterministic effects and modeling errors are represented by the process noise, W. In (3.14), gyro biases are assumed to be constant. This model is known as a *Wiener process* and can be considered as a special case of *Gauss-Markov process* [117].

Remark I. Gyro biases can also be modeled using *Singer Model*. This model assumes that the gyro bias is a zero-mean stationary *first order Markov process* [30]. The continuous time bias model is defined as:

$$\dot{b}_g = -\beta b_g + w \tag{3.15}$$

where w is a zero mean white noise and β is the reciprocal of the time constant. Note that $\beta = 0$ implies constant bias model.

To estimate the state vector X in (3.13), an extended Kalman filter that utilizes sensor measurements was implemented. To run the EKF, we need to compute ω, α and γ that appear on the right hand side of (3.14). Since there are no additional sensors to measure angular accelerations and jerks, they need to be estimated from gyro measurements. To this end, a slave type inverse Φ-algorithm is introduced to estimate ω, α and γ using bias compensated gyro readings. Since biases will be estimated by EKF and used as inputs to the inverse Φ-algorithm, we have a master-slave configuration in Figure 3 where the master estimator feeds the slave estimator with bias estimates and the slave estimator returns estimated angular velocity, accelerations and jerks to the master estimator.

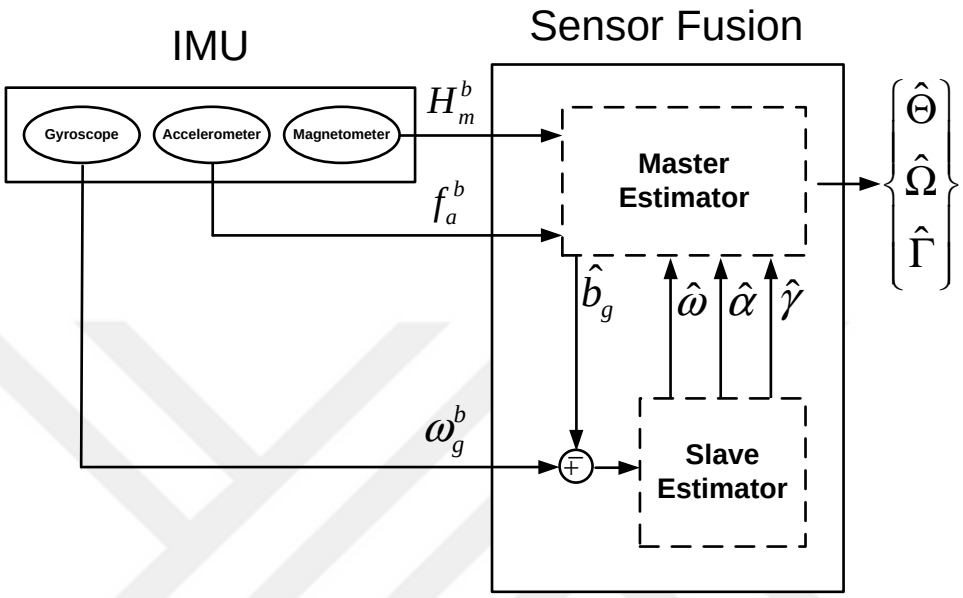

Figure 3: Block diagram of the master-slave Kalman filter.

3.2.1 Master Estimator

Process dynamics of the master estimator is given by (3.14). Applying Euler's forward discretization to the process dynamics leads to:

$$\begin{bmatrix} \Theta \\ \Omega \\ \Gamma \\ b_g \end{bmatrix}_{k+1} = \begin{bmatrix} \Theta \\ \Omega \\ \Gamma \\ b_g \end{bmatrix}_k + T_s \begin{bmatrix} \mathbb{B}\omega \\ \mathbb{F}\omega + \mathbb{B}\alpha \\ \mathbb{H}\omega + 2\mathbb{F}\alpha + \mathbb{B}\gamma \\ 0_{3\times 1} \end{bmatrix}_k + W_k \tag{3.16}$$

where $\mathbb{F} \equiv \dot{\mathbb{B}}$, $\mathbb{H} \equiv \dot{\mathbb{F}} = \ddot{\mathbb{B}}$, T_s is the sampling period and W_k is the white Gaussian process noise with zero mean. Measurement vector of the master estimator contains the specific force measurements, f_a^b, from accelerometer and the yaw angle, ψ_m, determined from the resolved components of the magnetic field measurements, H_m^b, in the horizontal plane along the heading axis [118]. In order to increase the observability of the state vector, the measurement vector of EKF is also extended

by using angular velocities, $\hat{\omega}$, and accelerations, $\hat{\alpha}$ estimated by the slave filter:

$$Y_k = \begin{bmatrix} f_a^b & \psi_m & \hat{\omega} & \hat{\alpha} \end{bmatrix}_k^T = \begin{bmatrix} R_n^b(\Theta)g \\ \psi \\ \mathbb{E}\Omega \\ \mathbb{E}\Gamma + \mathbb{G}\Omega \end{bmatrix}_k + V_k \tag{3.17}$$

where V_k is the time correlated measurement noise [119]:

$$V_k = \Lambda_{k-1} V_{k-1} + \zeta_{k-1} \tag{3.18}$$

with $\Lambda_{k-1} = e^{-\frac{T}{\kappa}} I_{3\times3}$ is the transition matrix of the time correlated errors with the time constant, κ, ζ_{k-1} represents the white Gaussian noise with zero mean, R_n^b is the rotation matrix from the inertial frame to the body frame in (3.4), $\mathbb{G} = \dot{\mathbb{E}}$, g is the gravitational acceleration vector and the inverse velocity transformation matrix, $\mathbb{E}$, is defined as:

$$\mathbb{E} = \mathbb{B}^{-1} = \begin{bmatrix} 1 & 0 & \sin\theta \\ 0 & \cos\phi & \cos\theta\sin\phi \\ 0 & -\sin\phi & \cos\phi\cos\theta \end{bmatrix} \tag{3.19}$$

As it is seen from (3.16) and (3.17), the process and measurement models of the master estimator are nonlinear so EKF will be implemented to estimate the state vector X.

Remark II. Larger the time constant leads to more correlated measurement noises. If κ approaches infinity, then the transition matrix becomes identity and $V_k = V_{k-1} + \zeta_{k-1}$, i.e. the measurement noises are time correlated. On the other hand, if the time constant is small, the measurement noises are less correlated and they behave like a white Gaussian noise with zero mean, i.e. $V_k = \zeta_{k-1}$.

3.2.2 Slave Estimator

The slave estimator provides estimates of angular velocities, accelerations and jerks to the master estimator. The following process dynamics is constructed in discrete time, based on the classical laws of motion using Taylor series where angular jerks are assumed to be constant:

$$\begin{bmatrix} \omega \\ \alpha \\ \gamma \end{bmatrix}_{k+1} = \begin{bmatrix} I_{3\times3} & T_s I_{3\times3} & 0.5T_s^2 I_{3\times3} \\ 0_{3\times3} & I_{3\times3} & T_s I_{3\times3} \\ 0_{3\times3} & 0_{3\times3} & I_{3\times3} \end{bmatrix} \begin{bmatrix} \omega \\ \alpha \\ \gamma \end{bmatrix}_k + \mathbb{W}_k \tag{3.20}$$

where T_s is the sampling period and $\mathbb{W}_k$ is the white Gaussian process noise with zero mean. The gyro bias estimated by the EKF is subtracted from the gyro readings to obtain bias compensated body angular velocity, $\omega_g^b - \hat{b}_g$, which is used as

the measurement for the slave estimator:

$$\Upsilon_k = \omega^b_{g_k} - \hat{b}_{g_k} = \begin{bmatrix} I_{3\times3} & 0_{3\times6} \end{bmatrix} \begin{bmatrix} \omega \\ \alpha \\ \gamma \end{bmatrix}_k + \mathbb{V}_k \tag{3.21}$$

where $\omega^b_g - \hat{b}_g = \begin{bmatrix} \omega^b_{g_x} - \hat{b}_{g_x} & \omega^b_{g_y} - \hat{b}_{g_y} & \omega^b_{g_z} - \hat{b}_{g_z} \end{bmatrix}^T$ and $\mathbb{V}_k$ is the time correlated measurement noise [119]:

$$\mathbb{V}_k = \lambda_{k-1}\mathbb{V}_{k-1} + \xi_{k-1} \tag{3.22}$$

with $\lambda_{k-1} = e^{-\frac{T}{\kappa}} I_{3\times3}$ is the transition matrix of the time correlated errors with the time constant, κ, and ξ_{k-1} is the white Gaussian noise with zero mean. When the measurement errors at different times are highly correlated, the classical Kalman filter provides an approximate solution to the estimation problem because R_k is the covariance matrix of only ξ_k, not $\mathbb{V}_k$, i.e. $\xi_k \sim N(0, R_k)$. Bryson and Henrikson [120] proposed a time-differencing algorithm also known as an *Inverse R-Algorithm* in order to handle with time correlated measurement errors. However, this algorithm introduces one step delay because the computation of apriori state estimate must use the current measurement. To resolve this problem, Petovello et al. [121]-[122] proposed a revised time-differencing algorithm which is known as an *Inverse* Φ*-Algorithm*. We employ the inverse Φ-algorithm to estimate angular velocity (ω), acceleration (α) and jerk (γ) using process and measurement models given by (3.20)-(3.22), respectively. The prediction stage of the inverse Φ-algorithm is the same with the prediction step of the Kalman filter. On the other hand, the update stage of the inverse Φ-algorithm is modified based on Kalman filter. The prediction and update stages of the inverse Φ-algorithm are presented in the Appendix A.

3.3 Cascaded High Gain Observers

This section develops cascaded high gain observers to estimate reliable link velocities and accelerations in addition to link positions by utilizing noisy position measurements from an IMU or an encoder. To illustrate this, consider the following second-order nonlinear system:

$$\begin{aligned} \dot{x}_{o_1} &= x_{o_2} \\ \dot{x}_{o_2} &= \Psi(x_o, u) \\ y_1 &= x_{o_1} \end{aligned} \tag{3.23}$$

where $x_o = \begin{bmatrix} x_{o_1} & x_{o_2} \end{bmatrix}^T$ is the state vector, x_{o_1} denotes link angles of the robotic manipulator, $x_{o_1} \triangleq q$, and x_{o_2} represent the link velocities, $x_{o_2} \triangleq \dot{q}$, u is the control

input, and y_1 is the position measurement provided by an IMU or an encoder. Suppose that the state feedback control, $u = \gamma_o(x_o)$, stabilizes the origin $x_o = 0$ of the closed loop system:

$$\begin{aligned} \dot{x}_{o_1} &= x_{o_2} \\ \dot{x}_{o_2} &= \Psi(x_o, \gamma_o(x_o)) \\ y_1 &= x_{o_1} \end{aligned} \tag{3.24}$$

To implement this feedback controller using only position measurements, a new observer which consists of two high gain observers in a cascaded structure is proposed as depicted in Figure 4. The first HGO uses position measurements by an

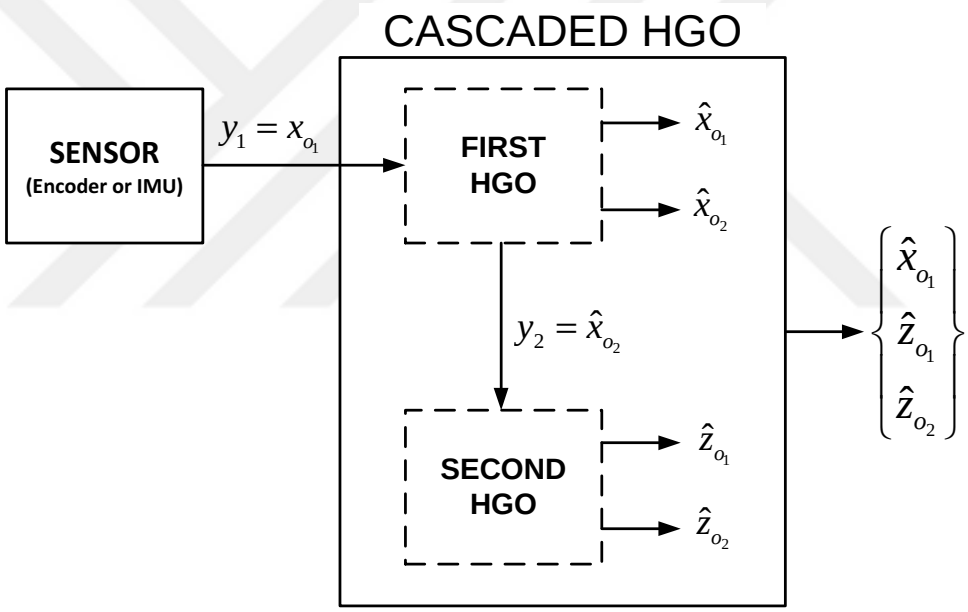

Figure 4: Block diagram of Cascaded HGO Structure

IMU or an encoder to estimate reliable position and velocity information. The second HGO, on the other hand, utilizes estimated velocities by the first HGO to provide estimates of acceleration signals. The dynamics of the first HGO is designed as:

$$\begin{aligned} \dot{\hat{x}}_{o_1} &= \hat{x}_{o_2} + L_1(y_1 - \hat{x}_{o_1}) \\ \dot{\hat{x}}_{o_2} &= \hat{\Psi}(\hat{x}_o, u) + L_2(y_1 - \hat{x}_{o_1}) \end{aligned} \tag{3.25}$$

where $y_1 = x_{o_1}$ is the position measurement, $\hat{\Psi}(\hat{x}_o, u)$ is a nominal model of the nonlinear function $\Psi(x_o, u)$, and L_1, L_2 are the observer gains. Since the exact

model of $\Psi(x_o, u)$ is not known, $\hat{\Psi}(\hat{x}_o, u) = 0$ can be considered. The dynamics of the second HGO is as follows:

$$\begin{aligned} \dot{\hat{z}}_{o_1} &= \hat{z}_{o_2} + L_3(y_2 - \hat{z}_{o_1}) \\ \dot{\hat{z}}_{o_2} &= L_4(y_2 - \hat{z}_{o_1}) \end{aligned} \tag{3.26}$$

where $y_2 = \hat{x}_{o_2}$ is the estimated velocity by the first HGO, and L_3, L_4 are the observer gains. Error dynamics in the first HGO are obtained as:

$$\begin{aligned} \dot{\tilde{x}}_{o_1} &= -L_1\tilde{x}_{o_1} + \tilde{x}_{o_2} \\ \dot{\tilde{x}}_{o_2} &= -L_2\tilde{x}_{o_1} + \delta_o(x_o, \tilde{x}_o) \end{aligned} \tag{3.27}$$

where the first HGO estimation error is defined as:

$$\tilde{x}_o = \begin{bmatrix} \tilde{x}_{o_1} \\ \tilde{x}_{o_2} \end{bmatrix} = \begin{bmatrix} x_{o_1} - \hat{x}_{o_1} \\ x_{o_2} - \hat{x}_{o_2} \end{bmatrix} \tag{3.28}$$

and $\delta_o(x_o, \tilde{x}_o) = \Psi(x_o, u) - \hat{\Psi}(x_o, u)$. The observer gain $L_{12} = \begin{bmatrix} L_1 & L_2 \end{bmatrix}^T$ should be designed such that

$$\lim_{t\to\infty} \tilde{x}_o(t) = 0 \tag{3.29}$$

and the disturbance effects of $\delta_o(x_o, \tilde{x}_o)$ on $\tilde{x}_o$ is rejected. The transfer function between δ_o and $\tilde{x}$ is defined as follows:

$$H_o(s) = \frac{1}{s^2 + L_1 s + L_2} \begin{bmatrix} 1 \\ s + L_1 \end{bmatrix} \tag{3.30}$$

When $\sup_{w\in\mathbb{R}} |H_o(jw)|$ is arbitrarily small, undesired disturbances can be eliminated. This can be achieved by choosing $L_2 \gg L_1 \gg 1$. Therefore, the first observer gains are designed as:

$$L_1 = \frac{e_1}{\epsilon_1}, \quad \text{and} \quad L_2 = \frac{e_2}{\epsilon_1^2} \tag{3.31}$$

for some positive constants e_1, e_2, and $\epsilon_1 \ll 1$. It is concluded that decreasing ϵ_1 diminishes the disturbance effect, δ_o. Since large observer gains, L_1, L_2, are used in order to achieve zero estimation errors by rejecting disturbances, these observers are referred as high gain observers. Based on similar arguments, L_3 and L_4 are designed as:

$$L_3 = \frac{e_3}{\epsilon_2}, \quad \text{and} \quad L_4 = \frac{e_4}{\epsilon_2^2} \tag{3.32}$$

for some positive constants e_3, e_4, and $\epsilon_2 \ll 1$. However, [123] shows that the transient response of the high gain observer suffers from a peaking phenomenon. The transient response contains a term of the form $\left(\frac{1}{\epsilon_1}\right) e^{-\frac{ft}{\epsilon_1}}$ for some $f > 0$. Thus, peaking is induced by the order $\left(\frac{1}{\epsilon_1}\right)$ when ϵ_1 is sufficiently small. This phenomenon is handled by saturating the control input, u, or the state, x_o.

Chapter 4

4 Stabilization Using Inner Loop Acceleration Control

The aim of stabilization control is to maintain the desired orientation of a robotic platform (e.g. a pan-tilt system) as in Figure 5 and reject all the external disturbances that act on the system. Pan and tilt axes can also be referred as azimuth and elevation axes.

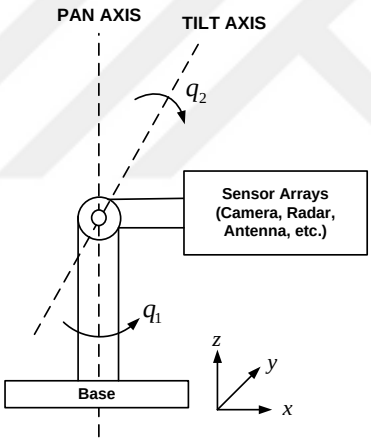

Figure 5: Pan-tilt mechanism.

The nonlinear model of the pan-tilt system based on the Euler-Lagrange formulation is as follows [124]:

$$M(q)\ddot{q} + C(q,\dot{q})\dot{q} + G(q) + F_v\dot{q} + F_s sgn(\dot{q}) = \tau + \tau_d \tag{4.1}$$

where

$$
\begin{aligned}
&q = \begin{bmatrix} q_1 & q_2 \end{bmatrix}^T, \quad \tau = \begin{bmatrix} \tau_1 & \tau_2 \end{bmatrix}^T, \quad \tau_d = \begin{bmatrix} \tau_{d_1} & \tau_{d_2} \end{bmatrix}^T \\
&M(q) = \begin{bmatrix} M_{11} & M_{12} \\ M_{21} & M_{22} \end{bmatrix}, \quad C(q, \dot{q}) = \begin{bmatrix} C_{11} & C_{12} \\ C_{21} & C_{22} \end{bmatrix} \\
&G(q) = \begin{bmatrix} 0 & 0.5 g m_2 l_2 \cos q_2 \end{bmatrix}^T, \quad F_v(\dot{q}) = \begin{bmatrix} v_1 \dot{q}_1 & v_2 \dot{q}_2 \end{bmatrix}^T \\
&F_s(\dot{q}) = \begin{bmatrix} k_1 \text{sgn}(\dot{q}_1) & k_2 \text{sgn}(\dot{q}_2) \end{bmatrix}^T \\
&M_{11} = \frac{1}{2} m_1 l_1^2 + m_2 l_1^2 + m_2 l_1 l_2 \cos q_2 + \frac{1}{3} m_2 l_2^2 \cos^2 q_2 + J_1 \\
&M_{22} = \frac{1}{3} m_2 l_2^2 + J_2, \quad M_{12} = M_{21} = 0 \\
&C_{11} = -m_2 l_1 l_2 \dot{q}_2 \sin q_2, \quad C_{12} = -\frac{1}{3} m_2 l_2^2 \dot{q}_1 \sin 2q_2 \\
&C_{21} = \dot{q}_1 \left(\frac{1}{2} m_2 l_1 l_2 \sin q_2 + \frac{1}{6} m_2 l_2^2 \sin 2q_2 \right), \quad C_{22} = 0
\end{aligned}
\tag{4.2}
$$

where $q, \dot{q}, \ddot{q} \in \mathbb{R}^2$ are the joint angles, velocities and accelerations, $M(q) \in \mathbb{R}^{2\times2}$ denotes the symmetric and positive-definite inertia matrix, $C(q, \dot{q}) \in \mathbb{R}^{2\times2}$ is the centripetal-Coriolis matrix, $G(q) \in \mathbb{R}^2$ is the gravity vector, F_v and $F_s \in \mathbb{R}^{2\times2}$ are constant, diagonal, positive-definite, viscous and static friction coefficient matrices, $sgn(\dot{q})$ is the signum function applied to the joint velocities, $\tau \in \mathbb{R}^2$ is the torque control input vector, $\tau_d \in \mathbb{R}^2$ defines the unknown disturbances acting on both azimuth and elevation axes. $J_1 \in \mathbb{R}$ and $J_2 \in \mathbb{R}$ are motor inertias, $m_1 \in \mathbb{R}$ and $m_2 \in \mathbb{R}$ are the masses of pan and tilt mechanisms, $l_1 \in \mathbb{R}$ is the radius, $l_2 \in \mathbb{R}$ is the length, $v_1 \in \mathbb{R}$ and $v_2 \in \mathbb{R}$ are viscous friction coefficients, and $k_1 \in \mathbb{R}$ and $k_2 \in \mathbb{R}$ are static friction coefficients.

Figure 6 depicts the block diagram of stabilization control. $\Omega_c = 0$ and Ω are the velocity command and measured velocity, e_Ω is the velocity error, V_c is the voltage applied to the motor, τ is the torque control input and τ_d represents the unknown disturbances acting on both azimuth and elevation axes. Since Ω is fed by a gyroscope, stabilization is also referred as gyro stabilization. Velocity controller is designed as a PI controller to follow the velocity command as closely as possible.

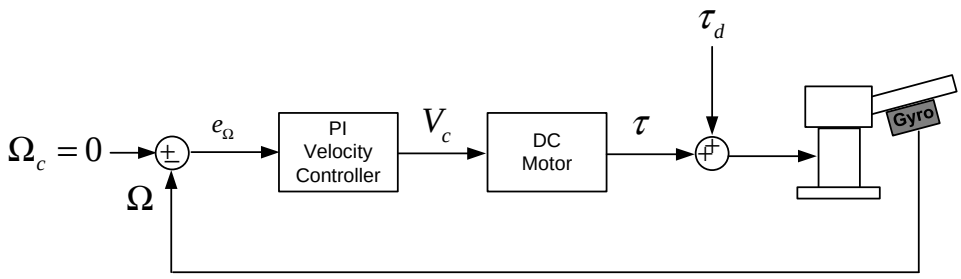

Figure 6: Block diagram of stabilization control.

The pan-tilt system converges from an initial orientation to the desired one by utilizing a PID position controller as shown in Figure 7. Θ_{ref} and Ω_{ref} are reference Euler angles and rates, $\hat{\Theta}$ and $\hat{\Omega}$ are estimated Euler angles and rates, and e_Θ defines the position error. Since both orientation and velocity information are used as feedback in the position controller, an IMU is needed to perform sensor fusion.

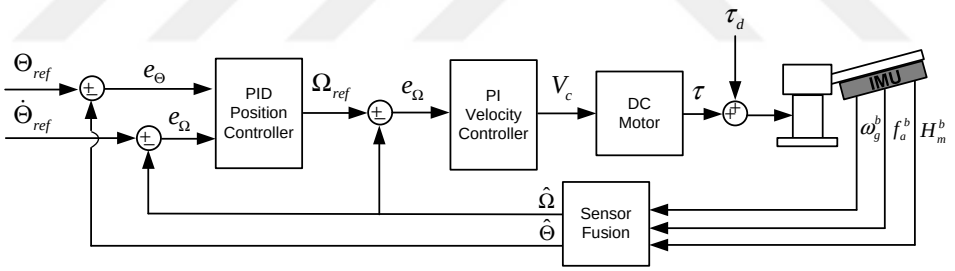

Figure 7: Block diagram of stabilization control with PID position control.

Stabilization control loop can be improved by using acceleration feedback in a PI current controller to achieve high precision stabilization as shown in Figure 8. J is the nominal inertia of motor, K_T is the motor torque constant, K_β is the acceleration feedback gain, I_{ref} and $\hat{I}$ represent reference and estimated currents, and e_I is the current error.

It is assumed that the center of rotation and the center of gravity of the pan-tilt mechanism are coincident. In light of this assumption, the nonlinear pan-tilt system given by (4.1) is decoupled along the azimuth and elevation axes. Therefore, two separate linear controllers are designed for these axes. In this thesis, the inner loop acceleration control detailed in [125] and [126] is implemented as depicted in Figure 8. The goal of acceleration control is to improve the stabilization per-

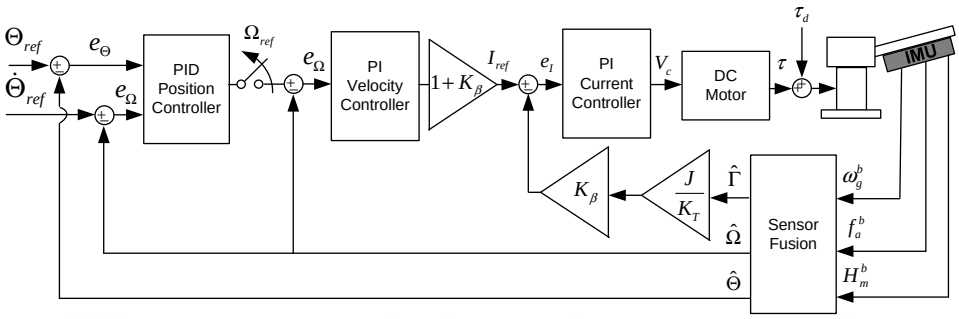

Figure 8: Block diagram of acceleration feedback control.

formance of the pan-tilt system by rejecting external disturbances. The position loop produces reference signals for the velocity loop, which in turn creates reference signals for the current loop. Reliable angular acceleration signals estimated by the master-slave Kalman filter are used as feedback in the current controller because the success of stabilization control largely depends on reliable acceleration feedback. However, estimated accelerations are not directly utilized in the current controller. When a torque is exerted on an object, it begins to rotate with an angular acceleration inversely proportional to its moment of inertia. This relation can be defined as $\tau = J\Gamma$. Also, the torque is proportional to the current in the armature windings of the rotor so it can be computed as $\tau = K_T I$. Using these relationships, an estimate of the current is calculated as $\hat{I} = \frac{J\hat{\Gamma}}{K_T}$ where $\hat{\Gamma}$ is the estimated angular acceleration. Then, the estimated current is scaled by the acceleration feedback gain, K_β, and used as feedback signal in the current controller.

Acceleration control is effective in disturbance rejection because the effects of disturbance will be sensed first in the acceleration signal before a significant velocity error can build up in the velocity loop. Higher acceleration gain adds more electronic inertia to the physical inertia of the total system [127]. Thus, the overall system exhibits high dynamic stiffness and has better disturbance rejection. The increase in effective inertia reduces the speed of the system's response. In order to preserve the loop gain, one should scale up the control loop gains by the factor $\left(1 + K_\beta\right)$ as in Figure 8.

The following PID controllers generate reference velocities for the velocity control loops for the azimuth and elevation axes:

$$\dot{\psi}_{ref} = K_{P_\psi} e_\psi + K_{I_\psi} \int e_\psi dt + K_{D_\psi} \dot{e}_\psi \tag{4.3}$$

$$\dot{\theta}_{ref} = K_{P_\theta} e_\theta + K_{I_\theta} \int e_\theta dt + K_{D_\theta} \dot{e}_\theta \tag{4.4}$$

where the orientation errors in the azimuth and elevation axes are defined respectively as follows:

$$e_{\psi} = \psi_{ref} - \hat{\psi} \tag{4.5}$$

$$e_{\theta} = \theta_{ref} - \hat{\theta} \tag{4.6}$$

Velocity and current controls are designed as PI controllers for the azimuth and elevation axes. Reference currents for the azimuth and elevation axes are generated as follows:

$$I_{ref_1} = (1 + K_{\beta_1})K_{P_{\dot{\psi}}}e_{\dot{\psi}} + (1 + K_{\beta_1})K_{I_{\dot{\psi}}}\int e_{\dot{\psi}}dt \tag{4.7}$$

$$I_{ref_2} = (1 + K_{\beta_2})K_{P_{\dot{\theta}}}e_{\dot{\theta}} + (1 + K_{\beta_2})K_{I_{\dot{\theta}}}\int e_{\dot{\theta}}dt \tag{4.8}$$

where

$$e_{\dot{\psi}} = \dot{\psi}_{ref} - \hat{\dot{\psi}} \tag{4.9}$$

$$e_{\dot{\theta}} = \dot{\theta}_{ref} - \hat{\dot{\theta}} \tag{4.10}$$

where $e_{\dot{\psi}}$ and $e_{\dot{\theta}}$ represent the velocity errors in the azimuth and elevation axes, respectively. Finally, torque control inputs are designed for the azimuth and elevation axes as follows:

$$\tau_1 = K_{P_1}e_{I_1} + K_{I_1}\int e_{I_1}dt \tag{4.11}$$

$$\tau_2 = K_{P_2}e_{I_2} + K_{I_2}\int e_{I_2}dt \tag{4.12}$$

where the current errors in the azimuth and elevation axes are defined as:

$$e_{I_1} = I_{ref_1} - \hat{I}_1 \tag{4.13}$$

$$e_{I_2} = I_{ref_2} - \hat{I}_2 \tag{4.14}$$

Chapter 5

5 Stabilization Using Acceleration Based LQR Control

This chapter derives a polytopic quasi-LPV model of the pan-tilt system and uses it to synthesize an acceleration based LQR controller. The proposed controller is applied on the nonlinear pan-tilt system for robust stabilization against external disturbances.

5.1 Derivation of the Quasi-LPV Model

Consider a linear parameter varying (LPV) model in the state-space form

$$\begin{aligned} \dot{x}(t) &= A(\sigma(t))x(t) + B(\sigma(t))u(t) \\ y(t) &= C(\sigma(t))x(t) + D(\sigma(t))u(t) \end{aligned} \tag{5.1}$$

where $x \in \mathbb{R}^n$, $u \in \mathbb{R}^{n_u}$ and $y \in \mathbb{R}^{n_y}$. The mappings $A(.)$, $B(.)$, $C(.)$ and $D(.)$ are continuous functions of the time-varying parameter vector $\sigma(t) \in \mathbb{R}^l$. This model can be represented as a linear input-output mapping:

$$P(\sigma) = \begin{bmatrix} A(\sigma) & B(\sigma) \\ C(\sigma) & D(\sigma) \end{bmatrix} \tag{5.2}$$

The parameter vector $\sigma(t)$ depends on measurable quantities

$$\sigma(t) = f(v(t)) \tag{5.3}$$

where $v(t) \in \mathbb{R}^k$ represents *scheduling signals* and $f : \mathbb{R}^k \rightarrow \mathbb{R}^l$ is a continuous mapping. A compact set can be defined as $\mathcal{P}_\sigma \subset R^l : \sigma \in \mathcal{P}_\sigma, \forall t > 0$ [128]. If it is assumed to be a polytope, then $\mathcal{P}_\sigma$ can be represented as the convex hull,

$$\mathcal{P}_\sigma := Co\{\sigma_{v_1}, \sigma_{v_2}, ..., \sigma_{v_L}\} \tag{5.4}$$

where $L = 2^l$ are the total number of vertices. If the state space model depends affinely on the parameters, then the LPV model is called as *parameter-affine*. Thus, $P(\sigma)$ in (5.2) becomes:

$$P(\sigma) = \sum_{i=0}^{l} \sigma_i P_i = P_0 + \sigma_1 P_1 + ... + \sigma_l P_l \tag{5.5}$$

LPV model in (5.6) is called polytopic since it can be represented by a linear combination of LTI models at the vertices. This is the case when (5.5) holds and σ can be expressed as a convex combination of L vertices σ_{v_i}.

$$P(\sigma) = Co\{P(\sigma_{v_1}), P(\sigma_{v_2}), ..., P(\sigma_{v_L})\} = \sum_{i=1}^{L} \alpha_i P(\sigma_{v_i}) \tag{5.6}$$

where $\sum_{i=1}^{L} \alpha_i = 1$, and $\alpha_i \geq 0$ are the convex coordinates. Since the aim is to obtain the quasi-LPV model of the pan-tilt system, (4.1) and (4.2) can be rewritten as:

$$\tau_1 = \left[a + bcosq_2 + ccos^2 q_2\right]\ddot{q}_1 - \left[bsinq_2 + csin2q_2\right]\dot{q}_1\dot{q}_2 \tag{5.7}$$

$$\tau_2 = c\ddot{q}_2 + \left[bsinq_2 + csin2q_2\right]\frac{\dot{q}_1^2}{2} + dcosq_2 \tag{5.8}$$

where a, b, c and d represent dynamic and kinematic parameters:

$$a = \frac{1}{2}m_1 l_1^2 + m_2 l_1^2, \quad b = m_2 l_1 l_2 \tag{5.9}$$

$$c = \frac{1}{3}m_2 l_2^2, \quad d = \frac{1}{2}m_2 g l_2 \tag{5.10}$$

From (5.7) and (5.8), $\ddot{q}_1$ and $\ddot{q}_2$ are calculated as follows:

$$\ddot{q}_1 = \frac{\tau_1 + \left[bsinq_2 + csin2q_2\right]\dot{q}_1\dot{q}_2}{a + bcosq_2 + ccos^2 q_2} \tag{5.11}$$

$$\ddot{q}_2 = \frac{\tau_2 - \left[bsinq_2 + csin2q_2\right]\frac{\dot{q}_1^2}{2} - dcosq_2}{c} \tag{5.12}$$

To construct the nonlinear dynamics given by (5.11) and (5.12) in the state-space form, the state vector is designed as:

$$x(t) = \begin{bmatrix} q_1 & q_2 & \dot{q}_1 & \dot{q}_2 \end{bmatrix}^T \tag{5.13}$$

where $x(t) \in R^4$. The polytopic quasi-LPV model of the pan-tilt system is derived by employing the ideas in [84]. Thus, the scheduling vector can be selected as the state vector of the system:

$$v(t) \triangleq x(t) = \begin{bmatrix} q_1 & q_2 & \dot{q}_1 & \dot{q}_2 \end{bmatrix}^T \tag{5.14}$$

By using the assumption in (5.14) and defining $h = a + b\cos q_2 + c\cos^2 q_2$, the polytopic quasi-LPV model of the pan-tilt system is computed from (5.11) and (5.12) as follows:

$$A = \begin{bmatrix} 0 & 0 & 1 & 0 \\ 0 & 0 & 0 & 1 \\ 0 & 0 & 0 & \sigma_1 \\ 0 & \sigma_2 & \sigma_3 & 0 \end{bmatrix}, \quad B = \begin{bmatrix} 0 & 0 \\ 0 & 0 \\ \sigma_4 & 0 \\ 0 & \frac{1}{c} \end{bmatrix},$$

$$C = \begin{bmatrix} I_{2\times 2} & 0_{2\times 2} \end{bmatrix}, \quad \text{and} \quad D = 0_{2\times 2} \tag{5.15}$$

where

$$\sigma_1 = \frac{(b\sin q_2 + c\sin 2q_2)\dot{q}_1}{h}$$

$$\sigma_2 = -\frac{d}{c}\frac{\cos q_2}{q_2}$$

$$\sigma_3 = -\frac{1}{2c}(b\sin q_2 + c\sin 2q_2)\dot{q}_1$$

$$\sigma_4 = \frac{1}{h} \tag{5.16}$$

with I and 0 being the identity and zero matrices, and $\sigma(t) \in R^4$. This model development appeared in [129].

In this thesis, the state vector, $x(t)$, is augmented to include the integral of the position errors to eliminate the steady state error. A new extended state vector, $z \in \mathbb{R}^6$, is designed as follows:

$$z = \begin{bmatrix} q_1 & q_2 & \dot{q}_1 & \dot{q}_2 & \int \big(r_1 - q_1\big)dt & \int \big(r_2 - q_2\big)dt \end{bmatrix}^T \tag{5.17}$$

where the desired joint angles are denoted by $r = \begin{bmatrix} r_1 & r_2 \end{bmatrix}^T \in \mathbb{R}^2$. In accordance with the new state vector in (5.17), an extended polytopic quasi-LPV model is designed as follows:

$$\dot{z}(t) = E(\sigma(t))z(t) + F(\sigma(t))u(t) + Hr(t)$$

$$y(t) = G(\sigma(t))z(t) + P(\sigma(t))u(t) \tag{5.18}$$

where

$$E = \begin{bmatrix} 0 & 0 & 1 & 0 & 0 & 0 \\ 0 & 0 & 0 & 1 & 0 & 0 \\ 0 & 0 & 0 & \sigma_1 & 0 & 0 \\ 0 & \sigma_2 & \sigma_3 & 0 & 0 & 0 \\ -1 & 0 & 0 & 0 & 0 & 0 \\ 0 & -1 & 0 & 0 & 0 & 0 \end{bmatrix}, \quad F = \begin{bmatrix} 0 & 0 \\ 0 & 0 \\ \sigma_4 & 0 \\ 0 & \frac{1}{c} \\ 0 & 0 \\ 0 & 0 \end{bmatrix},$$

$$H = \begin{bmatrix} 0_{4\times2} & I_{2\times2} \end{bmatrix}^T, \quad G = \begin{bmatrix} I_{2\times2} & 0_{2\times4} \end{bmatrix}, \quad P = 0_{2\times2} \tag{5.19}$$

and $u \in \mathbb{R}^2$ defines the control input, $y \in \mathbb{R}^2$ is the output. The system matrices $E(.)$ and $F(.)$ depend on the time varying parameter vector, $\sigma(t) \in \mathbb{R}^4$ obtained in (5.16).

Next section employs the extended polytopic quasi-LPV model given by (5.18) and (5.19) to synhesize the classical LMI-LQR controller and an acceleration based LMI-LQR controller.

5.2 LQR Synthesis Based on the Extended LPV Model

This section designs the classical LMI-LQR controller and an acceleration based LMI-LQR controller on the proposed LPV model given by (5.18) and (5.19). These controllers are used to stabilize the nonlinear pan-tilt system given by (4.1) and (4.2) against external disturbances. The aim is to increase dynamic stiffness of the pan-tilt system by incorporating acceleration feedback into the LMI-LQR controller. The performance of the developed controller is compared with the classical LMI based LQR controller in Chapter 7. The classical LQR controller is designed as

$$u_1 = Kz \tag{5.20}$$

that minimizes the following cost function:

$$J_1 = \int \left(z^T Q z + u_1^T R u_1 \right) dt \tag{5.21}$$

where $K \in \mathbb{R}^{2\times6}$ is the feedback gain matrix, $Q \in \mathbb{R}^{6\times6}$ and $R \in \mathbb{R}^{2\times2}$ are the state and control input weighting matrices. These matrices are symmetric and positive-definite, i.e. $Q > 0$ and $R > 0$. K is obtained by solving the following semidefinite programming problem:

$$\min \operatorname{tr}(P) \tag{5.22}$$

subject to

$$(E + FK)^T P + P(E + FK) \leq -Q - K^T R K \tag{5.23}$$

where $P \in \mathbb{R}^{6\times6} > 0$ is the Lyapunov matrix and tr denotes the trace. The non-convex optimization problem in (5.22)-(5.23) can be converted into a convex problem by multiplying left and right side of (5.23) with P^{-1} and applying Schur Complement [130]:

$$\max \operatorname{tr}(Y) \tag{5.24}$$

subject to

$$\begin{bmatrix} -(E+FK)-(E+FK)^T & Y & L^T \\ Y & Q^{-1} & 0_{6\times2} \\ L & 0_{2\times6} & R^{-1} \end{bmatrix} \geq 0 \tag{5.25}$$

and

$$Y = P^{-1} > 0 \tag{5.26}$$

where $L \in \mathbb{R}^{2\times6}$ is introduced as $L = KY$ and $Y \in \mathbb{R}^{6\times6}$ is the inverse of the Lyapunov matrix, $Y = P^{-1}$. The feedback matrix can be recovered as:

$$K = LY^{-1} \tag{5.27}$$

An acceleration based linear state feedback law is proposed as

$$u_2 = K_1 z + K_2 \dot{z} \tag{5.28}$$

where K_1, $K_2 \in \mathbb{R}^{2\times6}$ are the feedback gain matrices which will be designed by minimizing the following cost function:

$$J_2 = \int \left(z^T Q_1 z + \dot{z}^T Q_2 \dot{z} + u_2^T R u_2 \right) dt \tag{5.29}$$

where the cost function in (5.21) is modified such that acceleration signals are also included in the new cost function, J_2. $Q_2 > 0 \in \mathbb{R}^{6\times6}$ is a symmetric positive definite matrix that penalizes the derivative of the state vector. The overall control system is presented in Figure 9. Utilization of both z and $\dot{z}$ leads to redundancy in terms of position and velocity in the controller formulation given by (5.28). In this work, this redundancy is reduced by selecting smaller weights in Q_2 corresponding to velocity terms in $\dot{z}$.

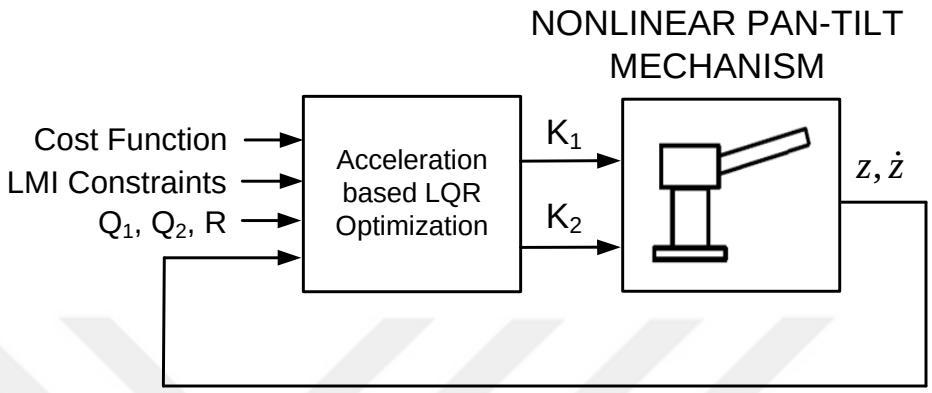

Figure 9: Control block diagram

The controller in (5.28) is designed by solving the following semidefinite programming problem:

$$\min\Big(\mathrm{tr}(P_1) + \mathrm{tr}(P_2)\Big) \tag{5.30}$$

subject to

$$(E + FK_1)^T P_1 + P_1(E + FK_1) \leq -Q_1 - K_1^T R K_1 \tag{5.31}$$

$$(E + FK_2)^T P_2 + P_2(E + FK_2) \leq -Q_2 - K_2^T R K_2 \tag{5.32}$$

where $P_1 \in \mathbb{R}^{6\times 6} > 0$ and $P_2 \in \mathbb{R}^{6\times 6} > 0$ are the Lyapunov matrices, and there exists a first-order, differentiable, positive-definite function $V(t) \in \mathbb{R}$ such that

$$\begin{aligned}\dot{V}(t) \leq & - z^T Q_1 z - \dot{z}^T Q_2 \dot{z} - u_2^T R u_2 + 2\dot{z}^T K_2^T F P_1 z \\ & + 2r^T H^T P_1 z + 2z^T K_1^T R K_2 \dot{z} \\ & - \dot{z}^T \Big[(E + FK_2)^T P_2 + P_2(E + FK_2)\Big]\dot{z}\end{aligned} \tag{5.33}$$

Proof: A Lyapunov function candidate, $V(t)$ is defined as

$$V = z^T P_1 z \tag{5.34}$$

The following expression is computed by taking the time derivative of (5.34), and using (5.18) and (5.33):

$$\begin{aligned}& z^T\Big[(E + FK_1)^T P_1 + P_1(E + FK_1)\Big]z + \dot{z}^T\Big[(E + FK_2)^T P_2 \\ & + P_2(E + FK_2)\Big]\dot{z} \leq -z^T Q_1 z - \dot{z}^T Q_2 \dot{z} - u_2^T R u_2 \\ & + 2z^T K_1^T R K_2 \dot{z}\end{aligned} \tag{5.35}$$

By substituting (5.28) into (5.35) and performing cancellations, one obtains

$$\begin{aligned} z^T\Big[(E+FK_1)^TP_1+P_1(E+FK_1)\Big]z+\dot{z}^T\Big[(E+FK_2)^TP_2 \\ +P_2(E+FK_2)\Big]\dot{z}\leq -z^T(Q_1+K_1^TRK_1)z \\ -\dot{z}^T(Q_2+K_2^TRK_2)\dot{z} \end{aligned} \tag{5.36}$$

The following constraints are derived in order to satisfy the inequality in (5.35):

$$(E+FK_1)^TP_1+P_1(E+FK_1)\leq -Q_1-K_1^TRK_1 \tag{5.37}$$

$$(E+FK_2)^TP_2+P_2(E+FK_2)\leq -Q_2-K_3^TRK_2 \tag{5.38}$$

(5.30)-(5.32) is a non-convex optimization problem. It can be converted into a convex problem by multiplying left and right side of (5.31)-(5.32) with P_1^{-1} and P_2^{-1}, and applying Schur Complement [130]:

$$\max\Big(\mathrm{tr}(Y_1)+\mathrm{tr}(Y_2)\Big) \tag{5.39}$$

subject to

$$\begin{bmatrix} -(E+FK_1)-(E+FK_1)^T & Y_1 & L_1^T \\ Y_1 & Q_1^{-1} & 0_{6\times 2} \\ L_1 & 0_{2\times 6} & R^{-1} \end{bmatrix}\geq 0 \tag{5.40}$$

$$\begin{bmatrix} -(E+FK_2)-(E+FK_2)^T & Y_2 & L_2^T \\ Y_2 & Q_2^{-1} & 0_{6\times 2} \\ L_2 & 0_{2\times 6} & R^{-1} \end{bmatrix}\geq 0 \tag{5.41}$$

and

$$Y_1=P_1^{-1}>0,\quad Y_2=P_2^{-1}>0 \tag{5.42}$$

where $L_1L_2\in\mathbb{R}^{2\times 6}$ and $L_2\in\mathbb{R}^{2\times 6}$ are defined as $L_1=K_1Y_1$ and $L_2=K_2Y_2$. $Y_1\in\mathbb{R}^{6\times 6}$ and $Y_2\in\mathbb{R}^{6\times 6}$ are the inverses of the Lyapunov matrices, $Y_1=P_1^{-1}$ and $Y_2=P_2^{-1}$. The controller matrices, K_1 and K_2 are recovered as:

$$K_1=L_1Y_1^{-1} \tag{5.43}$$

$$K_2=L_2Y_2^{-1} \tag{5.44}$$

The robust control toolbox YALMIP [131] is used to design the classical LMI based LQR controller and the proposed controller.

Chapter 6

6 Periodic Trajectory Tracking Using Hybrid Acceleration Based Learning-Adaptive Control

This chapter develops nonlinear controllers for robust periodic trajectory tracking problem where parametric uncertainties and unknown periodic dynamics are considered. The closed-loop stability proofs are provided.

6.1 Adaptive Controller with Acceleration Feedback

The nonlinear dynamical model of a n-rigid link robot with the actuator dynamics are obtained as follows [132]:

$$M(q)\ddot{q} + C(q,\dot{q})\dot{q} + F_v\dot{q} + F_s sgn(\dot{q}) + G(q) = \tau \tag{6.1}$$

where $M(q) \in \mathbb{R}^{n\times n}$ denotes the symmetric and positive-definite inertia matrix, and $M(q) \triangleq D(q) + J$. $D(q)$ and J are the robot and actuator inertia matrices. $C(q,\dot{q}) \in \mathbb{R}^{n\times n}$ is the centripetal-Coriolis matrix, $F_v \in \mathbb{R}^{n\times n}$ and $F_s \in \mathbb{R}^{n\times n}$ are constant, diagonal, positive-definite, viscous and static friction coefficient matrices, $sgn(\dot{q})$ is the signum function applied to the link velocities, and $G(q) \in \mathbb{R}^n$ is the gravity vector.

Some dynamical parameters in (6.1) can change unpredictably due to variations in the environmental conditions. This problem may also occur because the system parameters are slowly time-varying. Unmeasurable changes of the process parameters lead to unsatisfactory control performance. An adaptive controller adjusts itself to tackle unknown parameter uncertainties. Large variations generally occur in static friction coefficients. Thus, the adaptive controller uses the linear parametrization property given by (6.2).

Property 1: Linearity in the Static Friction Parameters

Due to large variations in static friction coefficients of the robotic dynamics, the static friction terms in (6.1) can also be linearly parameterized as

$$F_s sgn(\dot{q}) = W_1(\dot{q})\Phi_1 \tag{6.2}$$

where $\Phi_1 \in \mathbb{R}^n$ is the unknown constant static friction coefficients and $W_1(\dot{q}) \in \mathbb{R}^{n\times n}$ is the known regression matrix. The regression matrix, $W_1(\dot{q})$, includes known functions of the velocities.

According to data presented in [133], large variations occur in both motor inertias and static friction coefficients for some robotic manipulators. This motivates us to modify the unknown parameter vector, Φ_1, to include both motor moment of inertia terms and static friction coefficients. To illustrate this, a new linear parametrization property in (6.3) is defined.

Property 2: Linearity in the Motor Moment of Inertia and Static Friction Parameters

The motor moment of inertia terms and static friction coefficients in (6.1) can be linearly parameterized as

$$J\ddot{q} + F_s sgn(\dot{q}) = W_2(\dot{q}, \ddot{q})\Phi_2 \tag{6.3}$$

where unknown parameter vector, $\Phi_2 \in \mathbb{R}^{2n}$, consists of motor moment of inertia terms and static friction coefficients. Regression matrix, $W_2(\dot{q}, \ddot{q}) \in \mathbb{R}^{n\times 2n}$, includes both known velocities and accelerations. Using the new parametrization property in (6.3), the robot dynamics given by (6.1) can be rewritten as follows:

$$D(q)\ddot{q} + C(q, \dot{q})\dot{q} + F_v\dot{q} + G(q) + W_2(\dot{q}, \ddot{q})\Phi_2 = \tau \tag{6.4}$$

The subsequent subsections develop the control input, $\tau(t)$, and provide the closed-loop stability proof.

6.1.1 Controller Design

The control objective is to design the torque control input signal, $\tau(t)$, such that desired trajectories will be converged despite the parameter uncertainties in the dynamics of the robotic manipulator given by (6.4). The position tracking error, denoted by $e(t) \in \mathbb{R}^n$, is defined as follows:

$$e = q_d - q \tag{6.5}$$

where $q_d(t) \in \mathbb{R}^n$ is the desired link position. The control objective is based on the assumption that $q(t)$, $\dot{q}(t)$ and $\ddot{q}(t)$ are measurable, and the desired joint positions, velocities and accelerations are bounded. To facilitate the subsequent control development and stability analysis, the order of the robot dynamics given by (6.4) is reduced by defining a filtered tracking error variable, $r_a(t) \in \mathbb{R}^n$ as follows:

$$r_a = \dot{e} + \Gamma_a e \tag{6.6}$$

where $\dot{e}(t) \in \mathbb{R}^n$ is the joint velocity error, i.e. $\dot{e} \triangleq \dot{q}_d - \dot{q}$, and $\Gamma_a \in \mathbb{R}^{n\times n}$ is a constant, diagonal and positive-definite controller gain matrix. After taking the time derivative of (6.6), multiplying the resulting expression by the inertia matrix, $D(q)$, the open loop error system is obtained as

$$D(q)\dot{r}_a = D(q)(\ddot{q}_d + \Gamma_a\dot{e}) + C(q,\dot{q})\dot{q} + F_v\dot{q} + G(q) + W_2(\dot{q},\ddot{q})\Phi_2 - \tau \tag{6.7}$$

Based on (6.7) and the subsequent closed loop stability analysis, the proposed adaptive controller with acceleration feedback is designed as follows:

$$\tau = D(q)(\ddot{q}_d + \Gamma_a\dot{e}) + C(q,\dot{q})\dot{q}_d + F_v\dot{q}_d + G(q) + \tau_a + \Lambda_a e \tag{6.8}$$

where acceleration feedback is incorporated into the regression matrix as

$$\tau_a = W_2(\dot{q},\ddot{q})\hat{\Phi}_2 \tag{6.9}$$

and $\Lambda_a \in \mathbb{R}^{n\times n}$ is a constant, diagonal and positive-definite controller gain matrix. $\hat{\Phi}_2(t) \in \mathbb{R}^{2n}$ is an estimate of Φ_2, and updated based on the following adaptive law:

$$\dot{\hat{\Phi}}_2 = \Upsilon_a W_2^T(\dot{q},\ddot{q})r_a \tag{6.10}$$

with a constant, diagonal and positive-definite adaptation gain matrix, $\Upsilon_a \in \mathbb{R}^{2n\times 2n}$. Note that Craig et al. [134] developed adaptive inverse dynamics approach where joint accelerations are augmented into the regression matrix besides link velocities.

In the proposed controller development (6.8)-(6.10), except for motor moment of inertias and static friction parameters, it is assumed that the real system parameters are precisely known which is not possible in practice. For the case where all the real system parameters are unknown, the proposed adaptive controller is integrated with the designed learning controller in Section 6.3. Readers are referred to Section 6.3 for the hybrid control development with unknown system parameters.

When (6.8) is substituted into (6.7), the closed-loop error system for $r_a(t)$ is obtained as

$$D(q)\dot{r}_a = W_2(\dot{q},\ddot{q})\tilde{\Phi}_2 - C(q,\dot{q})\dot{e} - F_v\dot{e} - \Lambda_a e \tag{6.11}$$

where $\tilde{\Phi}_2(t) \in \mathbb{R}^{2n}$ is the parameter estimation error:

$$\tilde{\Phi}_2 = \Phi_2 - \hat{\Phi}_2 \tag{6.12}$$

6.1.2 Closed-Loop Stability Analysis

Theorem 1: The proposed controller developed in (6.8)-(6.10) can asymptotically drive the position error to zero, i.e.;

$$\lim_{t\to\infty} e(t) = 0 \tag{6.13}$$

if there exists a first-order differentiable, positive-definite function $V_1(e, \dot{e}, r_a, t) \in \mathbb{R}$ such that

$$\dot{V}_1 \leq -e^T \Gamma_a e + r_a^T \left(C(q, \dot{q}) + F_v \right) \dot{e} \tag{6.14}$$

Proof: To prove the conclusion of Theorem 1, a Lyapunov function candidate, $V_2(t)$ is defined as

$$V_2 = V_1 + \frac{r_a^T D r_a}{2} + \frac{\tilde{\Phi}_2^T \Upsilon_a^{-1} \tilde{\Phi}_2}{2} \tag{6.15}$$

The following is obtained by taking the time derivative of (6.15), and using the assumption in (6.14):

$$\dot{V}_2 \leq r_a^T D \dot{r}_a - e^T \Gamma_a e + r^T \left(C(q, \dot{q}) + F_v \right) \dot{e} + \tilde{\Phi}_2^T \Upsilon_a^{-1} \dot{\tilde{\Phi}}_2 \tag{6.16}$$

By substituting (6.10) and (6.11) into (6.16), it follows that:

$$\dot{V}_2 \leq -e^T \Gamma_a e - r_a^T \Lambda_a e \tag{6.17}$$

(6.17) can be simplified as:

$$\dot{V}_2 \leq -e^T \Gamma_a e \tag{6.18}$$

Signal Chasing: Based on (6.15) and (6.18), and using the positive-definite symmetric matrix Γ_a, it can be concluded that $V_2(t) \in \mathcal{L}_\infty$. It is observed that $r_a(t)$, $\tilde{\Phi}_2(t) \in \mathcal{L}_\infty$ since the signals in $V_2(t)$ given by (6.15) must remain bounded. The boundedness of $r_a(t)$ implies $e(t), \dot{e}(t) \in \mathcal{L}_\infty$ based on (6.6). Using Lemma 1 given in Appendix B, one obtains that

$$\|e\| = \sqrt{\int_0^\infty e^2(t) dt} < \infty \tag{6.19}$$

where $\| \cdot \|$ denotes 2-norm. Definition 1 provided in Appendix B is utilized to conclude that $e(t) \in \mathcal{L}_2$. Barbalat's Lemma which is presented in Appendix B implies (6.13) in Theorem 1 because $e(t), \dot{e}(t) \in \mathcal{L}_\infty$ and $e(t) \in \mathcal{L}_2$.

Using (6.5), the relationship $\dot{e} = \dot{q}_d - \dot{q}$, and the boundedness of $e(t), \dot{e}(t)$, it follows that $q(t), \dot{q}(t) \in \mathcal{L}_\infty$. Since $\Phi_2(t)$ represents bounded motor inertias and static friction coefficients, and $\tilde{\Phi}_2(t) \in \mathcal{L}_\infty$, it follows from (6.12) that $\hat{\Phi}_2(t) \in \mathcal{L}_\infty$.

6.2 Learning Controller with Acceleration Feedback for A General Error System

Learning controllers have been developed to compensate for the unknown nonlinear periodic dynamics with a known period. In this section, a standard learning controller which is utilized for a typical error system in the literature is reviewed.

Then, this learning controller is modified with acceleration feedback, and the use of new learning controller for a typical error system is shown with the closed loop stability analysis. Consider the system

$$\dot{x} = -f(x) + u \tag{6.20}$$

where $x \in \mathbb{R}$ is the state and $u \in \mathbb{R}$ is the control input. $f : \mathbb{R} \to \mathbb{R}$ represents a nonlinear function mapping. State error, $\varepsilon \in \mathbb{R}$, is defined as:

$$\varepsilon = x_d - x \tag{6.21}$$

with the desired state, $x_d \in \mathbb{R}$, and it follows that

$$\dot{\varepsilon} = \dot{x}_d - \dot{x} \tag{6.22}$$

By substituting (6.20) into (6.22), the open loop error dynamics is obtained as

$$\dot{\varepsilon} = \dot{x}_d + f(x) - u \tag{6.23}$$

Since unknown nonlinear dynamics, $f(x)$, are assumed to be periodic for learning control, we can obtain

$$f(x(t)) = f(x(t+T)) \tag{6.24}$$

for a known period, T. $f(x(t))$ can be considered as periodic disturbances, and so (6.23) can be rewritten as:

$$\dot{\varepsilon} = \dot{x}_d + d(t) - u \tag{6.25}$$

with the periodic disturbance, $d(t) \in \mathbb{R}$, i.e. $d(t) = d(t+T)$. The controller is designed as follows:

$$u = \dot{x}_d + k_\varepsilon \varepsilon + \hat{d}(t) \tag{6.26}$$

where $k_\varepsilon \in \mathbb{R}$ is positive constant control gain and $\hat{d}(t) \in \mathbb{R}$ is a learning based estimate of $d(t)$. Then, the closed loop error dynamics are derived by substituting (6.26) into (6.25):

$$\dot{\varepsilon} = -k\varepsilon + d(t) - \hat{d}(t) \tag{6.27}$$

The goal is to design $\hat{d}(t)$ in (6.27). The repetitive update law for the system in (6.27) is usually developed as:

$$\hat{d}(t) = \hat{d}(t-T) + k_1 \varepsilon \tag{6.28}$$

with a positive control gain, $k_1 \in \mathbb{R}$. It is mentioned in [98] that $\hat{d}(t) \in \mathcal{L}_\infty$ cannot be satisfied when $\hat{d}(t)$ is updated by (6.28). Sadegh et al. [135] solved this boundedness problem by saturating the entire right-hand side of (6.28) as follows:

$$\hat{d}(t) = sat(\hat{d}(t-T) + k_1 \varepsilon) \tag{6.29}$$

where $sat(\cdot)$ denotes the standard linear piecewise bounded saturation function. The update law in (6.29) guarantees that $\hat{d}(t)$ is bounded for all time. However, Dixon et al. [99] stated that the effect of saturation function on the stability is not clearly analyzed in [135] using the Lyapunov theory. Therefore, the following update law is developed in [99]:

$$\hat{d}(t) = sat(\hat{d}(t-T)) + k_1\varepsilon \tag{6.30}$$

where the error term on the right-hand side of the general repetitive update law given by (6.28) is not saturated. The update law in (6.30) guarantees $\hat{d}(t) \in \mathcal{L}_\infty$, and provides how Lyapunov-based stability analysis comply with the use of saturation function.

In this thesis, acceleration feedback is incorporated into the repetitive update law given by (6.30) to increase the robustness of the system exposed to periodic disturbances. The proposed repetitive update law is designed as follows:

$$\hat{d}(t) = sat(\hat{d}(t-T)) + k_1\lambda + k_2\ddot{\varepsilon} \tag{6.31}$$

where the filtered tracking error, $\lambda \in \mathbb{R}$, is defined as:

$$\lambda = \dot{\varepsilon} + k_3\varepsilon \tag{6.32}$$

with a positive constant gain, $k_3 \in \mathbb{R}$.

The proposed learning controller given in (6.31)-(6.32) achieves globally asymptotically tracking for a typical error system with unknown periodic disturbances. To illustrate this, the following first-order error dynamics are obtained as [100]:

$$\dot{e} = h(t,e) + G(t,e)\left[\nu(t) - \hat{\nu}(t)\right] \tag{6.33}$$

where $e(t) \in \mathbb{R}^n$ is the error, $\nu(t) \in \mathbb{R}^m$ is an unknown nonlinear function, $\hat{\nu}(t) \in \mathbb{R}^m$ is designed learning based estimate of $\nu(t)$, and the auxiliary functions $h(t,e) \in \mathbb{R}^n$ and $G(t,e) \in \mathbb{R}^{n\times m}$ are bounded provided that $e(t)$ is bounded.

Assumption 1: Asymptotic Stability

The origin of the error system $e(t) = 0$ is uniformly asymptotically stable for

$$\dot{e} = h(t,e) \tag{6.34}$$

and there exists a first-order differentiable positive-definite function $V_3(e,\ddot{e},s,t) \in \mathbb{R}$, positive-definite symmetric matrix $Q_3 \in \mathbb{R}^{n\times n}$, and known matrices $\mathcal{K}_1$, $\mathcal{K}_2 \in \mathbb{R}^{m\times n}$ such that

$$\dot{V}_3 \leq -e^T Q_3 e + (\nu - \hat{\nu})^T \mathcal{K}_1 s + (\nu - \hat{\nu})^T \mathcal{K}_2 \ddot{e} + s^T \mathcal{K}_1^T \mathcal{K}_2 \ddot{e} \tag{6.35}$$

where the filtered tracking error variable, $s \in \mathbb{R}^n$, is defined as:

$$s = \dot{e} + \mathcal{K}_3 e \tag{6.36}$$

for a constant, diagonal, positive-definite, controller gain matrix, $\mathcal{K}_3 \in \mathbb{R}^{n \times n}$.

Assumption 2: Periodicity and Boundedness

The unknown nonlinear disturbance, $\nu(t)$ is periodic with a known period, T. Thus,

$$\nu(t) = \nu(t - T) \tag{6.37}$$

An upper bound also exists for the unknown function as follows:

$$|\nu_i| \leq \pi_i \quad \text{for} \quad i = 1, 2, ..., m \tag{6.38}$$

where $\pi_i = \begin{bmatrix} \pi_1 & ... & \pi_m \end{bmatrix} \in \mathbb{R}^m$ is a vector of known, positive bounding constants.

6.2.1 Controller Design

The control objective for the general error problem given in (6.33) is to design a learning based estimate, $\hat{\nu}(t)$, such that

$$\lim_{t \to \infty} e(t) = 0 \tag{6.39}$$

for any bounded initial condition, $e(0)$. Estimation error is defined as:

$$\tilde{\nu}(t) = \nu(t) - \hat{\nu}(t) \tag{6.40}$$

where the learning based feedforward term is designed as:

$$\hat{\nu}(t) = sat_{\pi}(\hat{\nu}(t - T)) + \mathcal{K}_1 s + \mathcal{K}_2 \ddot{e} \tag{6.41}$$

using the error dynamics in (6.33) and the subsequent stability analysis. $sat_{\pi}(\cdot)$ denotes the saturation function and it is obtained using the known, positive bounding constants given by (6.38):

$$sat_{\pi_i}(\omega_i) = \begin{cases} \pi_i, & \omega_i \geq \pi_i \\ \omega_i, & -\pi_i < \omega_i < \pi_i \\ -\pi_i, & \omega_i \leq -\pi_i \end{cases} \tag{6.42}$$

with $\forall \omega_i \in \mathbb{R}, i = 1, 2, .., m$. In light of (6.42), the following inequality will be utilized in the subsequent stability analysis:

$$(\omega_{1i} - \omega_{2i})^2 \geq (sat_{\alpha_i}(\omega_{1i}) - sat_{\pi_i}(\omega_{2i}))^2 \tag{6.43}$$

where $\forall|\varpi_{1i}| \leq \pi_i, \varpi_{1i} \in \mathbb{R}, i = 1, 2, ..., m$. Note that the update law given in (6.41) has the same structure with (6.31). In light of the Assumption 2 and (6.42), the following relationship is derived:

$$\nu(t) = sat_{\pi}(\nu(t)) = sat_{\pi}\left(\nu(t-T)\right) \tag{6.44}$$

$\tilde{\nu}(t)$ is obtained by substituting (6.41) and (6.44) into (6.40):

$$\tilde{\nu} = sat_{\pi}\left(\nu(t-T)\right) - sat_{\pi}(\hat{\nu}(t-T)) - \mathcal{K}_1 s - \mathcal{K}_2 \ddot{e} \tag{6.45}$$

It should be noted that the learning based feedforward term given in (6.41) is bounded for all time, i.e. $\hat{\nu}(t) \in \mathcal{L}_{\infty}$, provided that $\ddot{e}(t), s(t) \in \mathcal{L}_{\infty}$.

6.2.2 Closed-Loop Stability Analysis

Theorem 1: The proposed learning controller developed in (6.41) ensures that

$$\lim_{t\to\infty} e(t) = 0 \tag{6.46}$$

for any bounded initial condition, $e(0)$.

Proof: To prove the conclusion of Theorem 1, a Lyapunov function candidate, $V_4(t)$ is defined as

$$V_4 = V_3 + \frac{1}{2}\int_{t-T}^{t} \Big(sat_{\pi}\nu(\phi) - sat_{\pi}\hat{\nu}(\phi)\Big)^T \Big(sat_{\pi}\nu(\phi) - sat_{\pi}\hat{\nu}(\phi)\Big) d\phi \tag{6.47}$$

Taking the time derivative of (6.47), and using the Leibniz's Rule provided in Appendix B and the assumption given in (6.35) yields

$$\begin{aligned}
\dot{V}_4 \leq & -e^T Q_3 e + (\nu - \hat{\nu})^T \mathcal{K}_1 s + (\nu - \hat{\nu})^T \mathcal{K}_2 \ddot{e} + s^T \mathcal{K}_1^T \mathcal{K}_2 \ddot{e} \\
& - \frac{1}{2}\Big[\Big(sat_{\alpha}\vartheta(t-T) - sat_{\alpha}\hat{\vartheta}(t-T)\Big)^T \Big(sat_{\alpha}\vartheta(t-T) - sat_{\alpha}\hat{\vartheta}(t-T)\Big)\Big] \\
& + \frac{1}{2}\Big[\Big(sat_{\alpha}\vartheta(t) - sat_{\alpha}\hat{\vartheta}(t)\Big)^T \Big(sat_{\alpha}\vartheta(t) - sat_{\alpha}\hat{\vartheta}(t)\Big)\Big]
\end{aligned} \tag{6.48}$$

Using (6.45), (6.48) can be observed as follows:

$$\begin{aligned}
\dot{V}_4 \leq & -e^T Q_3 e + (\nu - \hat{\nu})^T \mathcal{K}_1 s + (\nu - \hat{\nu})^T \mathcal{K}_2 \ddot{e} + s^T \mathcal{K}_1^T \mathcal{K}_2 \ddot{e} \\
& + \frac{1}{2}\Big[\Big(sat_{\alpha}\vartheta(t) - sat_{\alpha}\hat{\vartheta}(t)\Big)^T \Big(sat_{\alpha}\vartheta(t) - sat_{\alpha}\hat{\vartheta}(t)\Big)\Big] \\
& - \frac{1}{2}\Big[\Big(\tilde{\nu} + \mathcal{K}_1 s + \mathcal{K}_2 \ddot{e}\Big)^T \Big(\tilde{\nu} + \mathcal{K}_1 s + \mathcal{K}_2 \ddot{e}\Big)\Big]
\end{aligned} \tag{6.49}$$

By expanding the last line of (6.49), and performing cancellations, it is obtained that:

$$\begin{aligned}\dot{V}_4 \leq & -e^T Q_3 e - s^T \frac{\mathcal{K}_1^T \mathcal{K}_1}{2} s - \ddot{e}^T \frac{\mathcal{K}_2^T \mathcal{K}_2}{2} \ddot{e} \\ & + \frac{1}{2}\left[\left\| sat_\pi \nu(t) - sat_\pi \hat{\nu}(t) \right\|^2 - \left\| \nu(t) - \hat{\nu}(t) \right\|^2\right]\end{aligned} \tag{6.50}$$

(6.50) can be rewritten by exploiting the property given in (6.43):

$$\dot{V}_4 \leq -e^T Q_3 e - s^T \frac{\mathcal{K}_1^T \mathcal{K}_1}{2} s - \ddot{e}^T \frac{\mathcal{K}_2^T \mathcal{K}_2}{2} \ddot{e} \tag{6.51}$$

(6.51) can be simplified as follows:

$$\dot{V}_4 \leq -\left[\min\left(\|Q_3\|, \left\|\frac{\mathcal{K}_1^T \mathcal{K}_1}{2}\right\|, \left\|\frac{\mathcal{K}_2^T \mathcal{K}_2}{2}\right\|\right)\right]\|Y\|^2 \tag{6.52}$$

where an auxiliary signal, $Y(t) \in \mathbb{R}^{3n}$, is defined as

$$Y = \begin{bmatrix} e^T & s^T & \ddot{e}^T \end{bmatrix}^T \tag{6.53}$$

Signal Chasing: Based on (6.47) and (6.52), and using the positive-definite symmetric matrix Q_3, it can be obtained that $V_4(t) \in \mathcal{L}_\infty$. Utilizing Lemma 1 given in Appendix B, it can be observed that

$$\|Y\| = \sqrt{\int_0^\infty Y^2(t) dt} < \infty \tag{6.54}$$

and this implies $Y(t) \in \mathcal{L}_2$ based on Definition 1 given in Appendix B.

Property 3: Equivalent p-Norms

All p-norms are equivalent in the sense that if $\|\cdot\|_\alpha$ and $\|\cdot\|_\beta$ are two different p-norms, then there exists positive constants c_1 and c_2 such that

$$c_1\|y\|_\alpha \leq \|y\|_\beta \leq c_2\|y\|_\alpha \tag{6.55}$$

for all $y \in \mathbb{R}^n$. For $\mathcal{L}_1$, $\mathcal{L}_2$, and $\mathcal{L}_\infty$ norms, these inequalities take the following forms

$$\begin{gathered}\|y\| \leq \|y\|_1 \leq \sqrt{n}\|y\|, \quad \|y\|_\infty \leq \|y\| \leq \sqrt{n}\|y\|_\infty, \\ \text{and} \quad \|y\|_\infty \leq \|y\|_1 \leq n\|y\|_\infty\end{gathered} \tag{6.56}$$

where $\|\cdot\|_1$ and $\|\cdot\|_\infty$ represent 1-norm and ∞-norm, respectively.

(6.55) and (6.56) imply that $\|Y\|_\infty \leq \|Y\|$. Using $\|Y\| < \infty$ in (6.54), it can be obtained that $\|Y\|_\infty \leq \|Y\| < \infty$, and so $\|Y\|_\infty < \infty$. Based on Definition 2 presented in Appendix B, $\|Y\|_\infty = \sup|Y(t)| < \infty$ is observed, and it is concluded that $Y(t) \in \mathcal{L}_\infty$. Thus, $Y(t) \in \mathcal{L}_2 \cap \mathcal{L}_\infty$. It is observed that $e(t), \ddot{e}(t), s(t) \in \mathcal{L}_2 \cap \mathcal{L}_\infty$ because the signals in $Y(t)$ given by (6.53) must remain bounded.

Utilizing the boundedness of $s(t)$ and $\ddot{e}(t)$ in (6.41) and (6.45), it follows that $\hat{v}(t)$, $\tilde{v}(t) \in \mathcal{L}_\infty$. By applying saturation function on $v(t)$ as shown in (6.44), $v(t) \in \mathcal{L}_\infty$ is guaranteed. Since $v(t)$ and $\hat{v}(t) \in \mathcal{L}_\infty$, and using the fact that $h(t,e)$ and $G(t,e)$ are bounded for bounded $e(t)$, it is obtained that $\dot{e}(t) \in \mathcal{L}_\infty$ in (6.33). Barbalat's Lemma that is provided in Appendix B implies (6.46) in Theorem 1 because $e(t), \dot{e}(t) \in \mathcal{L}_\infty$ and $e(t) \in \mathcal{L}_2$.

6.3 Hybrid Acceleration Based Learning-Adaptive Controller for Robotic Manipulators

This section develops a new hybrid learning based adaptive controller using the acceleration feedback to achieve a global position tracking for n-rigid link robotic manipulators despite the parameter uncertainties and unknown periodic dynamics. The proposed hybrid controller utilizes learning based feedforward terms given in (6.31) to compensate for periodic disturbances, and adaptive based feedforward terms given in (6.9)-(6.10) to reject aperiodic disturbances.

For the subsequent control development and stability analysis, the following important properties will be utilized.

Property 4: Symmetric and Positive-Definite Inertia Matrix

It is previously mentioned that the robot inertia matrix, $D(q)$, is symmetric and positive-definite, and satisfies the following inequality:

$$\beta_1\|\eta\|^2 \leq \eta^T D(q)\eta \leq \beta_2\|\eta\|^2 \quad \forall \eta \in \mathbb{R}^n \tag{6.57}$$

where $\beta_1, \beta_2 \in \mathbb{R}$ are known positive constants, $\|\cdot\|$ denotes the standard Euclidean norm.

Property 5: Skew-Symmetry

The inertia and centripetal-Coriolis matrices satisfy the following skew-symmetric relationship:

$$\eta^T\left(\frac{1}{2}\dot{D}(q) - C(q,\dot{q})\right)\eta = 0 \quad \forall \eta \in \mathbb{R}^n \tag{6.58}$$

where $\dot{D}$ is the time derivative of the inertia matrix.

Property 6: Bounding Inequalities

The upper bounds for the norms of the centripetal-Coriolis, gravity, and viscous friction terms can be obtained as follows:

$$\|C(q,\dot{q})\|_{i\infty} \leq \sigma_{c1}\|\dot{q}\|,\ \|G(q)\| \leq \sigma_g,\ \|F_v\|_{i\infty} \leq \sigma_{f_v} \tag{6.59}$$

where $\sigma_{c1}, \sigma_g, \sigma_{f_v} \in \mathbb{R}$ represents known positive constants and $\|\cdot\|_{i\infty}$ is the induced infinity norm of a matrix.

Remark 1: Using the assumptions given in (6.57)-(6.59), it can be concluded that the torque control input is bounded when all the terms on the left-hand side of (6.4) are bounded provided that $q(t), \dot{q}(t), \ddot{q}(t) \in \mathcal{L}_\infty$.

6.3.1 Controller Design

The control objective is to design the torque control input signal, $\tau(t)$, such that the robot link positions will converge to desired trajectories despite the parameter uncertainties in the dynamic model given by (6.4), i.e. $q(t) \Rightarrow q_d(t)$ as $t \Rightarrow \infty$. To quantify the control objective, the position tracking error, denoted by $e(t) \in \mathbb{R}^n$, is defined as follows:

$$e = q_d - q \tag{6.60}$$

where $q_d(t) \in \mathbb{R}^n$ is the desired link position. The control objective is based on the assumption that $q(t)$, $\dot{q}(t)$ and $\ddot{q}(t)$ are measurable, and the desired link positions, velocities and accelerations are bounded, periodic functions of time that are defined as follows:

$$q_d(t) = q_d(t-T), \quad \dot{q}_d(t) = \dot{q}_d(t-T), \tag{6.61}$$

and

$$\ddot{q}_d(t) = \ddot{q}_d(t-T)$$

with a known period of T. To facilitate the subsequent control development and stability analysis, the order of the robot dynamics in (6.4) is reduced by defining a filtered tracking error variable, $r_h(t) \in \mathbb{R}^n$ as follows:

$$r_h = \dot{e} + \Gamma_1 e + \Gamma_2 \int e dt \tag{6.62}$$

where $\dot{e} \in \mathbb{R}^n$ is the velocity error, i.e. $\dot{e} \triangleq \dot{q}_d - \dot{q}$, and $\Gamma_1, \Gamma_2 \in \mathbb{R}^{n\times n}$ are constant, diagonal and positive-definite controller gain matrices. After taking the time derivative of (6.62) and multiplying the resulting expression by the inertia matrix, $D(q)$, the open loop error system is obtained as

$$D(q)\dot{r}_h = -C(q,\dot{q})r_h + \vartheta + \xi + W_2(\dot{q},\ddot{q})\Phi_2 - \tau \tag{6.63}$$

where the auxiliary expression $\vartheta, \xi \in \mathbb{R}^n$ are defined as follows:

$$\vartheta = D(q_d)\ddot{q}_d + C(q_d, \dot{q}_d)\dot{q}_d + G(q_d) + F_v\dot{q}_d \tag{6.64}$$

and

$$\begin{aligned}\xi =& D(q)(\ddot{q}_d + \Gamma_1\dot{e} + \Gamma_2 e) + G(q) + F_v\dot{q} - \vartheta \\ &+ C(q, \dot{q})\left(\dot{q}_d + \Gamma_1 e + \Gamma_2 \int e dt\right)\end{aligned} \tag{6.65}$$

Since the real system parameters are not exactly known, the auxiliary signal, ϑ, as a function of desired periodic trajectories, is an unknown periodic signal. In light of (6.57), (6.59) and (6.61), it follows that

$$|\vartheta_i| \leq \alpha_i \quad \text{for} \quad i = 1, 2, ..., n \tag{6.66}$$

where $\alpha_i = \begin{bmatrix}\alpha_1 & ... & \alpha_n\end{bmatrix} \in \mathbb{R}^n$ is a vector of known, positive bounding constants.

By utilizing (6.57), (6.59), (6.60) and (6.62), and motivated by the result in [100], it is obtained that:

$$\|\xi\| \leq \delta\left(\|Z\|\right)\|Z\| \tag{6.67}$$

where the auxiliary signal $Z(t) \in \mathbb{R}^{3n}$ is defined as:

$$Z(t) = \begin{bmatrix}e^T(t) & r_h^T(t) & \ddot{e}^T(t)\end{bmatrix}^T \tag{6.68}$$

and $\delta(\cdot) \in \mathbb{R}$ is a known and positive bounding function. On the basis of the structure of the open-loop error system in (6.63), the proposed hybrid control law is designed by using an adaptive controller along with a learning based feedforward term as follows:

$$\tau = \Lambda r_h + \kappa\delta^2\left(\|Z\|\right) r_h + \hat{\vartheta} + \tau_a \tag{6.69}$$

where $\hat{\vartheta} \in \mathbb{R}^n$ is an estimate of ϑ in (6.64) and generated by incorporating acceleration feedback into the standard feedforward term in [100]:

$$\hat{\vartheta}(t) = sat_\alpha(\hat{\vartheta}(t - T)) + K_1 r_h + K_2\ddot{e} \tag{6.70}$$

and the adaptive controller, τ_a, is designed as follows:

$$\tau_a = W_2(\dot{q}, \ddot{q})\hat{\Phi}_2 \tag{6.71}$$

with the update law given by (6.10):

$$\dot{\hat{\Phi}}_2 = \Upsilon_h W_2^T(\dot{q}, \ddot{q}) r_h \tag{6.72}$$

where $\ddot{e} \in \mathbb{R}^n$ is the acceleration error, i.e. $\ddot{e} \triangleq \ddot{q}_d - \ddot{q}$, $\Lambda \in \mathbb{R}^{n\times n}$ is a constant, diagonal, positive-definite, controller gain matrix, $\kappa \in \mathbb{R}$ is a constant positive gain, K_1, $K_2 \in \mathbb{R}^{n\times n}$, $\Upsilon_h \in \mathbb{R}^{2n\times 2n}$ represent constant, diagonal, positive-definite, learning control and adaptation gain matrices. Saturation function is denoted by $sat_\alpha(\cdot)$ and defined using the known, positive bounding constants given by (6.66):

$$sat_{\alpha_i}(\varsigma_i) = \begin{cases} \alpha_i, & \varsigma_i \geq \alpha_i \\ \varsigma_i, & -\alpha_i < \varsigma_i < \alpha_i \\ -\alpha_i, & \varsigma_i \leq -\alpha_i \end{cases} \tag{6.73}$$

with $\forall \varsigma_i \in \mathbb{R}, i = 1, 2, .., n$. In light of (6.73), the following inequality will be utilized in the subsequent stability analysis:

$$(\varsigma_{1i} - \varsigma_{2i})^2 \geq (sat_{\alpha_i}(\varsigma_{1i}) - sat_{\alpha_i}(\varsigma_{2i}))^2 \tag{6.74}$$

where $\forall |\varsigma_{1i}| \leq \alpha_i, \varsigma_{1i} \in \mathbb{R}, i = 1, 2, ..., n$.
When (6.69) is substituted into (6.63), the closed-loop error system for $r_h(t)$ is obtained as:

$$D\dot{r}_h = -Cr_h - \Lambda r_h + W_2\tilde{\Phi}_2 + \tilde{\vartheta} + \xi - \kappa\delta^2 (\|z\|) r_h \tag{6.75}$$

where the parameter estimation error, denoted by $\tilde{\Phi}_2 \in \mathbb{R}^{2n}$ is defined as:

$$\tilde{\Phi}_2 = \Phi_2 - \hat{\Phi}_2 \tag{6.76}$$

and $\tilde{\vartheta} \in \mathbb{R}^n$ is the learning estimation error:

$$\tilde{\vartheta} = \vartheta - \hat{\vartheta} \tag{6.77}$$

In light of (6.61), (6.64), (6.66) and (6.73), the following is derived:

$$\vartheta(t) = sat_\alpha(\vartheta(t)) = sat_\alpha(\vartheta(t - T)) \tag{6.78}$$

$\tilde{\vartheta}$ is obtained by substituting (6.70) and (6.78) into (6.77):

$$\tilde{\vartheta} = sat_\alpha(\vartheta(t - T)) - sat_\alpha(\hat{\vartheta}(t - T)) - K_1 r_h - K_2 \ddot{e} \tag{6.79}$$

6.3.2 Closed-Loop Stability Analysis

Theorem 1: The proposed hybrid controller developed in (6.69)-(6.72) can asymptotically drive the position error to zero, i.e.;

$$\lim_{t\to\infty} e(t) = 0 \tag{6.80}$$

where the controller gains Γ_1, Λ, κ, K_1 and K_2 given in (6.62), (6.69) and (6.70) are selected to satisfy the following sufficient condition

$$\min\left(\|\Gamma_1\|, \left\|\Lambda + \frac{K_1^T K_1}{2}\right\|, \left\|\frac{K_2^T K_2}{2}\right\|\right) > \frac{1}{4\kappa} \tag{6.81}$$

where $\|\cdot\|$ is the 2-norm of a matrix, and there exists a first-order differentiable, positive definite function $V_5(e, \dot{e}, \ddot{e}, t) \in \mathbb{R}$ such that

$$\dot{V}_5 \leq -e^T\Gamma_1 e + r_h^T K_1^T K_2 \ddot{e} + \tilde{\vartheta}^T K_2 \ddot{e} + r_h^T (K_1 - I)\tilde{\vartheta} \tag{6.82}$$

where $I \in \mathbb{R}^{n\times n}$ is the identity matrix.

Proof: To prove the conclusion of Theorem 1, a Lyapunov function candidate, $V(t)$ is defined as

$$\begin{aligned} V_6 =& V_5 + \frac{r_h^T D r_h}{2} + \frac{\tilde{\Phi}_2^T \Upsilon_h^{-1} \tilde{\Phi}_2}{2} + \frac{1}{2}\int_{t-T}^{t} \left(sat_\alpha \vartheta(\phi) - sat_\alpha \hat{\vartheta}(\phi)\right)^T \\ & \left(sat_\alpha \vartheta(\phi) - sat_\alpha \hat{\vartheta}(\phi)\right) d\phi \end{aligned} \tag{6.83}$$

Taking the time derivative of (6.83), and using the Leibniz's Rule provided in Appendix B and the assumption given in (6.82) yields

$$\begin{aligned} \dot{V}_6 \leq & -e^T\Gamma_1 e + r_h^T K_1^T K_2 \ddot{e} + \tilde{\vartheta}^T K_2 \ddot{e} + r_h^T (K_1 - I)\tilde{\vartheta} + r_h^T M \dot{r}_h \\ & + \frac{r_h^T \dot{D} r_h}{2} - \tilde{\Phi}_2^T W_2^T r_h + \frac{1}{2}\Big[\left(sat_\alpha \vartheta(t) - sat_\alpha \hat{\vartheta}(t)\right)^T \left(sat_\alpha \vartheta(t) - sat_\alpha \hat{\vartheta}(t)\right) \\ & - \left(sat_\alpha \vartheta(t-T) - sat_\alpha \hat{\vartheta}(t-T)\right)^T \left(sat_\alpha \vartheta(t-T) - sat_\alpha \hat{\vartheta}(t-T)\right)\Big] \end{aligned} \tag{6.84}$$

Using (6.58) and (6.75), the following is obtained:

$$\begin{aligned} \dot{V}_6 \leq & -e^T\Gamma_1 e + r_h^T K_1^T K_2 \ddot{e} + \tilde{\vartheta}^T K_2 \ddot{e} + r_h^T K_1 \tilde{\vartheta} - r_h^T \Lambda r_h \\ & + r_h^T \xi - r_h^T \kappa \delta^2 r_h + \frac{1}{2}\left\|sat_\alpha \vartheta(t) - sat_\alpha \hat{\vartheta}(t)\right\|^2 \\ & - \frac{1}{2}\left(sat_\alpha \vartheta(t-T) - sat_\alpha \hat{\vartheta}(t-T)\right)^T \left(sat_\alpha \vartheta(t-T) - sat_\alpha \hat{\vartheta}(t-T)\right) \end{aligned} \tag{6.85}$$

The expression given in (6.85) can be rewritten based on (6.67) and (6.79) as follows:

$$\begin{aligned} \dot{V}_6 \leq & -e^T\Gamma_1 e + r_h^T K_1^T K_2 \ddot{e} + \tilde{\vartheta}^T K_2 \ddot{e} + r_h^T K_1 \tilde{\vartheta} - r_h^T \Lambda r_h \\ & + \left[\delta \|Z\| \|r_h\| - \kappa \delta^2 \|r_h\|^2\right] + \frac{1}{2}\left\|sat_\alpha \vartheta(t) - sat_\alpha \hat{\vartheta}(t)\right\|^2 \\ & - \frac{1}{2}\Big[(\tilde{\vartheta} + K_1 r_h + K_2 \ddot{e})^T (\tilde{\vartheta} + K_1 r_h + K_2 \ddot{e})\Big] \end{aligned} \tag{6.86}$$

By expanding the last line of (6.86), and performing cancellations, one obtains

$$\begin{aligned}\dot{V}_6 \leq & -e^T\Gamma_1 e - r_h^T\left(\Lambda + \frac{K_1^T K_1}{2}\right) r_h - \ddot{e}^T \frac{K_2^T K_2}{2}\ddot{e} \\ & + \frac{1}{2}\left[\left\|sat_\alpha \vartheta(t) - sat_\alpha \hat{\vartheta}(t)\right\|^2 - \left\|\vartheta(t) - \hat{\vartheta}(t)\right\|^2\right] \\ & + \left[\delta\|Z\|\|r_h\| - \kappa\delta^2\|r_h\|^2\right]\end{aligned} \tag{6.87}$$

By exploiting the property given in (6.74), completing the square on the bracketed term in the last line of (6.87), and using (6.68), (6.87) can be simplified as:

$$\dot{V}_6 \leq -\left[\min\left(\|\Gamma_1\|, \left\|\Lambda + \frac{K_1^T K_1}{2}\right\|, \left\|\frac{K_2^T K_2}{2}\right\|\right) - \frac{1}{4\kappa}\right]\|Z\|^2 \tag{6.88}$$

where $\|\cdot\|$ is the 2-norm of a matrix.

Signal Chasing: When (6.81) is satisfied, it follows that $V_6(t) \in \mathcal{L}_\infty$ based on (6.83) and (6.88). Since the signals in $V_6(t)$ must remain bounded, it can be concluded that $r_h(t), \tilde{\Phi}_2(t) \in \mathcal{L}_\infty$. If the sufficient condition in (6.81) is satisfied and using Lemma 1 given in Appendix B, it is obtained that

$$\|Z\| = \sqrt{\int_0^\infty Z^2(t)dt} < \infty \tag{6.89}$$

and this implies $Z(t) \in \mathcal{L}_2$ based on Definition 1 given in Appendix B. Using (6.55) and (6.56) in Property 3, $\|Z\|_\infty \leq \|Z\|$. From $\|Z\| < \infty$ in (6.89), it is concluded that $\|Z\|_\infty \leq \|Z\| < \infty$ so $\|Z\|_\infty < \infty$. According to Definition 2 presented in Appendix B, $\|Z\|_\infty = \sup|Z(t)| < \infty$ is obtained, and it follows that $Z(t) \in \mathcal{L}_\infty$. Therefore, $Z(t) \in \mathcal{L}_2 \cap \mathcal{L}_\infty$.

The definition of $Z(t)$ given in (6.68) implies $e(t), \ddot{e}(t), r_h(t) \in \mathcal{L}_2 \cap \mathcal{L}_\infty$. It is observed that $\dot{e}(t) \in \mathcal{L}_2 \cap \mathcal{L}_\infty$ because the signals in $r_h(t)$ given by (6.53) must remain bounded based on (6.62). Since $e(t), \dot{e}(t) \in \mathcal{L}_\infty$ and $e(t) \in \mathcal{L}_2$, Barbalat's Lemma which is provided in Appendix B implies (6.80) in Theorem 1.

In light of (6.60) and (6.61), and using the boundedness of $e(t), \dot{e}(t), \ddot{e}(t)$, it follows that $q(t), \dot{q}(t), \ddot{q}(t) \in \mathcal{L}_\infty$. By exploiting the fact that the learning feedforward term given in (6.70) is composed of a saturation function, and $r(t), \ddot{e}(t) \in \mathcal{L}_\infty$, it can be concluded that $\hat{\vartheta}(t) \in \mathcal{L}_\infty$. Since Φ_2 represents bounded static friction coefficients and $\tilde{\Phi}_2(t) \in \mathcal{L}_\infty$, it follows from (6.76) that $\hat{\Phi}_2(t) \in \mathcal{L}_\infty$. It is observed that $\tau_a(t) \in \mathcal{L}_\infty$ using $\dot{q}(t), \ddot{q}(t), \hat{\Phi}_2(t) \in \mathcal{L}_\infty$ in (6.71). Finally, $\tau_a(t), \hat{\vartheta}(t), r_h(t) \in \mathcal{L}_\infty$ implies $\tau(t) \in \mathcal{L}_\infty$ based on (6.69). Therefore, all system signals remain bounded.

Chapter 7

7 Simulation Results

Simulation results for the proposed control algorithms and estimation methods are presented in this section where the proposed estimation methods are incorporated into a high fidelity simulation model to test the stabilization performance of the pan-tilt system subject to various external disturbances, and also evaluate periodic trajectory tracking performance on the same platform which suffers from parameter uncertainties and periodic disturbances with a known period. An inner loop acceleration approach that is given in Figure 8 is utilized to achieve high precision stabilization by using reliable estimates provided by the proposed master-slave Kalman filter algorithm that fuses 3-axis gyroscope, 3-axis accelerometer and 3-axis magnetometer measurements. The proposed acceleration based LMI-LQR controller is applied on the pan-tilt system to ensure high precision stabilization where reliable estimates are predicted by a cascaded high gain observer structure from noisy encoder measurements. On the other hand, the proposed hybrid learning based adaptive controller in (6.69)-(6.72) is used to obtain satisfactory periodic trajectory tracking performance by estimating reliable feedback signals with a cascaded high gain observer structure from noisy encoder measurements.

In order to construct a high fidelity simulation model, both nonlinear dynamics of the pan-tilt platform given by (4.1) and realistic sensor models given by (3.1), (3.6), (3.7), (3.8) are utilized. Biases and noises that corrupt sensor outputs are tabulated in Table 1 where SNR denotes signal to noise ratio. The update rates of MEMS inertial sensors that are provided in Table 1 are selected based on the specifications given in the inertial sensor market[1].

[1] Advanced Navigation, Spatial FOG (GPS aided INS and AHRS)

Table 1: Simulation Parameters

Parameter	Description	Value
Bw_g	Bandwidth of gyro	440 Hz
Bw_a	Bandwidth of accelerometer	200 Hz
Bw_m	Bandwidth of magnetometer	110 Hz
b_g	Gyro bias	$[1\ -1\ 0.5]^T\ deg/s$
b_a	Accelerometer bias	$[0.01\ -0.01\ 0.005]^T\ g$
b_m	Magnetometer bias	$[0.01\ -0.01\ 0.02]^T\ Wb/m^2$
S_{η_g}	SNR of gyro	65 dB
S_{η_a}	SNR of accelerometer	45 dB
S_{η_m}	SNR of magnetometer	61 dB
S_{η_e}	SNR of encoder	55 dB

7.1 Results of the Proposed Master-Slave Kalman Filter Algorithm

This section evaluates the performance of the proposed filter that employs both an extended Kalman filter (EKF) and an inverse Φ-algorithm in a master-slave configuration by using reliable angles, velocities and accelerations as feedback signals in the stabilization control of the pan-tilt system. Sections 7.1.1 and 7.1.2 present the first and second scenario results, respectively.

Since we assume that EKF and the inverse Φ-algorithm run at 1000 Hz, the proposed sensor fusion algorithm executes faster than these inertial sensors. Therefore, the master-slave Kalman filter algorithm may generate estimates before one of the gyroscope, accelerometer and magnetometer measurements are completed.

The quality of the estimated signals with the incomplete measurements due to the different rates for the MEMS inertial sensors will be deteriorated if proper action is not taken. This leads to the loss of data integrity. In order to ensure data integrity, we add a rate transition block at the output of each sensor in the simulations. We use this rate transition as a double buffer. The gyroscope provides angular velocity measurements to the slave estimator. When the gyro measurement is obtained, this data is transferred to the first buffer. The slave estimator takes the gyro data from this buffer until a new measurement is available. When a new gyro measurement is available, it is saved to the second buffer, the buffer index is changed, and the new measurement is used by the inverse Φ-algorithm. Similar double buffers are also used for accelerometer and magnetometer.

The reference trajectories in the inertial frame are selected to be smooth step functions of time in the simulations. Once the system reaches the target orientation, the PID position controller is deactivated and the reference velocity becomes zero,

$\Omega_{ref} = 0$, as shown in Figure 8. Thus, the pan-tilt system is stabilized by the PI velocity controller instead of PID position controller. Since the goal is to improve robustness of the stabilized pan-tilt system under external disturbances, acceleration feedback is introduced into the PI current controller. External disturbances are applied to the system to mimic realistic conditions in both scenarios. When the external disturbances are discarded, PID controller is not activated but the velocity controller is still utilized. The time synchronization between EKF and the inverse Φ-algorithm is achieved by introducing a unit delay to the output of EKF. The inverse Φ-algorithm uses the inverse of the state transition matrix. Thus, this algorithm produces stable and converging estimates if the transition matrix is not ill-conditioned. Since EKF is based on the linearization of nonlinear models given by (3.16)-(3.18), convergence is not guaranteed; however, by the proper choice of process and measurement noise covariance matrices, Q and R, and by increasing the observability of the state vector, one usually achieves stable filter operation with good convergence. In simulations, the filter parameters (Q and R) are tuned as follows:

$$Q_{master} = \begin{bmatrix} 10I_{3\times3} & 0_{3\times3} & 0_{3\times3} & 0_{3\times3} \\ 0_{3\times3} & 11I_{3\times3} & 0_{3\times3} & 0_{3\times3} \\ 0_{3\times6} & 0_{3\times3} & 12I_{3\times3} & 0_{3\times3} \\ 0_{3\times3} & 0_{3\times3} & 0_{3\times3} & 13I_{3\times3} \end{bmatrix}, \quad R_{master} = \begin{bmatrix} 10^{-4}I_{4\times4} & 0_{4\times6} \\ 0_{6\times4} & 10^{-3}I_{6\times6} \end{bmatrix}$$

$$Q_{slave} = \begin{bmatrix} I_{3\times3} & 0_{3\times3} & 0_{3\times3} \\ 0_{3\times3} & 2I_{3\times3} & 0_{3\times3} \\ 0_{3\times3} & 0_{3\times3} & 3I_{3\times3} \end{bmatrix}, \quad R_{slave} = 10^{-2}I_{3\times3}$$

where I and 0 represent the identity and zero matrices.

7.1.1 First Scenario

The pan-tilt platform is exposed to continuous, random and small amplitude disturbances. Figure 10 shows the disturbances applied to the azimuth and elevation axes. Gaussian distributed noises are used to generate these disturbances.
Azimuth and elevation angle responses are presented in Figures 11 and 12, respectively. Desired values of azimuth and elevation references are 45 deg and 55 deg. When the acceleration feedback is not used in the current controller, oscillations occur in the azimuth angle response. The maximum overshoot from the azimuth angle response curve is about 12%. On the other hand, the azimuth angle converges to the reference value in a smoother way when the acceleration feedback is introduced, e.g. $K_\beta = 5$. For the elevation angle response, the system does not exactly

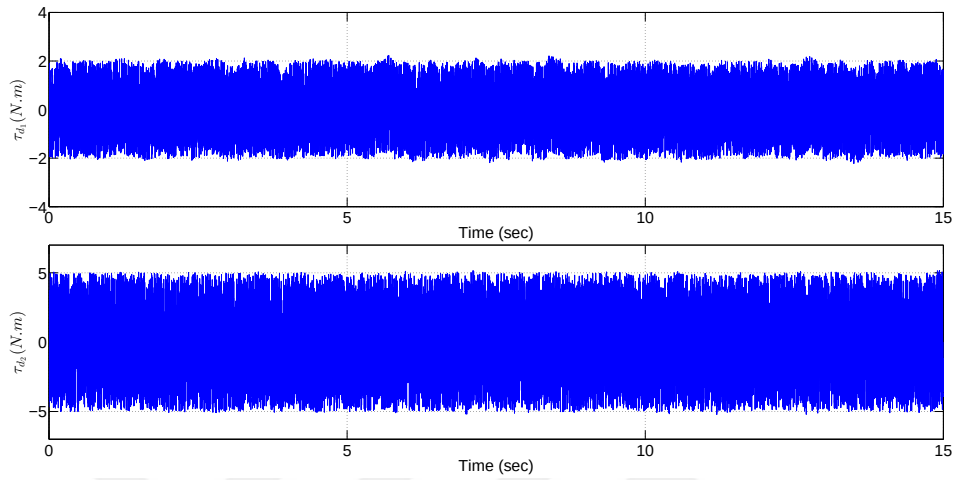

Figure 10: External disturbances applied on the azimuth and elevation axes.

converge to 55 *deg* without the use of acceleration feedback. The elevation angle oscillates between 54.5 *deg* and 55.2 *deg* at the steady state. As the acceleration feedback is introduced, sufficiently small steady state error is achieved in the elevation angle response. Figure 13 shows control efforts for $K_\beta = 0$ and $K_\beta = 5$. The

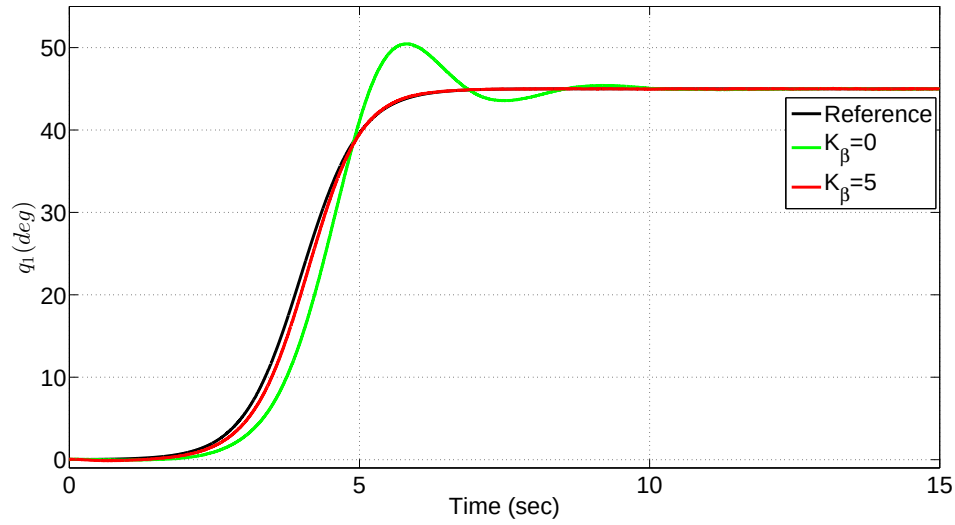

Figure 11: Azimuth angle responses.

amplitudes of the control inputs which are provided by the acceleration control are similar to those that are obtained without the use of acceleration feedback. RMS

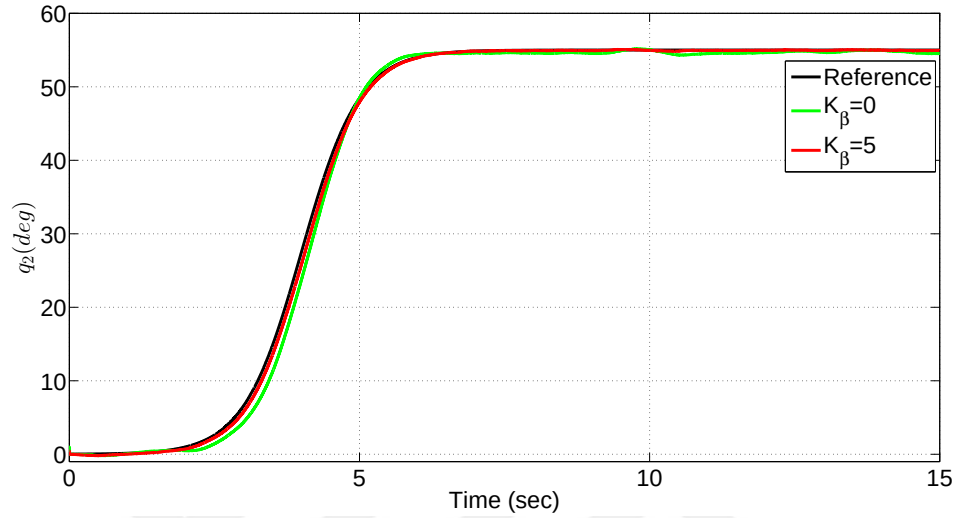

Figure 12: Elevation angle responses.

value of the control input for the azimuth axis is 2.83 $N.m$ and slightly decreases to 2.35 $N.m$ with the use of acceleration feedback. When the acceleration feedback is used in the PI current control loop, RMS value of the control input changes from 89.47 $N.m$ to 89.13 $N.m$ for the elevation axis. These results show that acceleration control does not require larger control inputs to obtain better output angle responses when the system is exposed to continuous disturbances. The master esti-

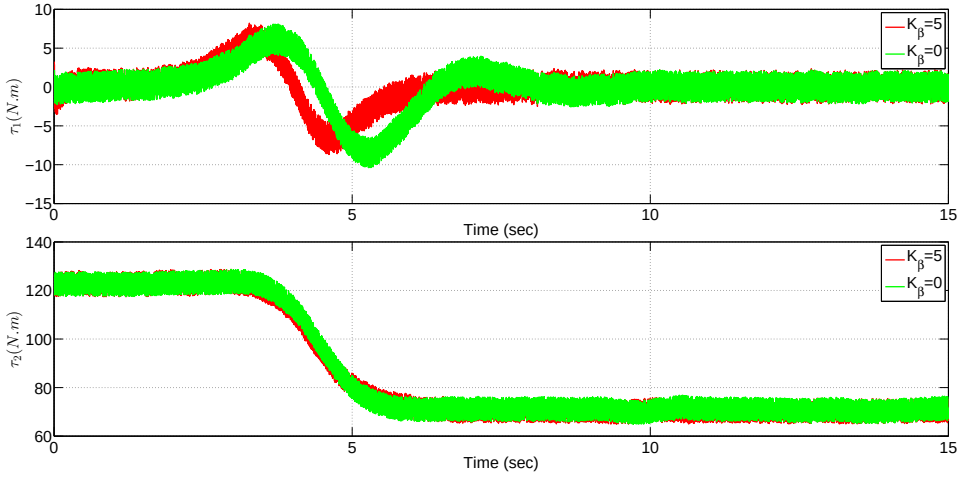

Figure 13: Torque control inputs of the azimuth and elevation axes.

mator which is implemented by using the EKF provides the estimates of pitch and yaw angles, velocities and accelerations based on (3.16)-(3.18). In Figures 14 and 15, estimated Euler angles are provided. EKF performance is evaluated by RMS value of the errors between measured and estimated pitch and yaw angles. RMS values of the estimation errors of the pitch angle are 0.0057 deg and 0.0168 deg for $K_\beta = 0$ and $K_\beta = 5$, respectively. Also, RMS values of the estimation errors of the yaw angle are obtained as 4.48×10^{-7} deg and 4.66×10^{-7} deg for $K_\beta = 0$ and $K_\beta = 5$, respectively. Since all the estimation errors are small, estimated signals converge to measured values successfully for both $K_\beta = 0$ and $K_\beta = 5$.

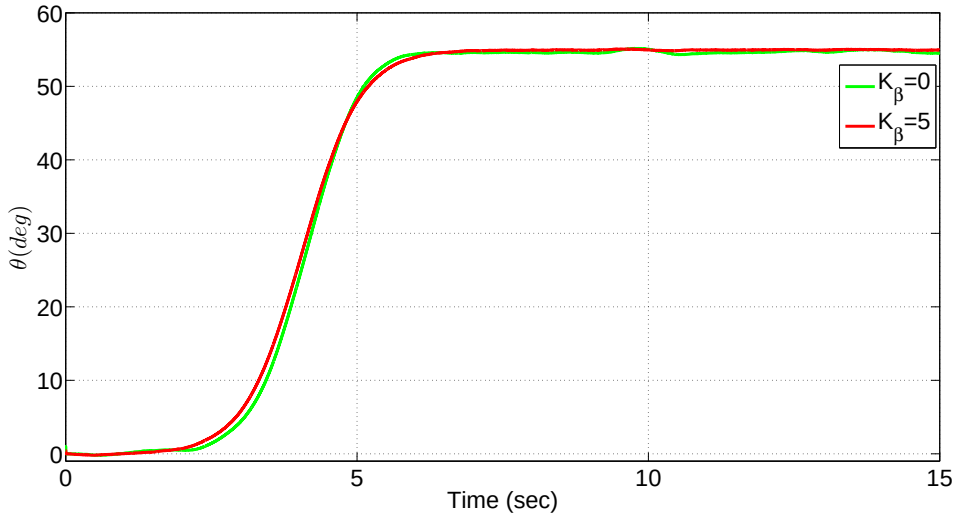

Figure 14: Estimated pitch angles.

On the other hand, Euler velocities and accelerations are estimated as depicted in Figures 16 and 17. The amplitude of oscillations are larger in both velocity and acceleration responses for $K_\beta = 0$ because the angle responses are not smooth when the acceleration feedback is not utilized. Angular velocities, accelerations and jerks are estimated by the slave filter using the process and measurement models in (3.20)-(3.22). When the acceleration feedback is utilized, small amplitude angular velocities are obtained in Figures 18-20. These results are not surprising because better angle responses are achieved with the use of acceleration feedback in the current controller. Similar observations can be also done for estimated angular accelerations and jerks in Figures 21 and 22.

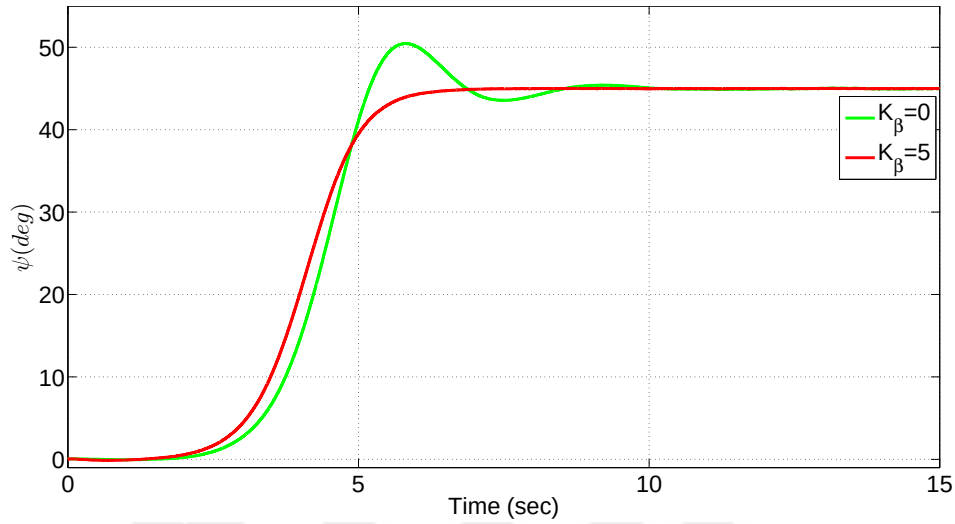

Figure 15: Estimated yaw angles.

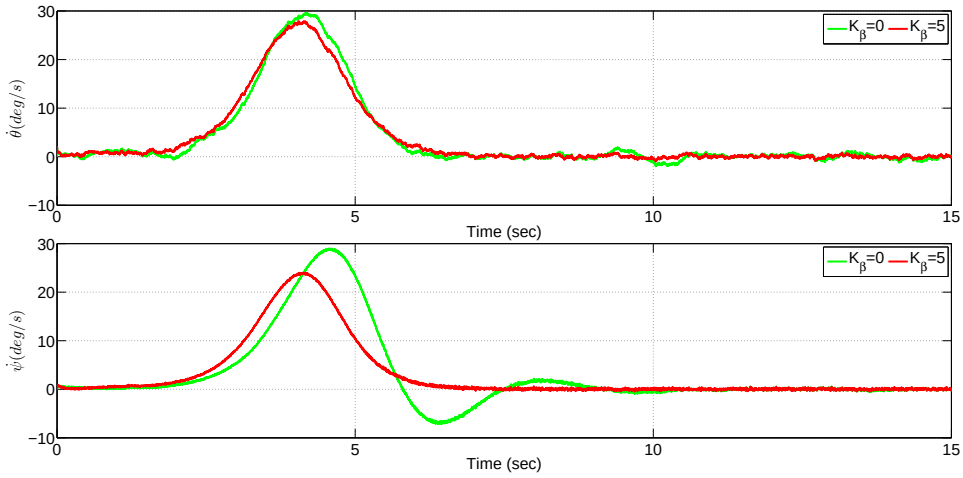

Figure 16: Estimated Euler velocities.

7.1.2 Second Scenario

In the second scenario, the pan-tilt platform is exposed to external disturbances after the desired positions are reached. In order to illustrate this case, disturbance torques are modeled as high amplitude step pulses with short durations. The amplitudes of the step pulses are assumed as 10 $N.m$ and 15 $N.m$. Step disturbances are applied on the system between $t = 8$ *sec* and $t = 12$ *sec* as shown in Figure 23.

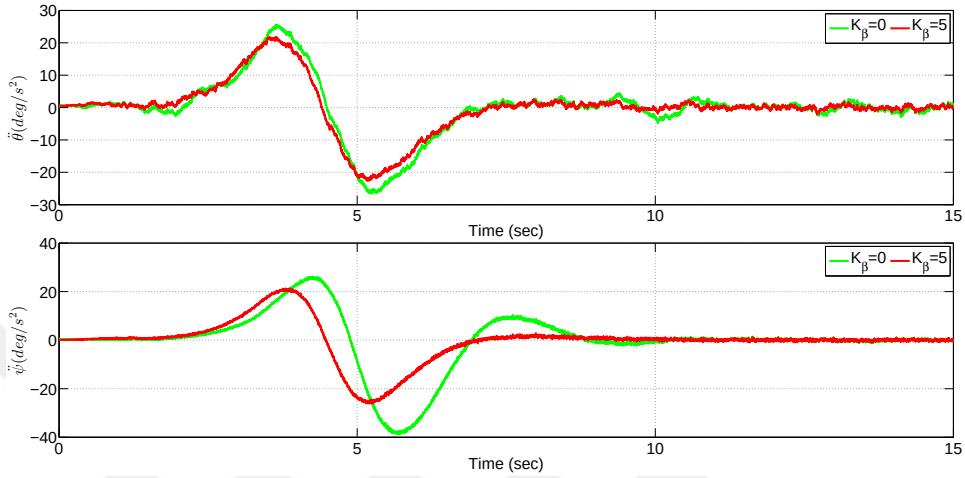

Figure 17: Estimated Euler accelerations.

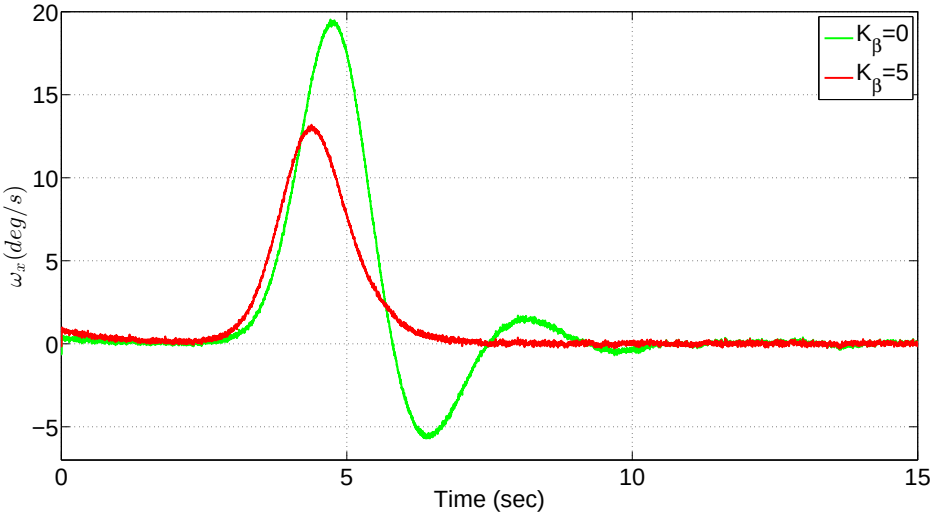

Figure 18: Estimated angular velocities about x axis.

Figures 24 and 25 show the tracking performance for the azimuth and elevation axes. When the acceleration feedback is not used, azimuth and elevation angles cannot follow the reference trajectories successfully due to step pulses. The azimuth angle reaches to approximately 59 *deg*. When the acceleration feedback is used, small amplitude oscillations occur. Azimuth angle oscillates between 44.5 *deg* and 46 *deg* with the use of acceleration controller. In other words, azimuth an-

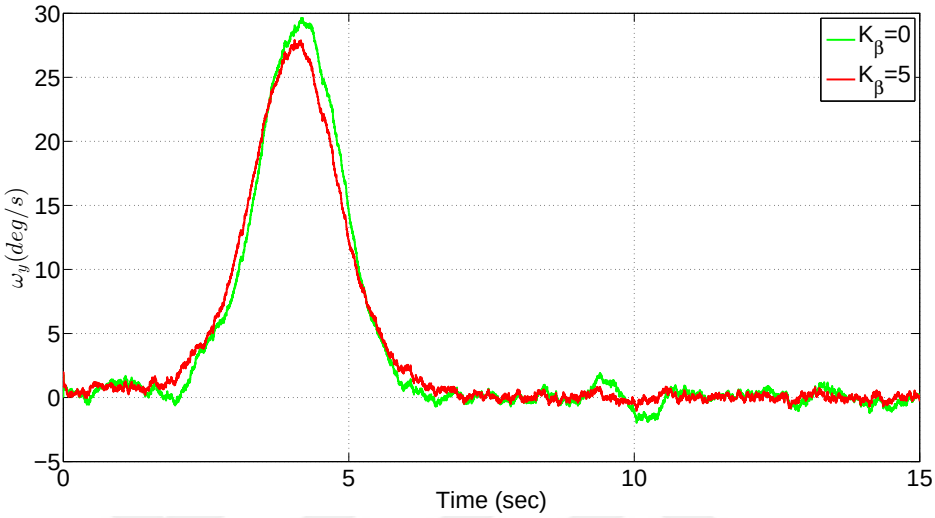

Figure 19: Estimated angular velocities about y axis.

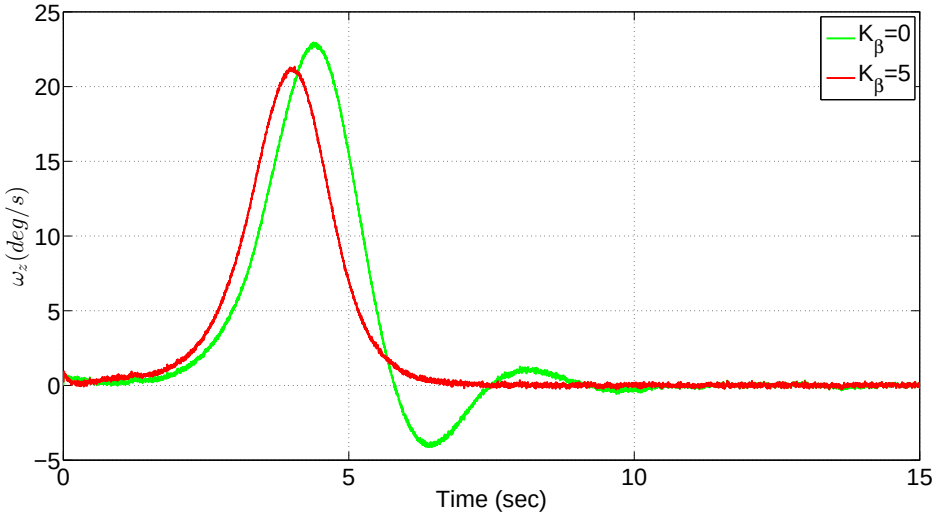

Figure 20: Estimated angular velocities about z axis.

gle is successfully stabilized despite the step pulses. Similar performances are also observed for the elevation angle responses. Smoother elevation angle response is achieved with the introduction of acceleration feedback. However, amplitudes of the oscillations increase to approximately 80 *deg* when the acceleration controller is not active.

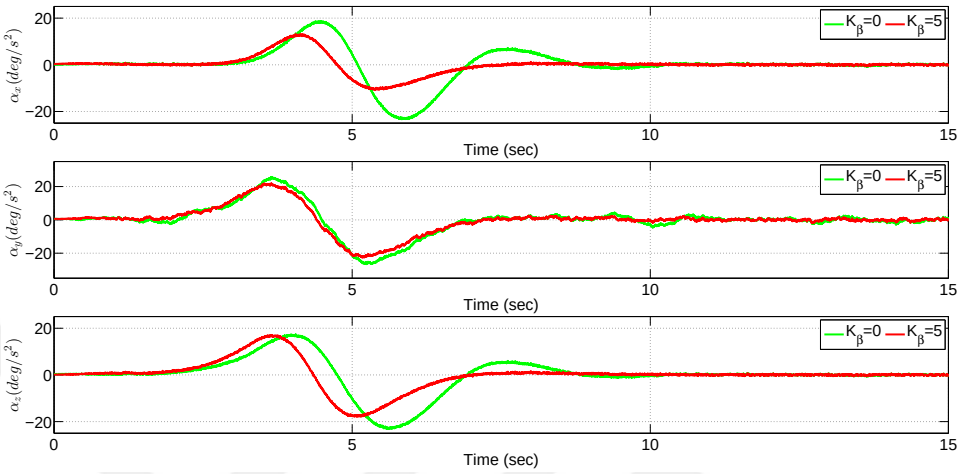

Figure 21: Estimated angular accelerations.

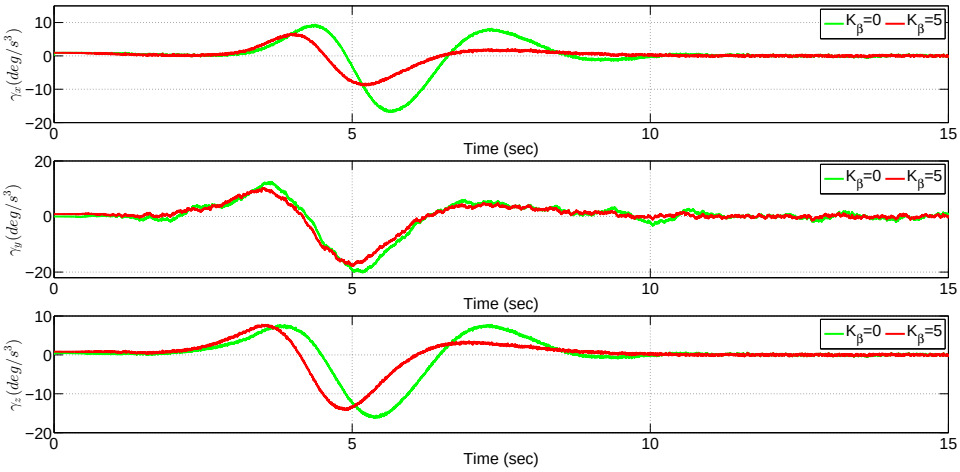

Figure 22: Estimated angular jerks.

In Figure 26, control efforts are provided for $K_\beta = 0$ and $K_\beta = 12$. In order to reject the external disturbances, large acceleration gain, $K_\beta = 12$, is used. As it is expected that when the disturbances are not applied on the system, this acceleration gain leads to high amplitude oscillations compared to the case where acceleration feedback is not utilized. On the other hand, when the disturbances are applied on the system, the amplitude of oscillations are larger without the use of acceleration feedback. As a result, pan and tilt axes are not stabilized due to disturbances even

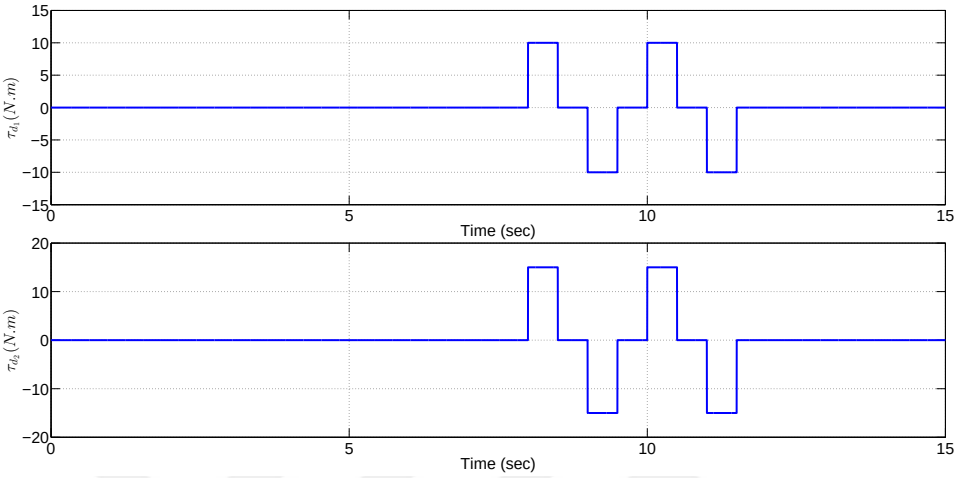

Figure 23: External disturbances applied on the azimuth and elevation axes.

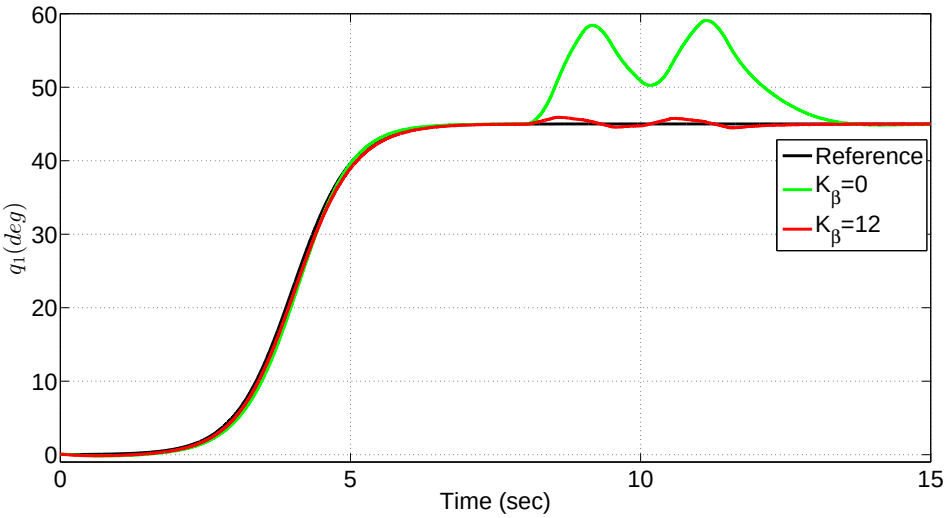

Figure 24: Azimuth angle responses.

high control efforts are obtained for $K_\beta = 0$. Similar to that of the first scenario, the master estimator is implemented by using the EKF based on (3.16)-(3.18). Figures 27 and 28 depict the estimated pitch and yaw angles. RMS values of the errors between the measured and estimated pitch angles are 0.0121 *deg* and 0.0095 *deg* for $K_\beta = 0$ and $K_\beta = 12$, respectively. On the other hand, RMS values of the errors between the measured and estimated yaw angles are 2.72×10^{-7} *deg* and

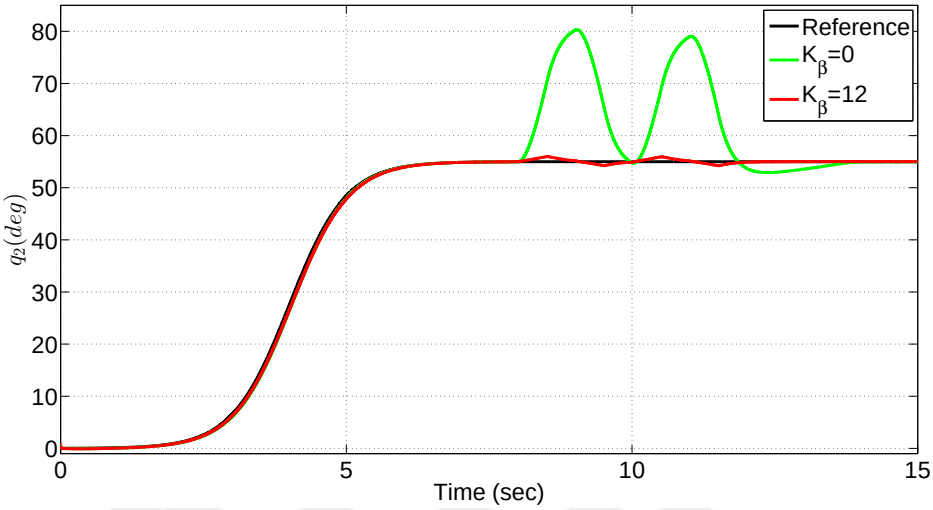

Figure 25: Elevation angle responses.

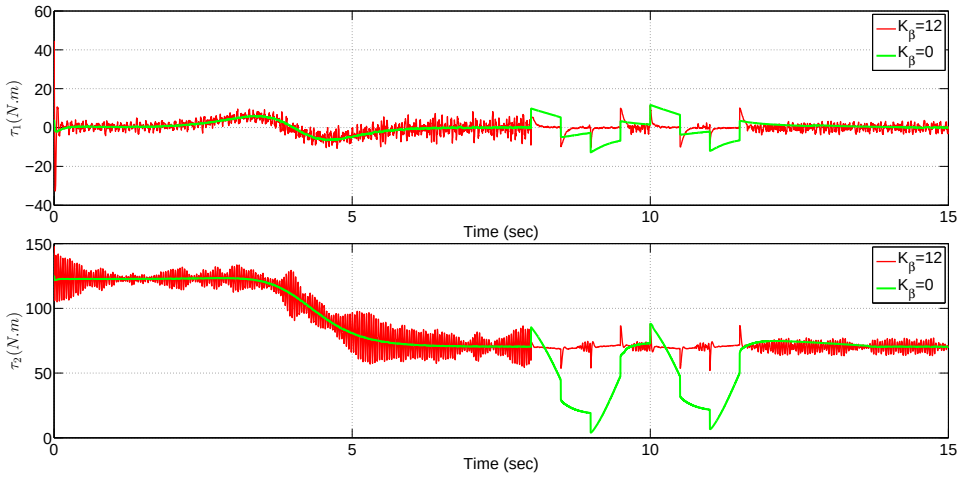

Figure 26: Torque control inputs of the azimuth and elevation axes.

2.05×10^{-7} *deg* for $K_\beta = 0$ and $K_\beta = 12$. Since these errors are small, satisfactory estimates of pitch and yaw angles are obtained for both $K_\beta = 0$ and $K_\beta = 12$. On the other hand, pitch and yaw velocities and accelerations are estimated as depicted in Figures 29 and 30. When the acceleration controller is not active, high amplitude oscillations are observed in the estimated values as expected.

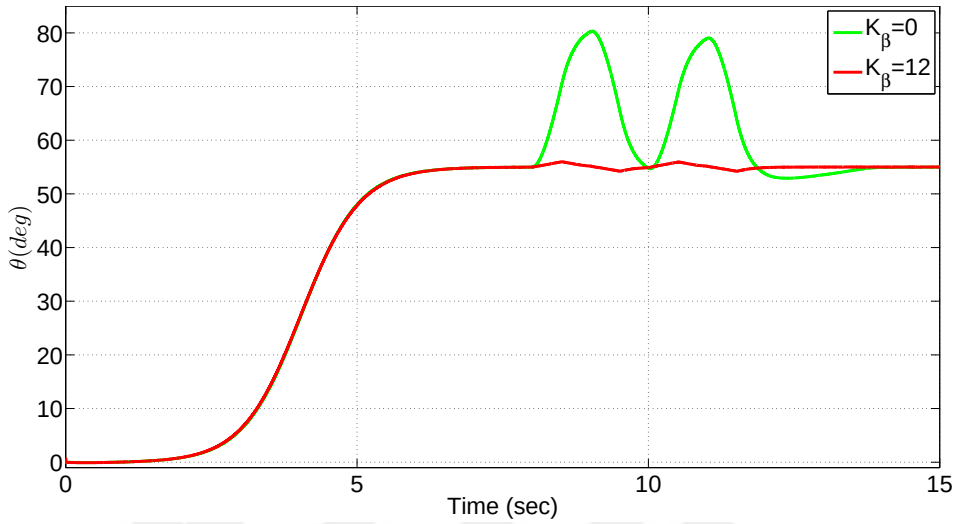

Figure 27: Estimated pitch angles.

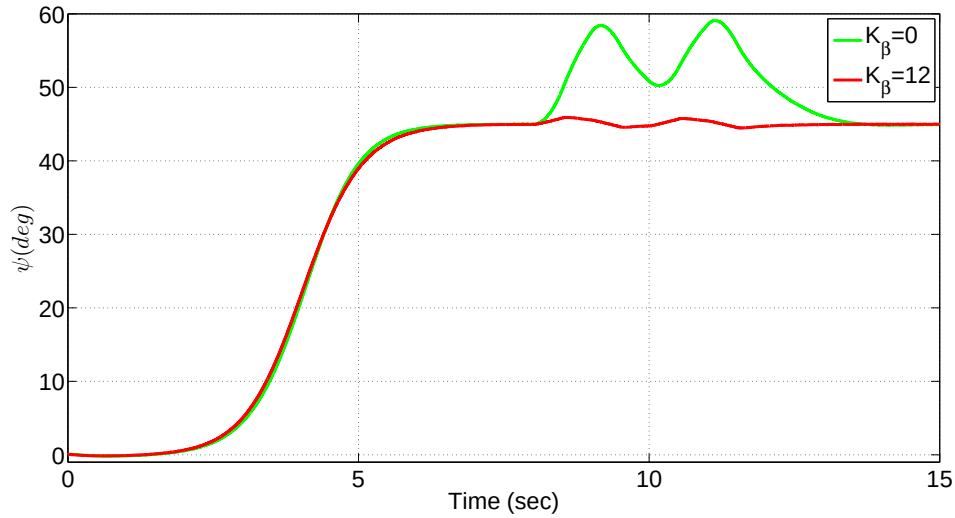

Figure 28: Estimated yaw angles.

Figures 31-33 present the estimated angular velocities by the slave filter. When the acceleration feedback is not used, high amplitude angular velocities are obtained between $t = 8$ *sec* and $t = 12$ *sec* due to the disturbances. The dramatic changes are also observed in the estimated angular accelerations and jerks when the disturbances are applied on the system as depicted in Figures 34 and 35.

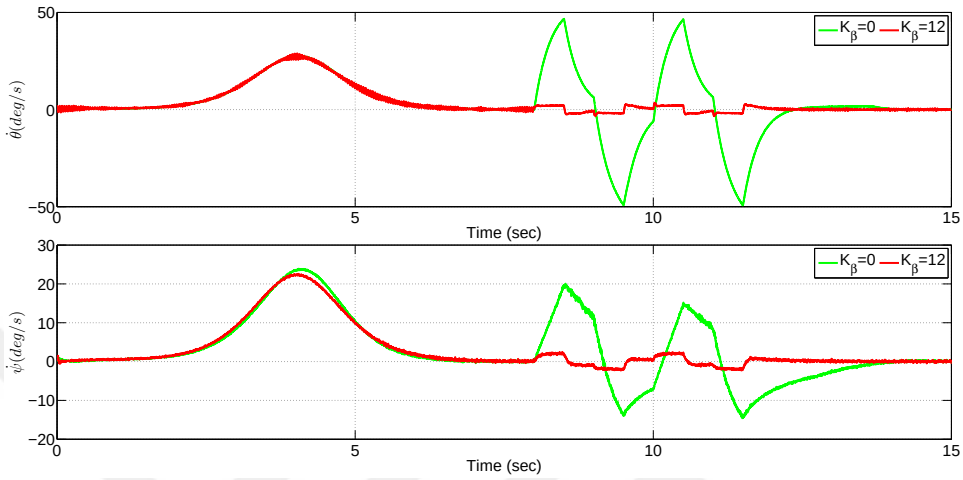

Figure 29: Estimated Euler velocities.

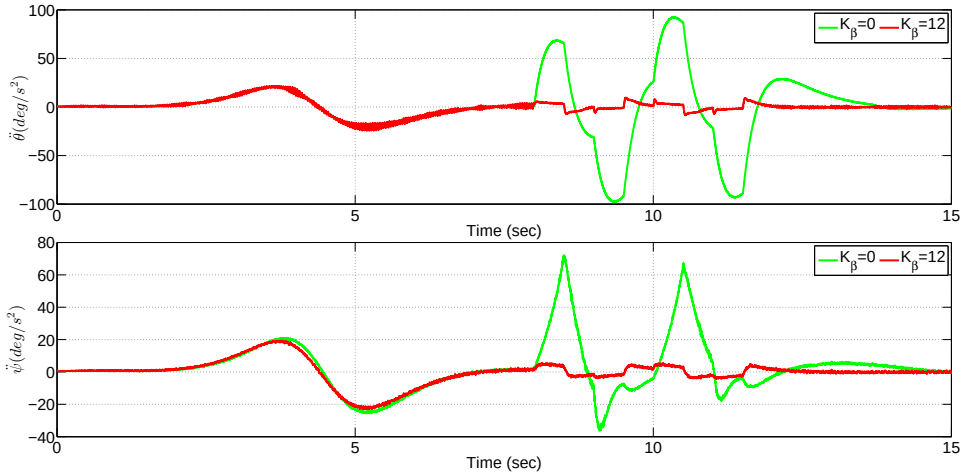

Figure 30: Estimated Euler accelerations.

7.2 Comparison with Other Sensor Fusion Algorithms

The performance of the proposed sensor fusion algorithm is compared to a Newton predictor enhanced Kalman filter (NPEKF) [136] and an error state Kalman filter (ErKF) [137]-[138]. In the NPEKF method, angular accelerations are estimated by a classical Kalman filter and then estimated accelerations are passed through the Newton predictor to further reduce the phase lag caused by the Kalman filter. To compare the performance of the proposed method with NPEKF, pitch and yaw

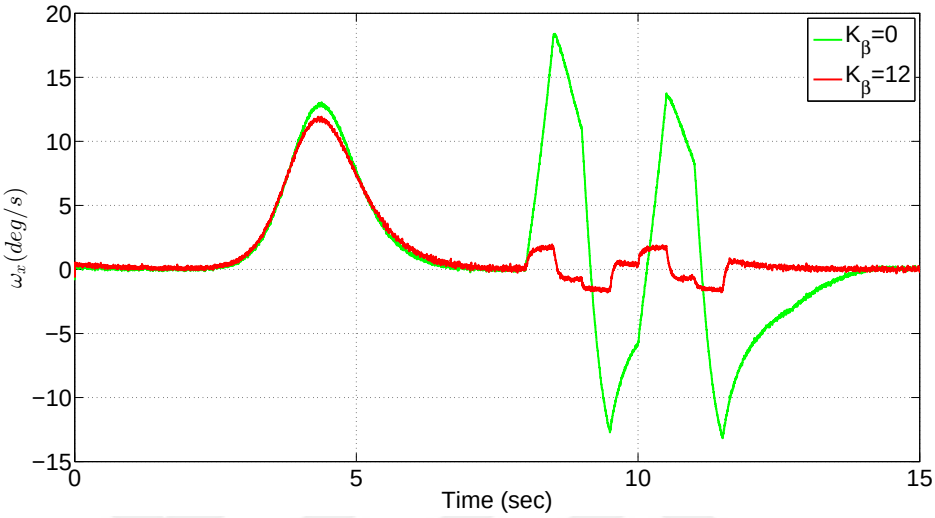

Figure 31: Estimated angular velocities about x axis.

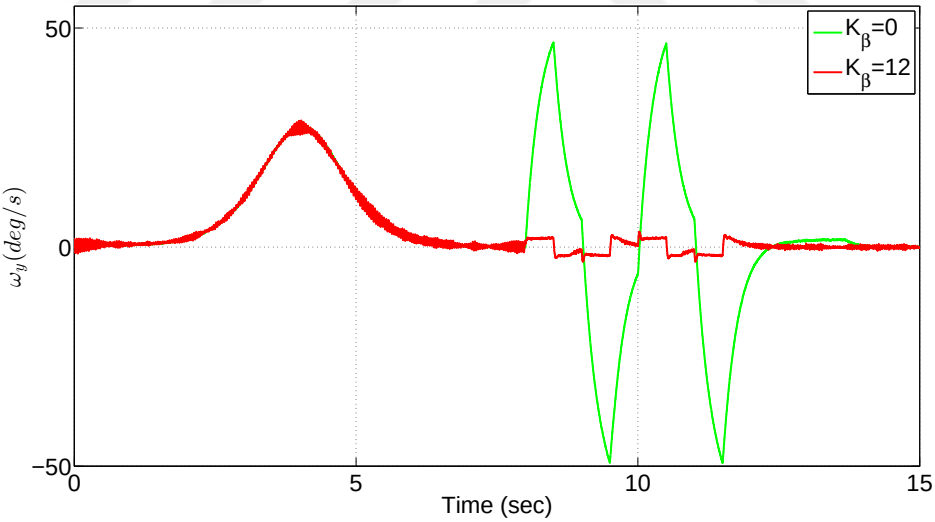

Figure 32: Estimated angular velocities about y axis.

accelerations are estimated by the proposed filter and then those estimated values are passed through the following predictor designed by Han et.al [136]:

$$\mathbb{H}_2^1(z) = 3 - 3z^{-1} + z^{-2} \tag{7.1}$$

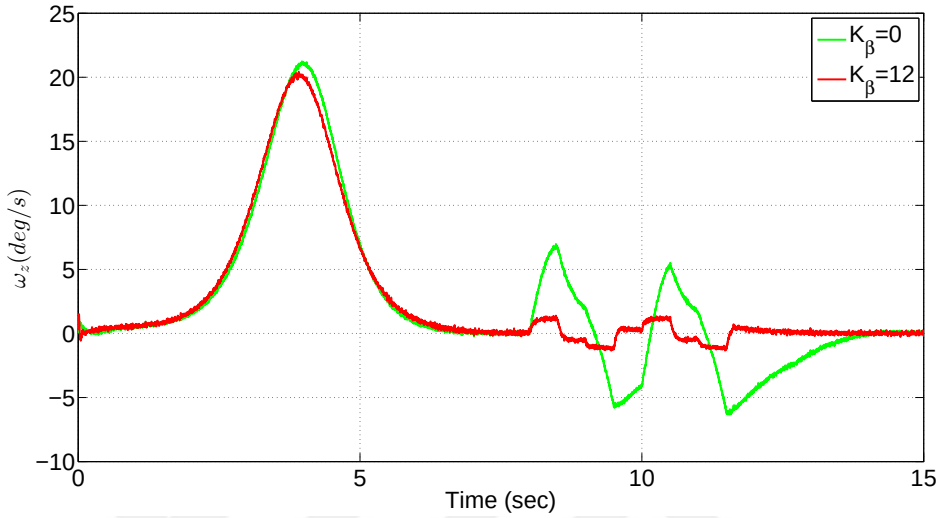

Figure 33: Estimated angular velocities about z axis.

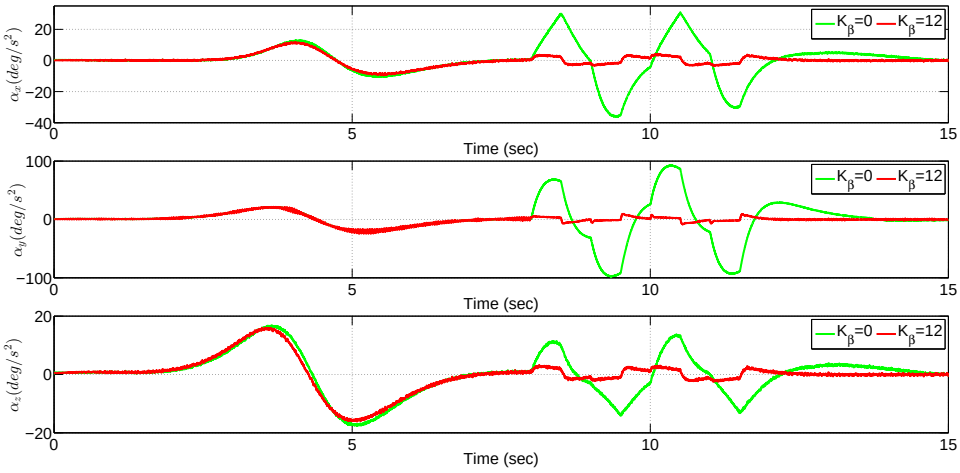

Figure 34: Estimated angular accelerations.

where $\mathbb{H}_2^1(z)$ represent 1-step 2nd-order Newton predictor. Thus, only three past states are required to predict pitch and yaw accelerations. To the best of our knowledge, the global Kalman filter and ErKF have not been used to estimate Euler and body frame angular accelerations. However, there are attempts to solve the attitude estimation problem by using ErKF and underline differences between EKF and ErKF [137]-[138]. Thus, advantages of ErKF over EKF are known for the attitude

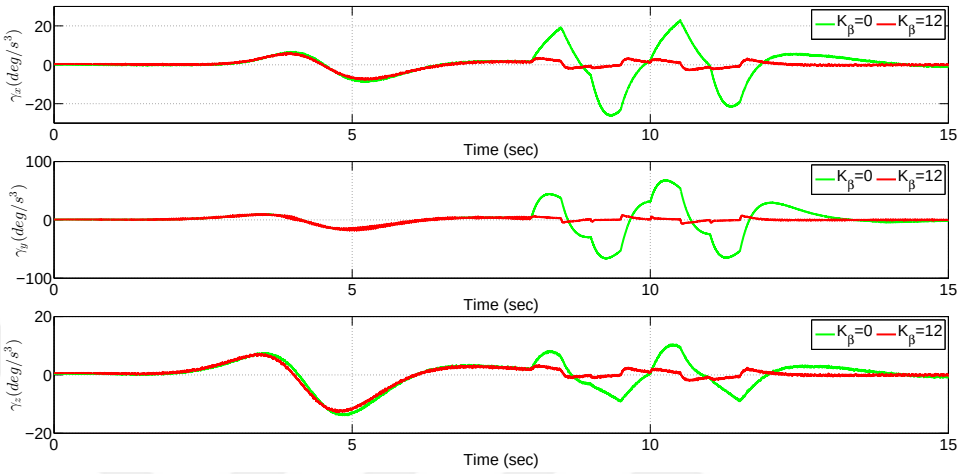

Figure 35: Estimated angular jerks.

estimation. While ErKF is used to only estimate the errors in the state, EKF is implemented to obtain the state estimate itself. In this work, the performance of EKF that is used in a master-slave configuration with the inverse Φ-algorithm is compared with ErKF for the velocity and acceleration estimation problem. ErKF is also used in a master-slave configuration with the inverse Φ-algorithm since the process dynamics of this estimation problem requires to use body frame angular accelerations and jerks estimated by the inverse Φ-algorithm. The estimated signals by the proposed filter, NPEKF and ErKF are presented in Sections 7.2.1 and 7.2.2.

7.2.1 First Scenario

The performance of the proposed filter is compared to the Newton predictor and the error state Kalman filter while the system is exposed to random and continuous disturbances given in Figure 10. Figures 36 and 37 present estimated pitch and yaw angles. The performance of the proposed filter is almost similar with the fusion algorithm where the master filter is designed as ErKF. However, estimated angles by NPEKF are noisy. Thus, the proposed method outperforms the Newton predictor.

Errors between measured and estimated pitch and yaw angles are provided in Figures 38 and 39. Estimation errors are almost the same when the master filter is implemented as either EKF or ErKF, but errors of NPEKF are larger than the ones obtained by the proposed filter. RMS values of the pitch angle estimation errors are

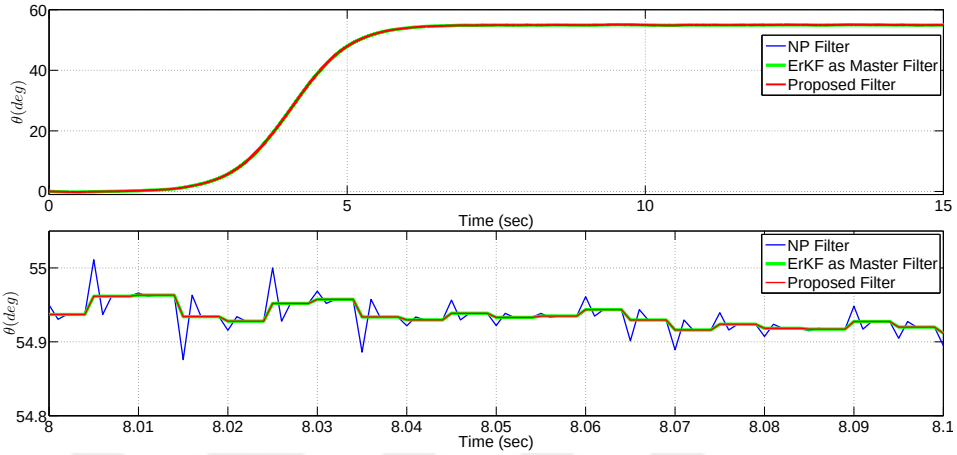

Figure 36: Comparison between estimated pitch angles.

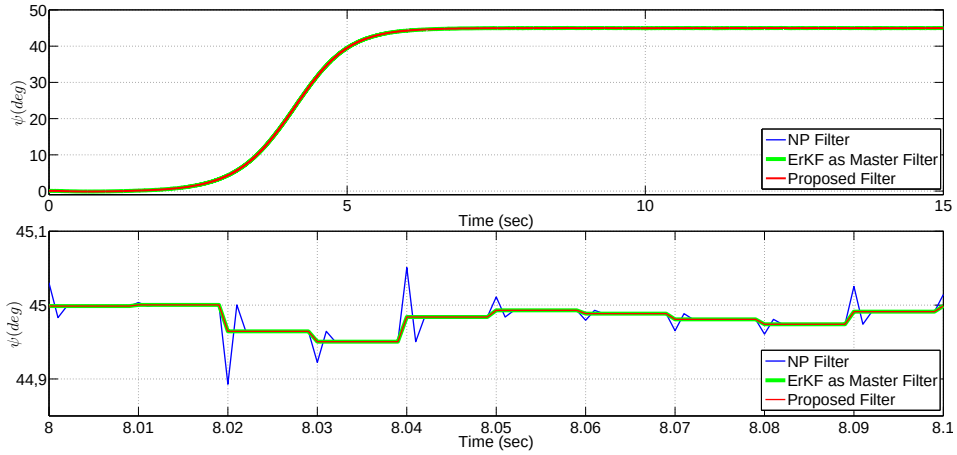

Figure 37: Comparison between estimated yaw angles.

2.11×10^{-6} *deg* and 0.0451 *deg* for the proposed filter and NPEKF, respectively. RMS value of the yaw angle estimation error is 0.0451 *deg* for NPEKF and smaller RMS error is obtained with the proposed method, i.e. 2.11×10^{-7} *deg*. Similar observations can be also done for the estimated values of pitch and yaw velocities and accelerations in Figures 40-43. Estimated velocity and acceleration signals by the proposed method are closer to the ones estimated by the fusion algorithm in which the master estimator is implemented as ErKF. On the other hand, estimated signals are smoother with the proposed method compared to NPEKF.

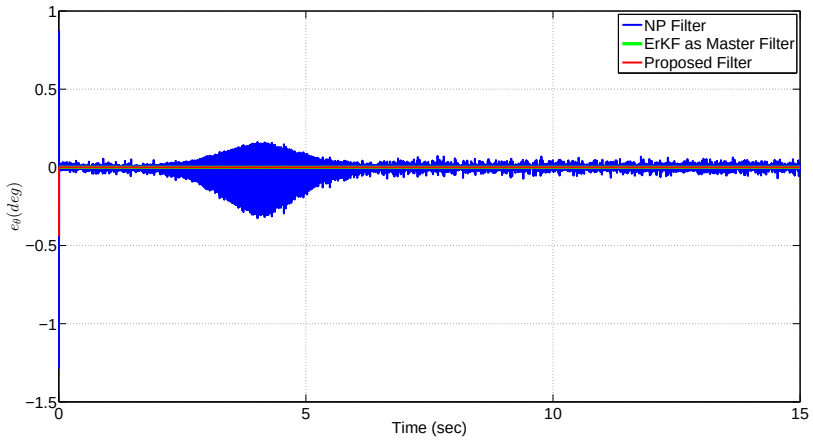

Figure 38: Error between measured and estimated pitch angles.

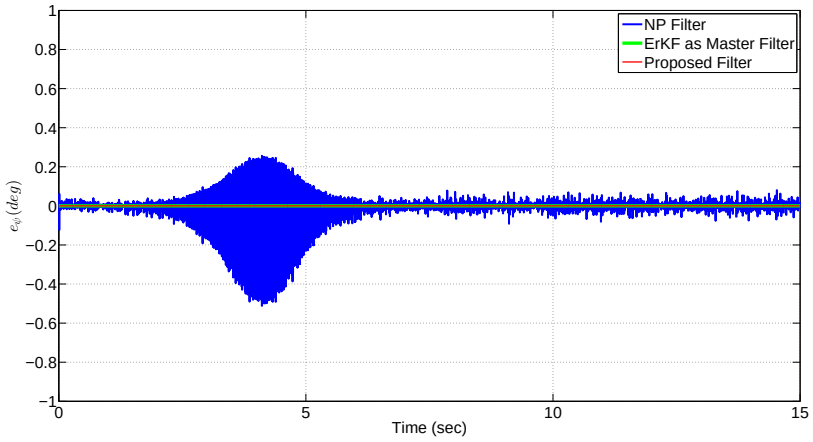

Figure 39: Error between measured and estimated yaw angles.

7.2.2 Second Scenario

The performance of the proposed filter is compared to the Newton predictor and the error state Kalman filter when the disturbances are applied on the system. Estimated pitch and yaw angles are provided in Figures 44 and 45. Similar to the case of the first scenario, estimated pitch and yaw angles by the proposed method and the fusion algorithm in which the master filter is implemented as ErKF, are almost the same. On the other hand, better estimation performance is achieved with the

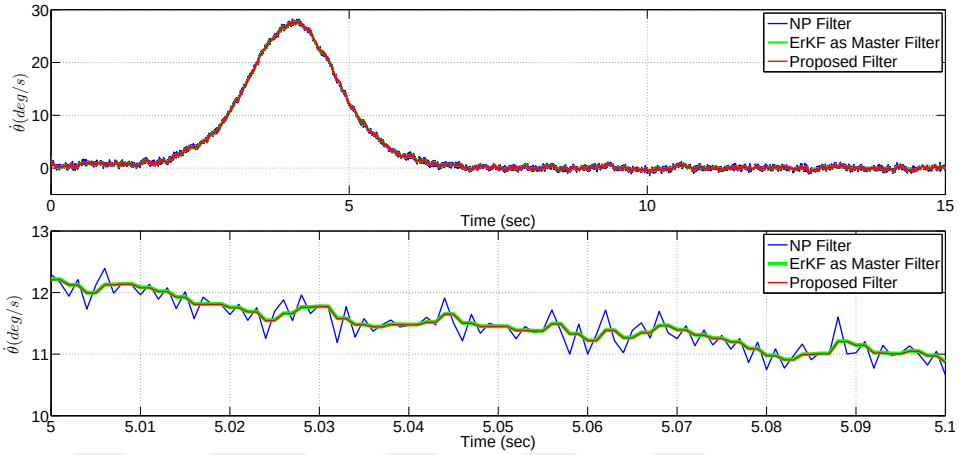

Figure 40: Comparison between estimated pitch velocities.

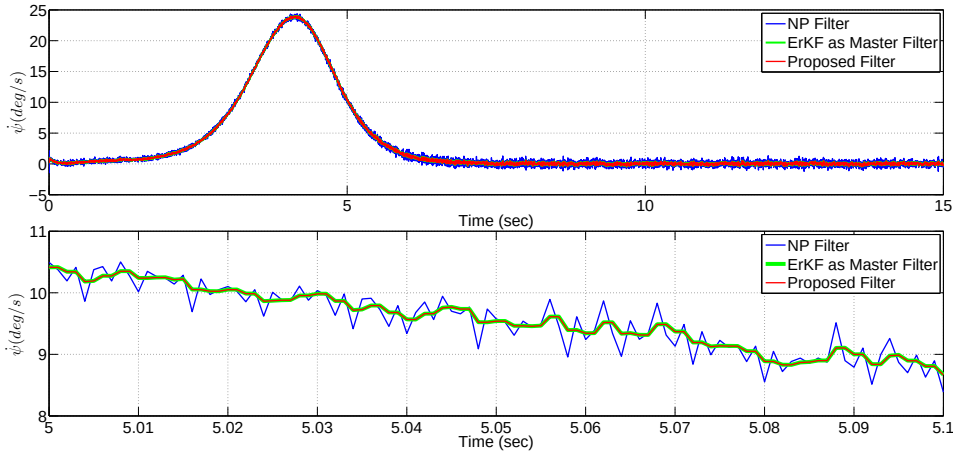

Figure 41: Comparison between estimated yaw velocities.

proposed filter compared to NPEKF because the proposed one provides smoother estimates than NPEKF. Newton predictor leads to high amplitude peaks in estimated pitch and yaw angles. Figures 46 and 47 also depict the errors between measured and estimated pitch and yaw angles. Estimation errors that are obtained by designing the master filter as either EKF or ErKF are similar. Those errors are also smaller than the ones computed with NPEKF. While RMS value of the pitch angle estimation error is 0.0481 *deg* for NPEKF, this RMS value decreases to 9.63×10^{-6} *deg* as the proposed method is utilized. On the other hand, RMS

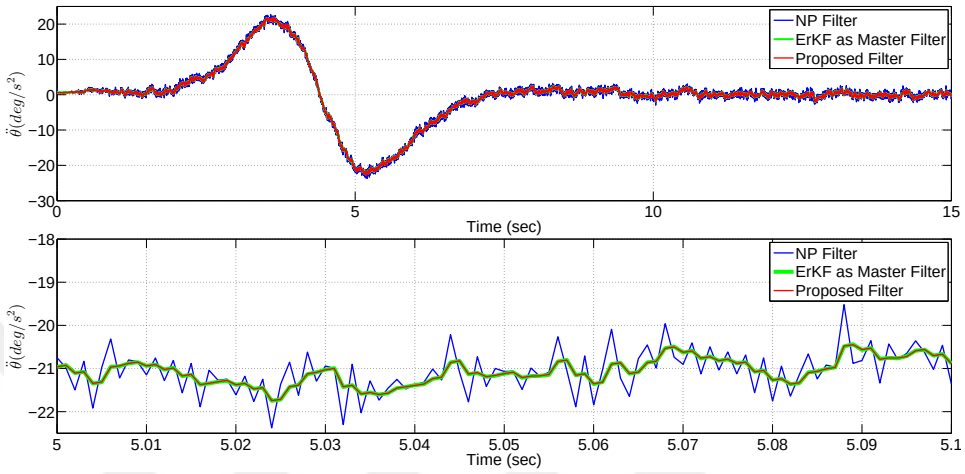

Figure 42: Comparison between estimated pitch accelerations.

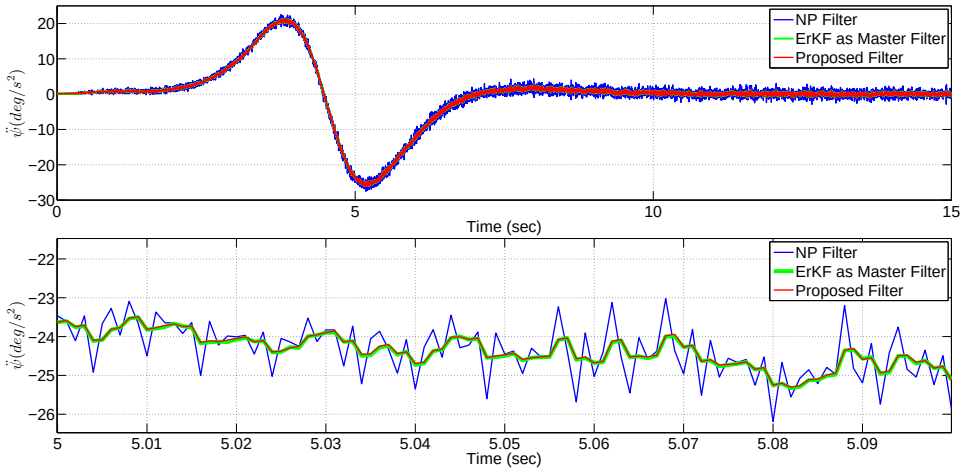

Figure 43: Comparison between estimated yaw accelerations.

values of the yaw angle estimation errors are 2.05×10^{-7} *deg* and 0.0483 *deg* for the proposed filter and NPEKF, respectively. Estimated pitch and yaw velocities and accelerations are also presented in Figures 48-51. Similar velocities and accelerations are estimated by the proposed method and the fusion algorithm where the master estimator is implemented as ErKF. However, estimated signals by NPEKF have much more noise than the proposed filter. When the disturbances are applied on the system, oscillations occur in all estimated velocity and acceleration signals

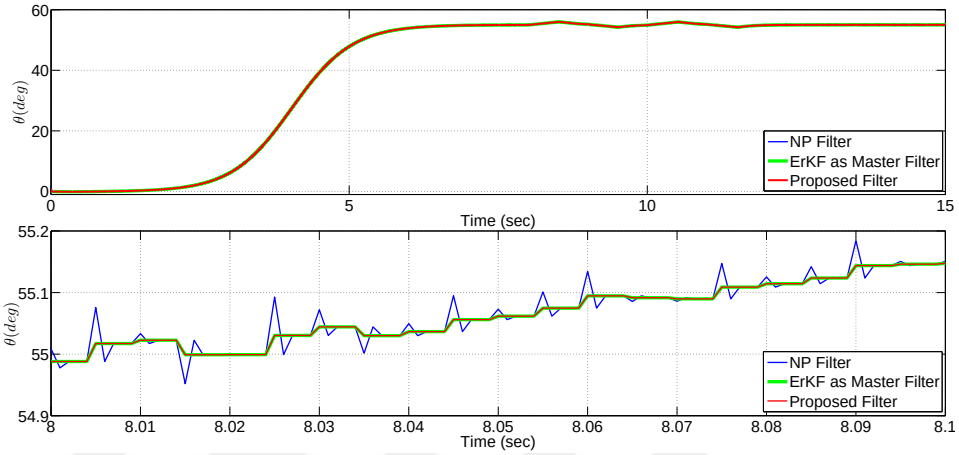

Figure 44: Comparison between estimated pitch angles.

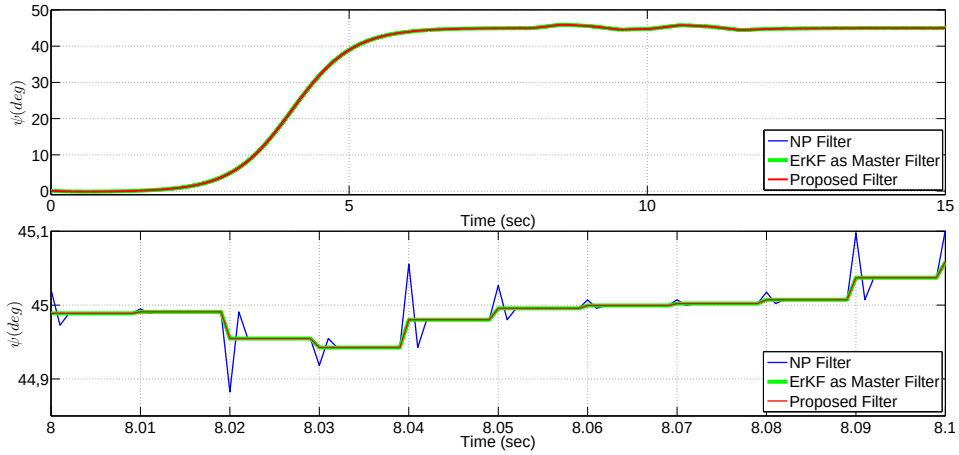

Figure 45: Comparison between estimated yaw angles.

between $t = 8$ *sec* and $t = 12$ *sec*, but the amplitudes of those oscillations are larger with NPEKF.

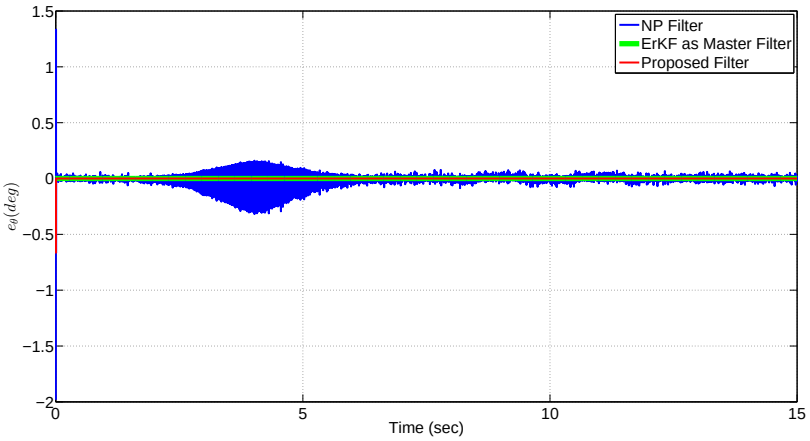

Figure 46: Error between measured and estimated pitch angles.

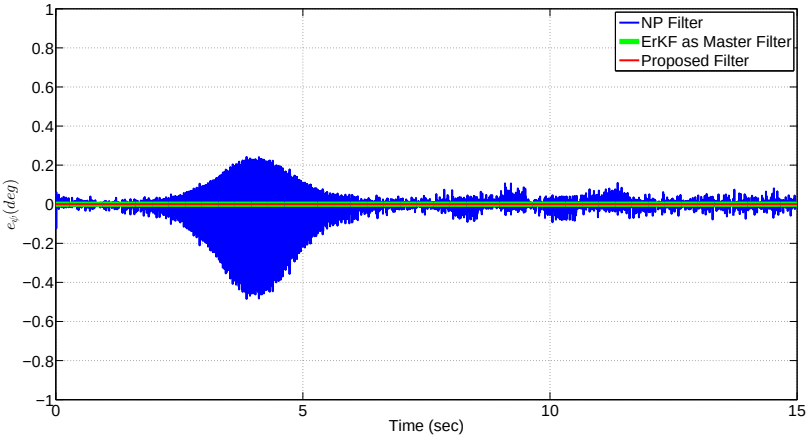

Figure 47: Error between measured and estimated yaw angles.

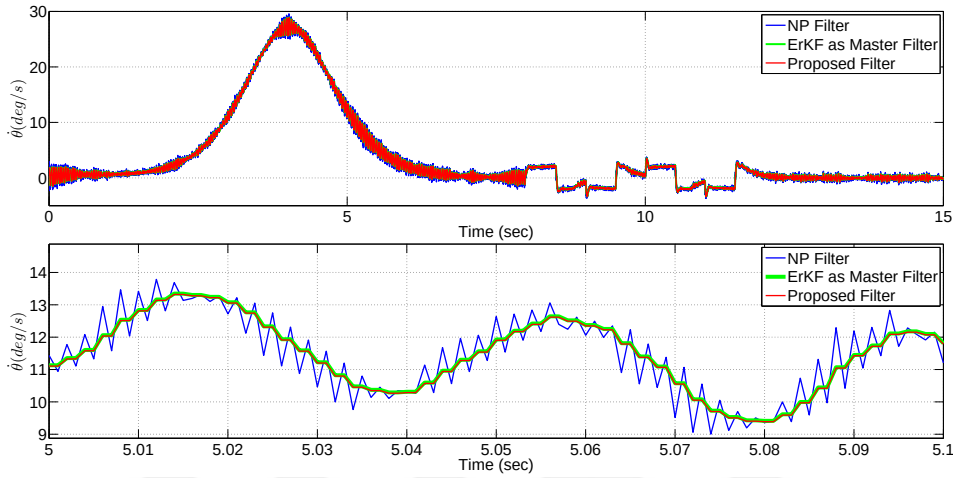

Figure 48: Comparison between estimated pitch velocities.

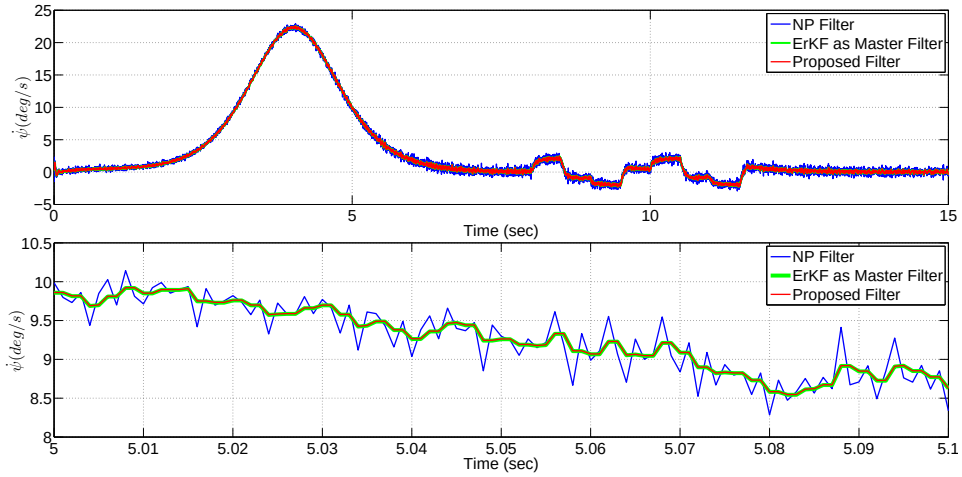

Figure 49: Comparison between estimated yaw velocities.

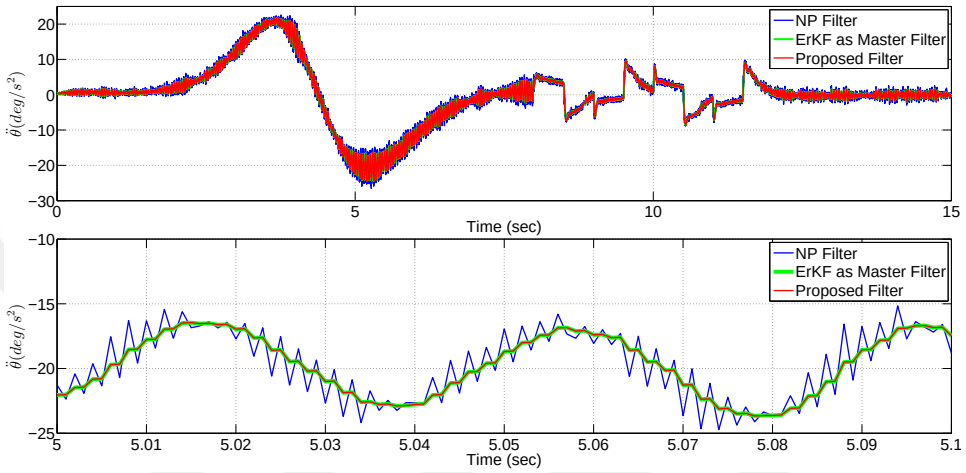

Figure 50: Comparison between estimated pitch accelerations.

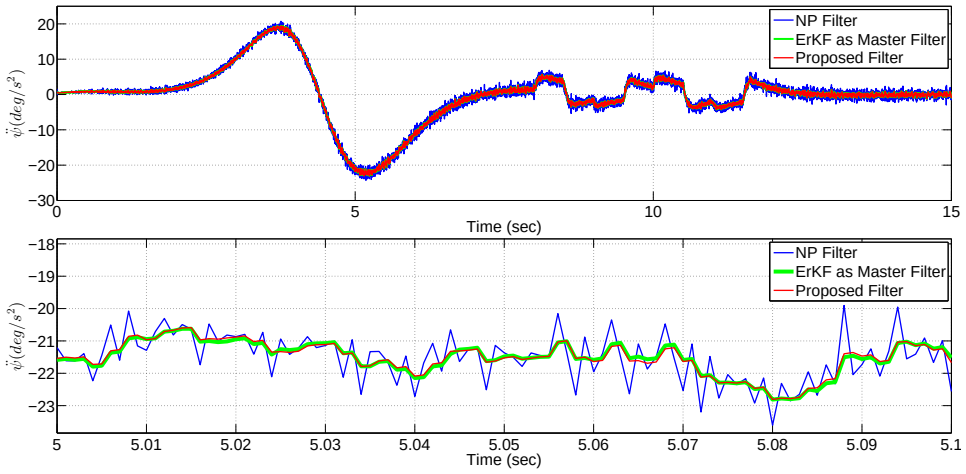

Figure 51: Comparison between estimated yaw accelerations.

7.3 Results of the Acceleration Based LQR Control

The physical constraints that are applied to the joints are as follow:

Table 2: Physical Constraints

Parameter	Minimum Value	Maximum Value
q_1	$-170°$	$170°$
q_2	$-85°$	$85°$
$\dot{q}_1$	$-150°/sec$	$150°/sec$
$\dot{q}_2$	$-50°/sec$	$50°/sec$

Using the physical constraint given in Table 2, scheduling position trajectories are designed as quintic polynomials in Figure 52. Since the position trajectories are designed as 5th degree polynomials, joint velocity and acceleration trajectories are 4th and 3rd degree polynomials as shown in Figures 53 and 54.

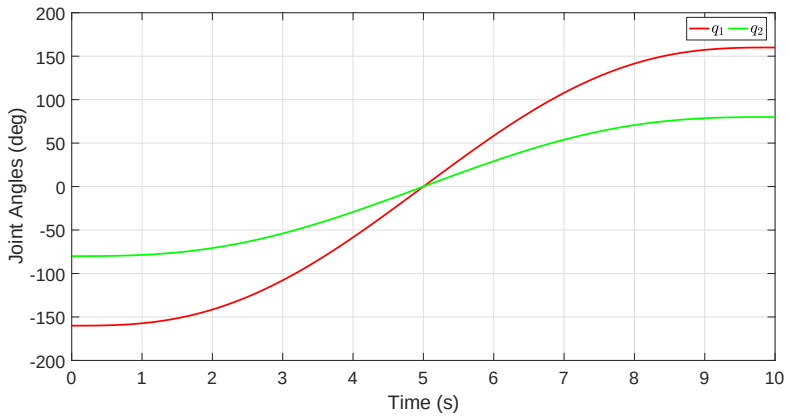

Figure 52: Scheduling joint position signals

The parameter trajectories, σ_j, are generated based on (5.16) in Figures 55-58. σ_1 and σ_3 depend on q_2 and $\dot{q}_1$. On the other hand, σ_2 and σ_4 are the function of only q_2. Due to this dependency, the parameter values have the upper and lower bounds given in Table 3.

External disturbances shown in Figure 59 are applied on the system after the desired positions are reached. These disturbances are modeled as high amplitude step pulses with short durations. The amplitudes of the step pulses are assumed as 10 $N.m$ and 15 $N.m$. The performance of the proposed controller in (5.28) is

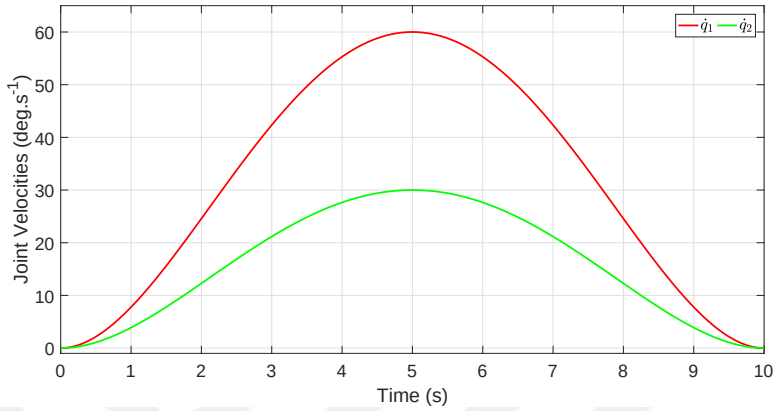

Figure 53: Scheduling joint velocity signals

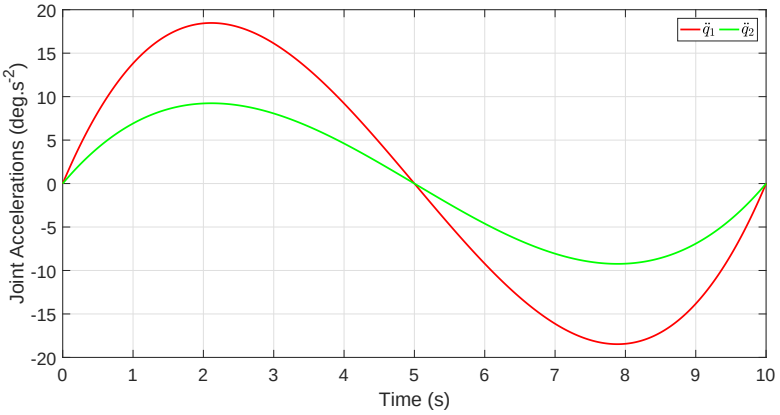

Figure 54: Scheduling joint acceleration signals

compared with the performance of the classical LQR controller in (5.20).

LQR controller is synthesized based on the developed polytopic quasi-LPV model in (5.18)-(5.19). The total number of vertices is $L = 2^4 = 16$. The proposed state feedback controller given in (5.28) is designed by interpolating LMIs at each vertex. The elements of the state feedback gain matrix, K, K_1 and K_2 are designed

Table 3: Upper and Lower Bounds of the Parameter Vector

Parameter		**Upper Bound**	**Lower Bound**
σ_1	$(rad.sec^{-1})$	0.4225	-0.4225
σ_2	$(rad.sec^2)^{-1}$	-1.2812	-14.7
σ_3	$(unitless)$	1.4405	-1.4405
σ_4	$(kg.m^2)^{-1}$	1.2581	0.7059

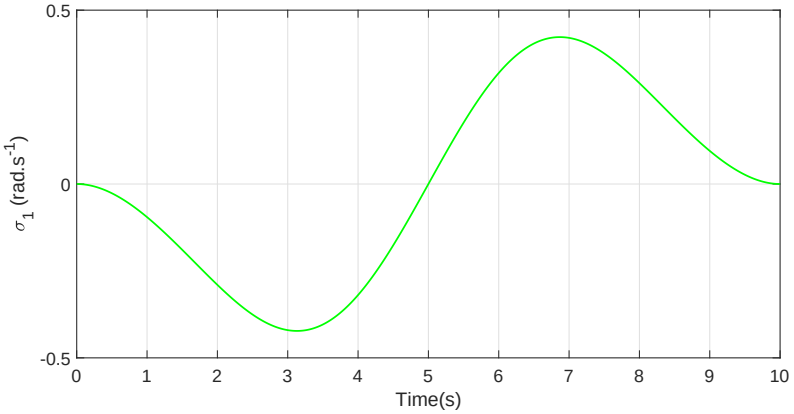

Figure 55: Parameter trajectory: σ_1

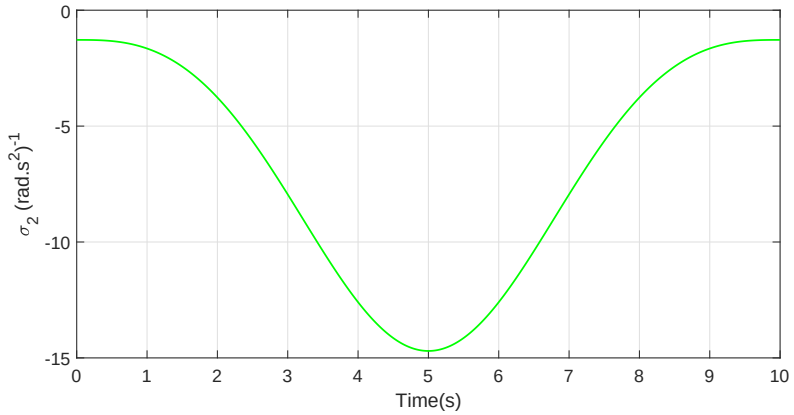

Figure 56: Parameter trajectory: σ_2

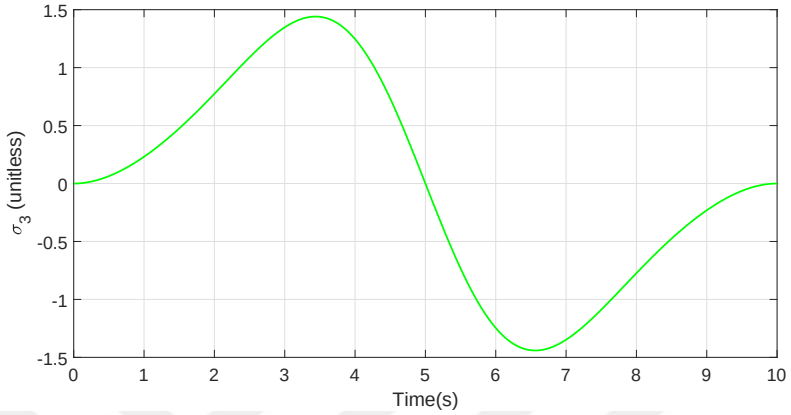

Figure 57: Parameter trajectory: σ_3

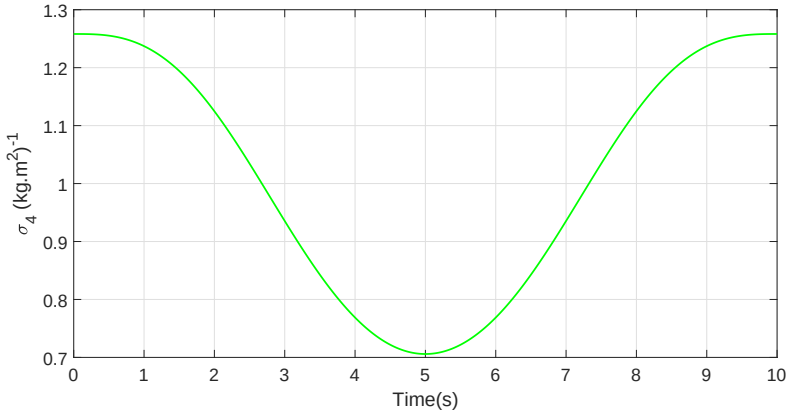

Figure 58: Parameter trajectory: σ_4

based on the weighting matrices, Q, Q_1, Q_2 and R given by (7.1) and (7.2).

$$Q = Q_1 = \begin{bmatrix} 1 & 0 & 0 & 0 & 0 & 0 \\ 0 & 1 & 0 & 0 & 0 & 0 \\ 0 & 0 & 1 & 0 & 0 & 0 \\ 0 & 0 & 0 & 1 & 0 & 0 \\ 0 & 0 & 0 & 0 & 5 & 0 \\ 0 & 0 & 0 & 0 & 0 & 5 \end{bmatrix}, \quad R = \begin{bmatrix} 0.001 & 0 \\ 0 & 0.01 \end{bmatrix} \tag{7.1}$$

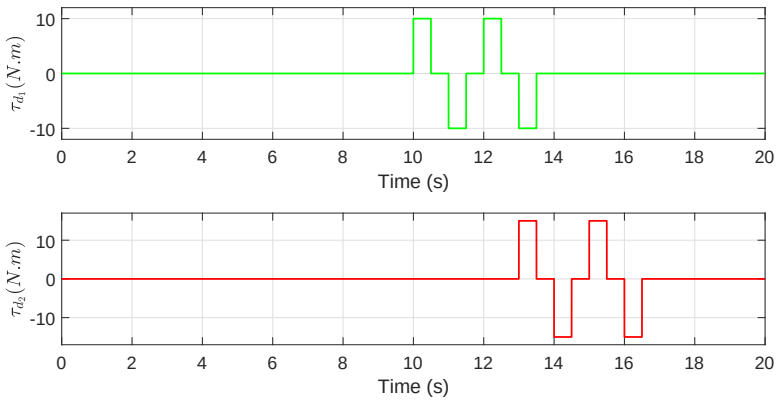

Figure 59: External disturbances on the pan and tilt axes

$$Q_2 = \begin{bmatrix} 0.001 & 0 & 0 & 0 & 0 & 0 \\ 0 & 0.001 & 0 & 0 & 0 & 0 \\ 0 & 0 & 100 & 0 & 0 & 0 \\ 0 & 0 & 0 & 100 & 0 & 0 \\ 0 & 0 & 0 & 0 & 0.001 & 0 \\ 0 & 0 & 0 & 0 & 0 & 0.001 \end{bmatrix} \tag{7.2}$$

More weighting is added to the integral of the position errors than the other states in Q_1 to eliminate the steady state error. R limits the amplitude of the control input and the elements of the matrix R are designed smaller than the elements of Q_1 matrix. This makes the system sensitive to the states of the system instead of the control input. As it is previously mentioned in Chapter 5, there is a redundancy in the controller due to common velocity terms in z and $\dot{z}$. This redundancy is eliminated by choosing the elements of Q_2 are small, i.e. $Q_{2_{11}} = Q_{2_{22}} = Q_{2_{55}} = Q_{2_{66}} = 0.001$.

Using the system model (5.18)-(5.19) and the weighting matrices in (7.1) and (7.2), the optimal feedback gain matrices, K, K_1, $K_2 \in R^{2\times 6}$, obtained by YALMIP is given in (7.3)-(7.5).

$$K = \begin{bmatrix} -81.5 & -7.8\times10^{-11} & -36.2 & -3.6\times10^{-12} & 75.8 & 1.9\times10^{-12} \\ -1\times10^{-11} & -27.7 & -8.8\times10^{-12} & -10.6 & 1.7\times10^{-11} & 24.7 \end{bmatrix} \tag{7.3}$$

$$K_1 = \begin{bmatrix} -88.3 & -3.4\times10^{-11} & -36.5 & -1.2\times10^{-12} & 85.4 & -5.6\times10^{-11} \\ -3.7\times10^{-9} & -30.6 & -3.7\times10^{-10} & -10.6 & 2.2\times10^{-8} & 29.7 \end{bmatrix} \tag{7.4}$$

$$K_2 = \begin{bmatrix} -135.8 & -2.7\times10^{-10} & -23.9 & -2.2\times10^{-11} & 384.3 & 5.8\times10^{-9} \\ -3.7\times10^{-9} & -24.3 & -3.7\times10^{-10} & -3 & 2.19\times10^{-8} & 105.6 \end{bmatrix} \tag{7.5}$$

The performance of the controller is tested on the nonlinear pan-tilt system. Initial joint angles are assumed as 150 deg and 75 deg. The desired angles are $r_1 = 65\,deg$ and $r_2 = 15\,deg$. Joint angles converge to reference values as depicted in Figure 60. Joint velocities converge to zero in Figure 61. Higher amplitude oscillations are obtained in all transient responses with the classical controller. As the external disturbances are applied on the system, acceleration feedback improves the system responses compared to the case where the acceleration feedback is not used in the controller.

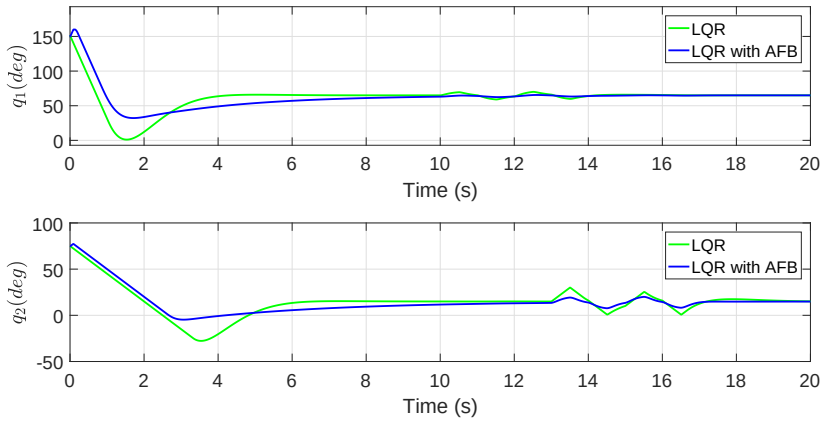

Figure 60: Output joint angles

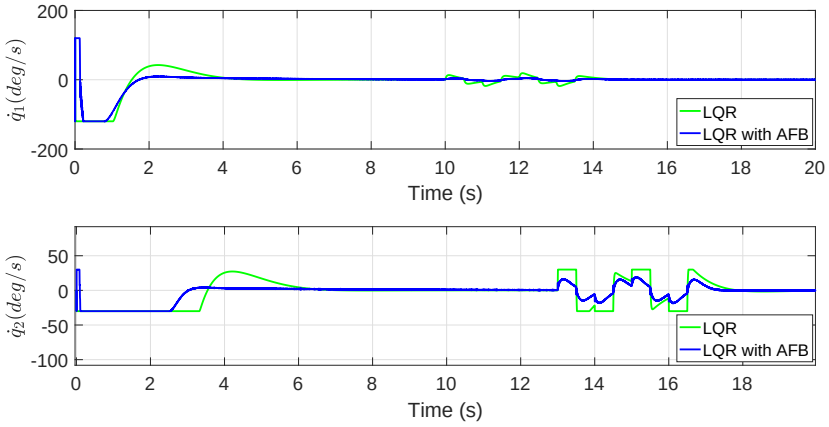

Figure 61: Output joint velocities

The performance specifications given in Tables 4 and 5 also show that the proposed controller outperforms the classical LMI based LQR controller.

Table 4: Pan Axis Performance Specification

Transient Responses ($t = 1 - 10$ *sec*)		
Performance Criteria	Proposed Controller	Classical Controller
Absolute Worst Case Position Error (deg)	20.55	55.08
RMS Position Error (deg)	19.30	20.38
RMS Control Input (N.m)	5.35	3.62
System Responses During Disturbances		
Performance Criteria	Proposed Controller	Classical Controller
Absolute Worst Case Position Error (deg)	1.28	4.92
RMS Position Error (deg)	2.64	3.27
RMS Control Input (N.m)	7.14	7.35

Table 5: Tilt Axis Performance Specification

Transient Responses ($t = 1 - 10$ *sec*)		
Performance Criteria	Proposed Controller	Classical Controller
Absolute Worst Case Position Error (deg)	20.51	23.96
RMS Position Error (deg)	8.77	9.13
RMS Control Input (N.m)	4.40	4.16
System Responses During Disturbances		
Performance Criteria	Proposed Controller	Classical Controller
Absolute Worst Case Position Error (deg)	5.42	20.27
RMS Position Error (deg)	3.71	12.37
RMS Control Input (N.m)	7.74	7.27

7.4 Results of the Hybrid Acceleration Based Learning-Adaptive Controller

The performance of the developed hybrid learning based adaptive controller given in (6.69)-(6.72) is evaluated on the pan-tilt platform and compared with the performance of the hybrid learning based adaptive controller where reliable accelerations are used as feedback in only adaptive controller, not the learning controller. The desired trajectories which are presented in Figure 62 are generated based on the following periodic functions:

$$\begin{bmatrix} q_{d_1} \\ q_{d_2} \end{bmatrix} = \begin{bmatrix} (2 + 0.2\sin(t))(\sin(\sin(t)))(1 + e^{-0.6t^3}) \\ (1 + 0.2\sin(t))(\sin(\sin(t)))(1 + e^{-0.6t^3}) \end{bmatrix} \tag{7.6}$$

with a period of $T = 6.28\,sec$ and the exponential term is used to provide a "smooth-start" to the system. The controller gains are tuned as follows:

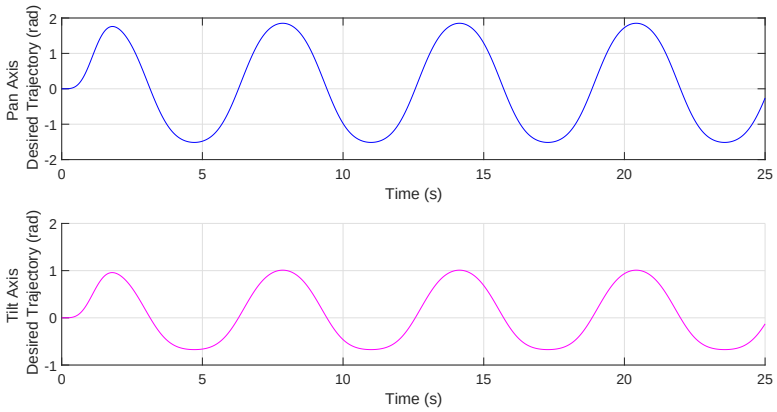

Figure 62: Desired trajectories

$$\Gamma_1 = \begin{bmatrix} 20 & 0 \\ 0 & 14 \end{bmatrix},\ \Lambda = \begin{bmatrix} 40 & 0 \\ 0 & 12 \end{bmatrix}$$

$$K_1 = \begin{bmatrix} 30 & 0 \\ 0 & 10 \end{bmatrix},\ K_2 = \begin{bmatrix} 0.01 & 0 \\ 0 & 0.01 \end{bmatrix},\ \Upsilon_h = 20I_{4\times 4}$$

Position and filtered errors reduce after each period of the desired trajectory and globally asymptotically converge to zero as depicted in Figures 63 and 64. Sudden peaks occur in the position errors due to the integration of discontinues created by signum functions in the static frictions terms of the dynamic model given in (4.1).

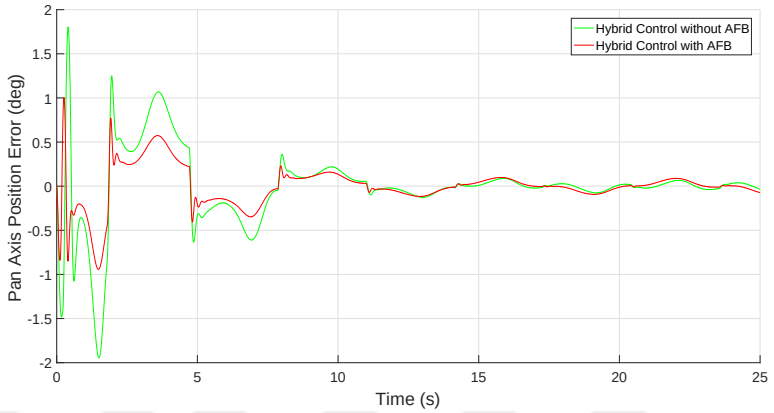

Figure 63: Pan axis position error, $e_1(t)$

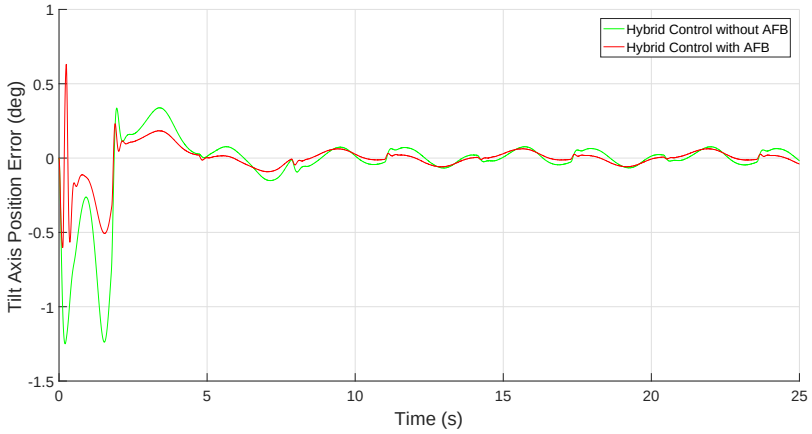

Figure 64: Tilt axis position error, $e_2(t)$

Figures 65-68 depict the torque control inputs and the learning feedforward control inputs. Due to the desired periodic trajectories, control inputs oscillate to reject the unknown periodic disturbances. The proposed controller outperforms the hybrid controller without acceleration feedback as shown in Tables 6 and 7.

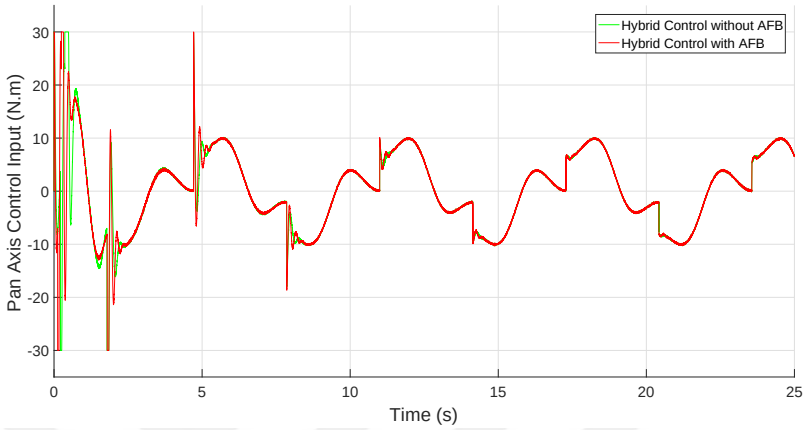

Figure 65: Pan axis control input, $\tau_1(t)$

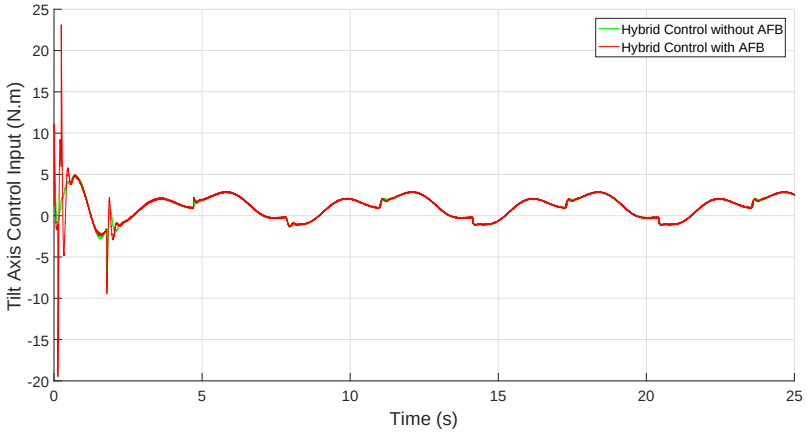

Figure 66: Tilt axis control input, $\tau_2(t)$

Table 6: Pan Axis Performance Specification

Performance Criteria	Proposed Controller	Hybrid Controller without AFB
Absolute Worst Case Position Error (deg)	1.0052	1.9450
RMS Position Error (deg)	0.2275	0.4213
RMS Control Input (N.m)	7.4996	7.4731

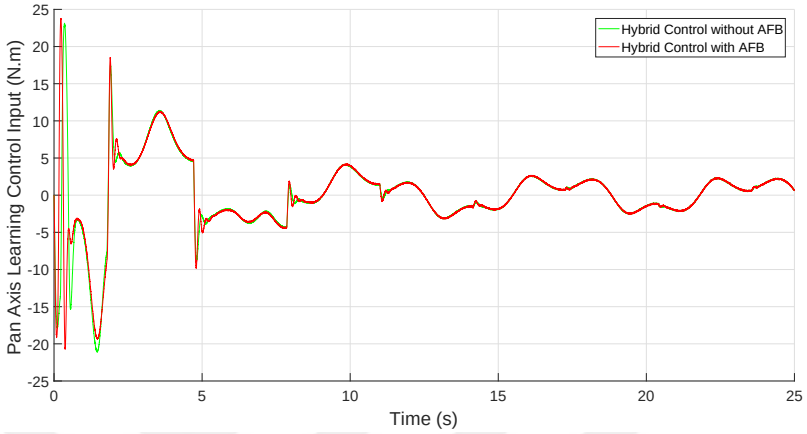

Figure 67: Pan axis learning feedforward control, $\vartheta_1(t)$

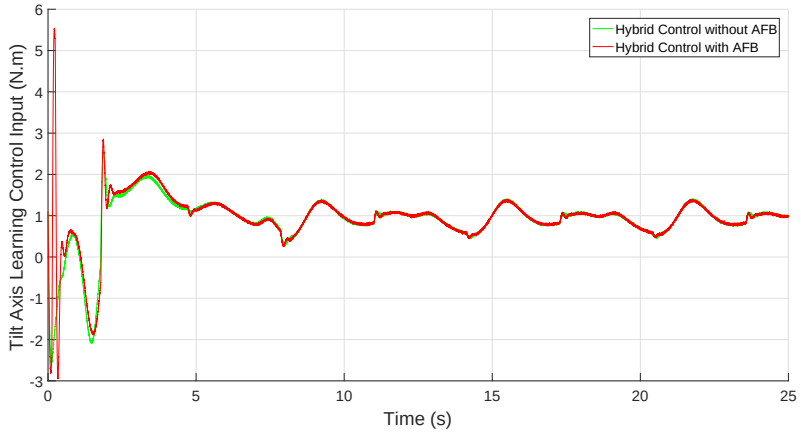

Figure 68: Tilt axis learning feedforward control, $\vartheta_2(t)$

Table 7: Tilt Axis Performance Specification

Performance Criteria	Proposed Controller	Hybrid Controller without AFB
Absolute Worst Case Error (deg)	0.6305	1.2496
RMS Error (deg)	0.1072	0.2372
RMS Control Input (N.m)	2.0086	1.8094

Static friction coefficients are satisfactorily estimated by the adaptive controller. Estimated values of the static friction parameters approximately converge to 3.1 Nm and 0.4 Nm as depicted in Figures 69 and 70. Motor moment of inertias are estimated as 2.7 $kg.m^2$ and 1.5 $kg.m^2$ as shown in Figures 71 and 72.

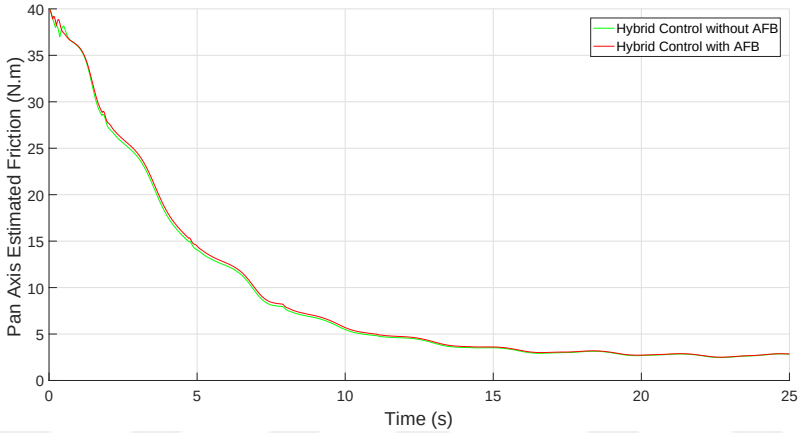

Figure 69: Pan axis estimated friction parameter, $\hat{f}_{s_1}$

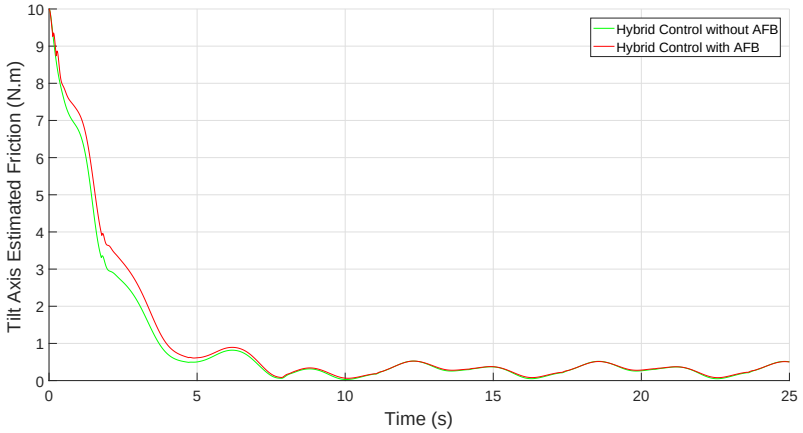

Figure 70: Tilt axis estimated friction parameter, $\hat{f}_{s_2}$

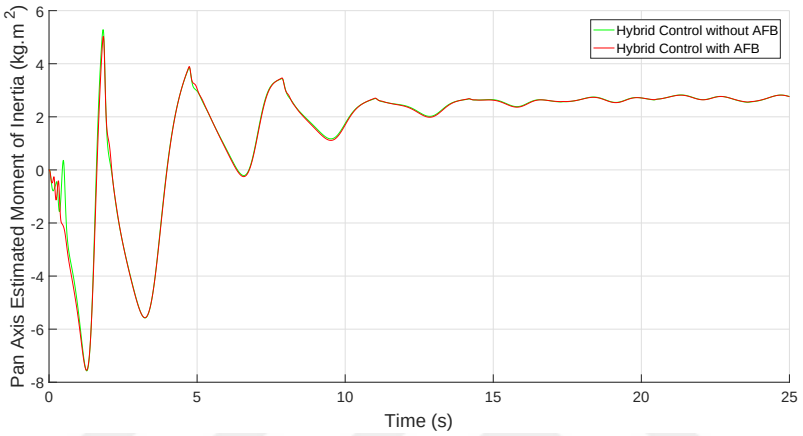

Figure 71: Pan axis estimated moment of inertia, $\hat{J}_{m_1}$

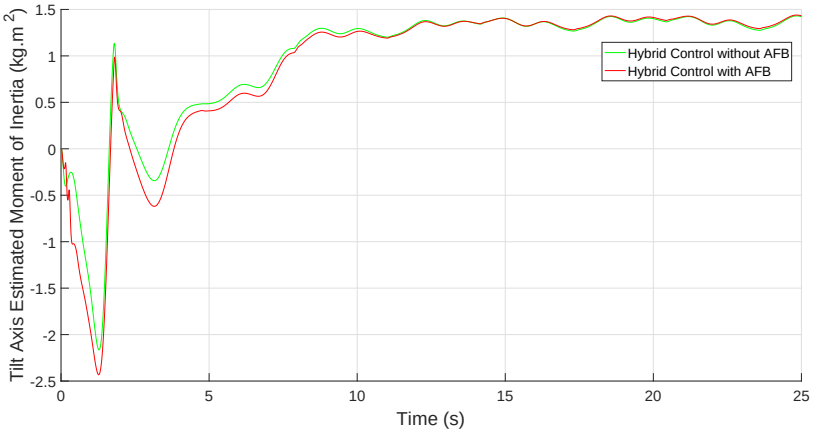

Figure 72: Tilt axis estimated moment of inertia, $\hat{J}_{m_2}$

Chapter 8

8 Conclusions

This thesis investigates the role of acceleration feedback in various stabilization and periodic trajectory tracking control algorithms to minimize effects of external disturbances and parameter uncertainties. Since obtaining reliable acceleration feedback signals is a challenging task, the work in this thesis has focused on estimating reliable acceleration signals from an IMU or an encoder. In order to tackle this problem, a novel master-slave Kalman filter algorithm and a cascaded high gain observer structure are developed.

The master-slave Kalman filter estimates reliable Euler velocity and acceleration signals in addition to Euler angles. Slave estimator based on the inverse Φ-algorithm estimates angular velocities, accelerations and jerks. When these estimates are used in the master estimator, Euler angles, velocities and accelerations are estimated. The stabilization performance of a pan-tilt system is assessed by using estimated Euler angles, velocities and accelerations in a high fidelity simulation model for two different disturbance scenarios. In the first scenario, the pan-tilt platform is subject to random and continuous time varying disturbances whereas step disturbances in the form of short duration pulses with relatively large amplitudes are applied to the system in the second scenario. In the first scenario, azimuth angle converges in a smooth way by utilizing acceleration controller whereas small steady state errors are observed in the elevation angle with the use of acceleration feedback. The amplitudes of the torque control inputs are almost the same with or without the use of acceleration feedback. Thus, acceleration control provides better performance without larger control efforts. Due to the step pulses in the second scenario, system responses have high amplitude oscillations when the acceleration controller is not active. As the acceleration feedback is introduced, the external disturbances are successfully rejected and much smoother responses are achieved. Although high control efforts were spent when the step pulses were exerted on the system, the system could not be stabilized without the acceleration controller. The performance of the proposed sensor fusion algorithm was compared to the Newton predictor enhanced Kalman filter (NPEKF) and the error state Kalman filter (ErKF) in both scenarios. Estimated angle, velocity and acceleration signals by the

proposed master-slave Kalman filter and the fusion algorithm in which the master estimator is implemented as ErKF, are similar to each other. On the other hand, the proposed method outperforms NPEKF. The Newton predictor leads to much more noisy estimates and has the largest estimation errors compared with the other methods.

A polytopic quasi-LPV model of the nonlinear pan-tilt system has been derived to synthesize acceleration based LMI-LQR controller for the pan-tilt stabilization. Acceleration signals are estimated by a new high gain observer structure where two different observers are employed in a cascaded structure. The first HGO uses position measurements from an encoder to estimate reliable position and velocity information. The second HGO, on the other hand, utilizes velocities estimated by the first HGO to provide estimates of acceleration signals. Obtained estimates by the proposed HGO are used in the proposed LMI-LQR controller. The feedback gain matrix is designed by interpolating LMIs at each vertex of the polytopic model. Step pulses are exerted on the system to compare the performance of the proposed LMI-LQR controller with the classical one. During the application of disturbances on the nonlinear system, the amplitude of oscillations gets smaller as acceleration feedback is utilized in optimal LQR controller.

This thesis also develops a novel hybrid control method by combining acceleration based learning controller with an adaptive controller for the trajectory tracking in repetitive robotic tasks. The use of acceleration feedback in the learning control provides robustness to the system against unknown periodic disturbances with a known period. Adaptive controller, on the other hand, compensates for the uncertainties in the actuator moment of inertia terms and the static friction parameters. Integral of the position error is also included in the filtered error variable. The developed cascaded nonlinear high gain observer structure is utilized to estimate reliable position, velocity and acceleration signals from noisy encoder measurements. Lyapunov based stability analysis show that all system signals remain bounded, and the proposed controller ensures global asymptotic position tracking for a n-rigid link manipulator. The performance of the proposed hybrid controller is tested on a high fidelity simulation model of a pan-tilt platform and it has been found as quite satisfactory.

Appendix

A The Method of Petovello

The inverse Φ-algorithm assumes the following process and measurement models [119]:

$$x_k = A_{k-1}x_{k-1} + \Upsilon_{k-1}\epsilon_{k-1} \tag{A-1}$$

$$y_k = C_k x_k + \varepsilon_k \tag{A-2}$$

$$\varepsilon_k = \Psi_{k-1}\varepsilon_{k-1} + \varsigma_{k-1} \tag{A-3}$$

$$\Psi_{k-1} = e^{-\frac{T}{\kappa}}, \quad R_k = \sigma^2\left(I - \Psi_{k-1}^2\right) \tag{A-4}$$

$$E(\epsilon_k) = E(\varsigma_k) = 0 \tag{A-5}$$

$$E\left(\epsilon_k\epsilon_l^T\right) = Q_k\delta_{kl}, \quad E\left(\varsigma_k\varsigma_l^T\right) = R_k\delta_{kl}, \quad E\left(\epsilon_k\varsigma_l^T\right) = 0 \tag{A-6}$$

where A_{k-1} is the state transition matrix, C_k is the output matrix, ϵ_{k-1} and ς_{k-1} are the white Gaussian noises with zero means, ε_k is time correlated noise, $E(x)$ is the expectation of x, δ_{kl} is the Kronecker delta function, Q_k and R_k are the covariance matrices of ϵ_k and ς_k, Ψ_{k-1} is the transition matrix of the time correlated error, T is the sampling time, κ is the time constant, I is the identity matrix, and σ is the standart deviation.
Prediction stage of the inverse Φ-algorithm:

$$\hat{x}_{k/k-1} = A_{k-1}\hat{x}_{k-1/k-1} \tag{A-7}$$

$$P_{k/k-1} = A_{k-1}P_{k-1/k-1}A_{k-1}^T + Q_{k-1} \tag{A-8}$$

Update stage of the inverse Φ-algorithm:

$$K_k = \left[P_{k/k-1}\bar{C}_k^T + S_k\right]\left[\bar{C}_k P_{k/k-1}\bar{C}_k^T + \bar{R}_k + \bar{C}_k S_k + S_k^T\bar{C}_k^T\right]^{-1} \tag{A-9}$$

$$\hat{x}_{k/k} = \hat{x}_{k/k-1} + K_k\left[\bar{y}_k - \bar{C}_k\hat{x}_{k/k-1}\right] \tag{A-10}$$

$$P_{k/k} = P_{k/k-1} - K_k\left[\bar{C}_k P_{k/k-1}\bar{C}_k^T + \bar{R}_k + \bar{C}_k S_k + S_k^T\bar{C}_k^T\right]K_k^T \tag{A-11}$$

where

$$\bar{y}_k = y_k - \Psi_{k-1}y_{k-1} \tag{A-12}$$

$$\bar{C}_k = C_k - \Psi_{k-1}C_{k-1}A_{k-1}^{-1} \tag{A-13}$$

$$S_k = Q_{k-1}\Upsilon_{k-1}^T A_{k-1}^{-T}C_{k-1}^T\Psi_{k-1}^T \tag{A-14}$$

$$\bar{R}_k = \Psi_{k-1}C_{k-1}A_{k-1}^{-1}\Upsilon_{k-1}Q_{k-1}\Upsilon_{k-1}^T A_{k-1}^{-T}C_{k-1}^T\Psi_{k-1}^T + R_{k-1} \tag{A-15}$$

B Important Lemmas and Definitions

B.1 Leibniz's Rule

The Leibniz integral rule provides a formula for differentiation of a definite integral whose limits are functions of the differential variable. Let $f(x,t)$ be a function such that both $f(x,t)$ and its partial derivative $f_x(x,t)$ are continuous in x and t in some region of the (x,t)-plane, including $u(x) \leq t \leq v(x)$ and $x_0 \leq x \leq x_1$. Suppose that the functions $u(x)$ and $v(x)$ are both continuous and both have continuous derivatives for $x_0 \leq x \leq x_1$:

$$\frac{d}{dx}\int_{u(x)}^{v(x)} f(x,t)dt = f(v(x))\frac{dv}{dx} - f(u(x))\frac{du}{dx} + \int_{u(x)}^{v(x)} \frac{\partial}{\partial x} f(x,t)dt \tag{A-1}$$

that is the general form of the Leibniz integral rule.

B.2 Lemma 1

Given a nonnegative function denoted by $V(t) \in \mathbb{R}$ as follows [100]:

$$V = \frac{1}{2}x^2 \tag{A-2}$$

with the following time derivative

$$\dot{V} = -k_1 x^2 \tag{A-3}$$

then $x(t) \in \mathbb{R}$ is square integrable, i.e. $V(t) \in \mathcal{L}_2$.

Proof: If both sides of (A-3) is integrated, then the following is computed as

$$-\int_0^\infty \dot{V}(t)dt = k_1 \int_0^\infty x^2(t)dt \tag{A-4}$$

and

$$k_1 \int_0^\infty x^2(t)dt = V(0) - V(\infty) \tag{A-5}$$

It is known that $V(0) \geq V(\infty) \geq 0$ based on (A-2) and (A-3). Therefore, the following relationships are obtained:

$$k_1 \int_0^\infty x^2(t)dt = V(0) - V(\infty) \leq V(0) < \infty \tag{A-6}$$

$$\sqrt{\int_0^\infty x^2(t)dt} \leq \sqrt{\frac{V(0)}{k_1}} < \infty \tag{A-7}$$

Definition 1 in the next page is used to conclude that $x(t) \in \mathcal{L}_2$.

B.3 Definition 1

Consider a function $f(t) : \mathbb{R}_+ \rightarrow R$. Let the 2-norm (denoted by $\|\cdot\|$) of a scalar function f(t) be defined as [100]:

$$\|f(t)\| = \sqrt{\int_0^\infty f^2(\tau)d\tau} \tag{A-8}$$

If $\|f(t)\| < \infty$, then it can be said that the function $f(t)$ belongs to the subspace $\mathcal{L}_2$ of the space of all possible functions, i.e. $f(t) \in \mathcal{L}_2$.

B.4 Definition 2

Let the ∞-norm (denoted by $\|\cdot\|_\infty$) of $f(t)$ be defined as [100]:

$$\|f(t)\|_\infty = sup|f(t)| \tag{A-9}$$

If $\|f(t)\|_\infty < \infty$, then it can be said that the function $f(t)$ belongs to the subspace $\mathcal{L}_\infty$ of the space of all possible functions, i.e. $f(t) \in \mathcal{L}_\infty$.

B.5 Barbalat's Lemma

Consider a function $f(t) : \mathbb{R}_+ \rightarrow R$. If $f(t), \dot{f}(t) \in \mathcal{L}_\infty$, and $f(t) \in \mathcal{L}_2$, then

$$\lim_{t\rightarrow\infty} f(t) = 0 \tag{A-10}$$

This lemma is often referred to as Barbalat's Lemma [17] .

References

[1] I. Kaminer, A. Pascoal, E. Hallberg, and C. Silvestre, "Trajectory tracking for autonomous vehicles: An integrated approach to guidance and control," *Journal of Guidance, Control, and Dynamics*, Vol. 21, No. 1, pp. 29-38, 1998.

[2] F. N. Martins, W. C. Celeste, R. Carelli, M. Sarcinelli-Filho, T.F. Bastos-Filho, "An adaptive dynamic controller for autonomous mobile robot trajectory tracking," *Control Engineering Practice*, Vol. 16, No. 11, pp. 1354-1363, 2008.

[3] A. P. Aguiar and J. P. Hespanha, "Trajectory-tracking and path-following of underactuated autonomous vehicles with parametric modeling uncertainty," *IEEE Transactions on Automatic Control*, Vol. 52, No. 8, pp. 1362-1379, 2007.

[4] L. Menini and A. Tornambe, "Asymptotic tracking of periodic trajectories for a simple mechanical system subject to nonsmooth impacts," *IEEE Transactions on Automatic Control*, Vol. 47, No. 7, pp. 1122-1126, 2001.

[5] H. Wong and V. Kapila, "Adaptive learning control-based periodic trajectory tracking for spacecraft formations," IEEE Transactions on Decision and Control, 2003.

[6] M. Gomes and A. M. Ferreira, "Gun-turret modeling and control," 18th International Congress of Mechanical Engineering, 2005.

[7] P. Kumar, A. Dick, T. S. Sheng, "Real time target tracking with pan-tilt zoom camera," Digital Image Computing: Techniques and Applications, pp. 492-497, 2009.

[8] J. Davis and X. Chen, "Calibrating pan-tilt cameras in wide area surveillance networks," International Conference on Computer Vision, 2003.

[9] C. H. Lee, S. H. Kim, S. C. Kang, M. S. Kim, Y. K. Kwak, "Double-track mobile robot for hazardous environment applications," *Advanced Robotics*, Vol. 17, No. 5, pp. 447-459, 2003.

[10] S. Mahmoudzadeh and H. Mojallali, "An optimized PID for legless capsubots using modified imperialist competitive algorithm," International Conference on Robotics and Mechatronics, 2013.

[11] J. P. Ferreira, M. M. Crisostomo, A. P. Coimbra, "Adaptive PD controller modeled via support vector regression for a biped robot," *IEEE Transactions on Control Systems Technology*, Vol. 21, No. 3, pp. 941-949, 2012.

[12] R. J. Wai and R. Muthusamy, "Fuzzy-neural-network inherited sliding-mode control for robot manipulator including actuator dynamics," *IEEE Transactions on Neural Networks and Learning Systems*, Vol. 24, No. 2, pp. 274-287, 2013.

[13] D. Simon, **Optimal State Estimation: Kalman, H_∞, and Nonlinear Approaches**, John Wiley and Sons, New Jersey, 2006.

[14] P. R. Belanger, "Estimation of angular velocity and acceleration from shaft encoder measurements," IEEE International Conference on Robotics and Automation, 1992.

[15] A. Tilli and M. Montanari, "A low-noise estimator of angular speed and acceleration from shaft encoder measurements," *Automatika: Journal for Control, Measurement, Electronics, Computing and Communications*, Vol. 42, No. 3-4, pp. 169-176, 2001.

[16] R. J. E. Merry, M. J. G. Molengraft, M. Steinbuch, "Velocity and acceleration estimation for optical incremental encoders," *Mechatronics*, Vol. 20, No. 1, pp. 20-26, 2010.

[17] H. K. Khalil, **Nonlinear Systems**, Prentice-Hall, New Jersey, 2002.

[18] S. I. Roumeliotis, G. S. Sukhatme, G. A. Bekey, "Circumventing dynamic modeling: Evaluation of the error-state Kalman filter applied to mobile robot localization," *IEEE International Conference on Robot Localization*, 1999.

[19] S. Panich, "Indirect Kalman filter in mobile robot application," *Journal of Mathematics and Statistics*, Vol. 6, No. 3, pp. 381-384, 2010.

[20] R. E. Kalman, "New approach to linear filltering and prediction problems," *Journal of Basic Engineering*, Vol. 82, No. 1, pp. 35-45, 1960.

[21] M. R. Rajamani and J. B. Rawlings, "Estimation of the disturbance structure from data using semidefinite programming and optimal weighting," *Automatica*, Vol. 45, No. 1, pp. 142-148, 2009.

[22] O. J. Woodman, "An introduction to inertial navigation," Technical Report, University of Cambridge, Computer Laboratory, UCAMCL-TR-696, 2007.

[23] A. Edelstein, "Advances in magnetometry," *Journal of Physics: Condensed Matter*, Vol. 19, No. 16, 2007.

[24] A. Kim and M. F. Golnaraghi, "A quaternion-based orientation estimation algorithm using an inertial measurement unit," IEEE Position Location and Navigation Symposium, pp. 268-272, 2004.

[25] A. M. Sabatini, "Kalman filter based orientation determination using inertial/magnetic sensors: Observability analysis and performance evaluation," *Sensors*, Vol. 11, No. 10, pp. 9182-9206, 2011.

[26] W. Li and J. Wang, "Effective adaptive Kalman filter for MEMS-IMU/magnetometers integrated attitude and heading reference systems," *Journal of Navigation*, Vol. 66, No. 1, pp. 99-113, 2013.

[27] M. St-Pierre and D. Gingras, "Comparison between the unscented Kalman Filter and the extended Kalman filter for the position estimation module of an integrated navigation information system," IEEE Intelligent Vehicles Symposium, pp. 831-835, 2004.

[28] C. W. Tan and S. Park, "Design of accelerometer-based inertial navigation systems," *IEEE Transactions on Instrumentation and Measurement*, Vol. 54, No. 6, pp. 2520-2530, 2005.

[29] E. Edwan, S. Knedlik, O. Loffeld, "Constrained angular motion estimation in a gyro-free IMU," *IEEE Transactions on Aerospace and Electronic Systems*, Vol. 47, No. 1, pp. 596-610, 2011.

[30] E. Edwan, S. Knedlik, O. Loffeld, "Angular motion estimation using dynamic models in a gyro-free inertial measurement unit," *Sensors*, Vol. 12, No. 5, pp. 5310-5327, 2012.

[31] D. S. Bayard and S. R. Ploen, "High accuracy inertial sensors from inexpensive components," US Patent, US20030187623, 2003.

[32] H. Chang, L. Xue, W. Qin, G. Yuan, W. Yuan, "An integrated MEMS gyroscope array with higher accuracy output," *Sensors*, Vol. 8, No. 4, pp. 2886-2899, 2008.

[33] Q. M. Lam, T. Hunt, P. Sanneman, S. Underwood, "Analysis and design of a fifteen state stellar inertial attitude determination system," AIAA Guidance, Navigation and Control Conference, No. 5483, pp. 11-14, 2003.

[34] Z. Diao, H. Quan, L. Lan, Y. Han, "Analysis and compensation of MEMS gyroscope drift," The 7th International Conference on Sensing Technology, 2013.

[35] X. Ruan and M. Yu, "Modeling research of MEMS gyro drift based on Kalman filter," The 26th Chinese Control and Decision Conference, pp. 2949-2952, 2014.

[36] K. Bikonis and J. Demkowicz, "Data integration from GPS and inertial navigation systems for pedestrians in urban area," *The International Journal on Marine Navigation and Safety of Sea Transportation*, Vol. 7, No. 3, pp. 401-406, 2013.

[37] J. A. Rios and E. White, "Fusion filter algorithm enhancements for a MEMS GPS/IMU," Proceedings of the 14th International Technical Meeting of the Satellite Division of the Institute of Navigation, pp. 1382-1393, 2001.

[38] P. Zhang, J. Gu, E. E. Milios, P. Huynh, "Navigation with IMU/GPS/digital compass with unscented Kalman filter," IEEE International Conference Mechatronics and Automation, 2005.

[39] E. Nebot and H. D. Whyte, "Initial calibration and alignment of low-cost inertial navigation units for land vehicle applications," *Journal of Robotic Systems*, Vol. 16, No. 2, pp. 81-92, 1999.

[40] F. Caron, E. Duflos, D. Pomorski, P. Vanheeghe, "GPS/IMU data fusion using multisensor Kalman filtering: Introduction of contextual aspects," *Information Fusion*, Vol. 7, No. 2, pp. 221-230, 2006.

[41] R. Mahony, T. Hamel, J. M. Pflimlin, "Nonlinear complementary filters on the special orthogonal group," *IEEE Transactions on Automatic Control*, Vol. 53, No. 5, pp. 1203-1218, 2008.

[42] E. R. Bachmann, R. B. McGhee, X. Yun, M. J. Zyda, "Inertial and magnetic posture tracking for inserting humans into networked virtual environments," Proceedings of the ACM Symposium on Virtual Reality Software and Technology, pp. 9-16, 2001.

[43] S. O. H. Madgwick, A. J. Harrison, R. Vaidyanathan, "Estimation of IMU and MARG orientation using a gradient descent algorithm," IEEE International Conference on Rehabilitation Robotics, 2011.

[44] H. K. Khalil and A. Saberi A, "Adaptive stabilization of a class of nonlinear systems using high-gain feedback," *IEEE Transactions on Automatic Control*, Vol. 32, No. 11, pp. 1031-1035, 1987.

[45] A. Tornambe, "Use of asymptotic observers having high gains in the state and parameter estimation," IEEE Conference on Decision and Control, 2002.

[46] F. Esfandiari and H. K. Khalil, "Observer-based design of uncertain systems: Recovering state feedback robustness under matching conditions," Proceedings of Allerton Conference, 1987.

[47] J. P. Gauthier, H. Hammouri, S. Othman, "A simple observer for nonlinear systems application to bioreactors," *IEEE Transactions on Automatic Control*, Vol. 37, No. 6, pp. 875-880, 1992.

[48] G. Besançon, "High-gain observation with disturbance attenuation and application to robust fault detection," *Automatica*, Vol. 39, No. 6, pp. 1095-1102, 2003.

[49] H. Hammouri, B. Targui, F. Armanet, "High-gain observer based on a triangular structure," *International Journal of Robust and Nonlinear Control*, Vol. 12, No. 6, pp. 497-518, 2002.

[50] F. Esfandiari and H. K. Khalil, "Output feedback stabilization of fully linearizable systems," *International Journal of Control*, Vol. 56, No. 5, pp. 1007-1037, 1991.

[51] V. N. Polotskiy, "On the maximal errors of an asymptotic state identifier," *Automation and Remote Control*, Vol. 39, No. 8, pp. 1116-1121, 1979.

[52] A. Teel and L. Praly, "Global stabilizability and observability imply semiglobal stabilizability by output feedback," *System and Control Letters*, Vol. 22, No. 5, pp. 313-325, 1994.

[53] A. Teel and L. Praly, "Tools for semiglobal stabilization by partial state and output feedback," *SIAM Journal on Control and Optimization*, Vol. 33, No. 5, pp. 1443-1488, 1995.

[54] A. Tornambe, "Output feedback stabilization of a class of nonminimum-phase nonlinear systems," *System and Control Letters*, Vol. 19, No. 3, pp. 193-204, 1992.

[55] A. N. Atassi and H. K. Khalil, "A separation principle for the stabilization of a class of nonlinear systems," *IEEE Transactions on Automatic Control*, Vol. 44, No. 9, pp. 1672-1687, 1999.

[56] C. I. Byrnes, F. Celani, A. Isidori, "Omega-limit sets of a class of nonlinear systems that are semiglobally practically stabilized," *International Journal of Robust and Nonlinear Control*, Vol. 15, No. 7, pp. 315-333, 2005.

[57] L. Imsland, R. Findeisen, E. Bullinger, F. Allgower, B. A. Foss, "A note on stability, robustness and performance of output feedback nonlinear model predictive control," *Journal of Process Control*, Vol. 13, No. 7, pp. 633-644, 2003.

[58] M. Maggiore and K. Passino, "Output feedback tracking: A separation principle approach," *IEEE Transactions on Automatic Control*, Vol. 50, No. 1, pp. 111-117, 2005.

[59] P. B. Schmidth and R. D. Lorenz, "Design principles and implementation of acceleration feedback to improve performance of DC drives," *IEEE Transactions on Industry Applications*, Vol. 28, No. 3, pp. 594-599, 1992.

[60] J. Deur and N. Peric, "A compative study of servosystems with acceleration feedback," IEEE Industrial Applications Conference, 2000.

[61] J. D. Han, Y. Q. He, W. L. Xu, "Angular acceleration estimation and feedback control: An experimental investigation," *Mechatronics*, Vol. 17, No. 9, pp. 524-532, 2007.

[62] Y. Hori, "Disturbance suppression on an acceleration control type DC servo system," IEEE Power Electronics Specialists Conference, 1988.

[63] S. H. Jeong, S. Jung, M. Tomizuka, "Attitude control of a quad-rotor system using an acceleration based disturbance observer: An emprical approach," IEEE/ASME Conference on Advanced Intelligent Mechatronics, 2012.

[64] H. Kobayashi, S. Katsura, K. Ohnishi, "An analysis of parameter variations of disturbance observer for haptic motion control," *IEEE Transactions on Industrial Electronics*, Vol. 54, No. 6, 2007.

[65] S. Katsura, K. Irie, K. Ohishi, "Wideband force control by position-acceleration integrated disturbance observer," *IEEE Transactions on Industrial Electronics*, Vol. 55, No. 4, pp. 1699-1706, 2008.

[66] M. Mizuochi, T. Tsuji, K. Ohnishi, "Multirate sampling method for acceleration control system," *IEEE Transactions on Industrial Electronics*, Vol. 54, No. 3, pp. 1462-1471, 2007.

[67] W. Shang and S. Cong, "Motion control of parallel manipulators using acceleration feedback," *IEEE Transactions on Control Systems Technology*, Vol. 22, No. 1, pp. 314-321, 2014.

[68] A. Rubaai, A. R. Ofoli, D. Cobbinah, "DSP-based real-time implementation of a hybrid H_∞ adaptive fuzzy tracking controller for servo-motor drives," *IEEE Transactions on Industry Applications*, Vol. 43, No. 2, pp. 476-484, 2007.

[69] V. P. Makkapati, M. Reichhartinger, M. Horn, "Performance improvement of servo drives with mechanical elasticity via extended acceleration feedback," IEEE International Conference on Control Applications, pp. 1279-1284, 2012.

[70] M. Rezac and Z. Hurak, "Vibration rejection for inertially stabilized double gimbal platform using acceleration feedforward," IEEE International Conference on Control Applications, pp. 363-368, 2011.

[71] C. Bai and Z. Zhang, "Acceleration based mass imbalance feedforward compensation for inertial stabilized platform," *International Journal of Control, Automation, and Systems*, Vol. 12, No. 3, pp. 609-617, 2014.

[72] W. L. Xu, J. D. Han, S. K. Tso, "Experimental study of contact transition control incorporating joint acceleration feedback," *IEEE/ASME Transactions on Mechatronics*, Vol. 5, No. 3, pp. 292-301, 2000.

[73] A. P. White, G. Zhu, J. Choi, **Linear Parameter-Varying Control for Engineering Applications**, Springer, 2013.

[74] G. Mercere, M. Lovera, E. Laroche, "Identification of a flexible robot manipulator using a linear parameter-varying descriptor state-space structure," 50th IEEE Conference on Decision and Control and European Control Conference, pp. 818-823, 2011.

[75] J. S. Shamma and M. Athans, "Analysis of gain scheduled control for nonlinear plants," *IEEE Transactions on Automatic Control*, Vol. 35, No. 8, pp. 898-907, 1990.

[76] W. J. Rugh and J. S. Shamma, "Research on gain scheduling," *Automatica*, Vol. 36, No. 10, pp. 1401-1425, 2000.

[77] O. Sename, P. Gaspar, and J. Bokor, **Robust Control and Linear Parameter Varying Approaches: Application to Vehicle Dynamics**, Springer, 2013.

[78] F. Casella and M. Lovera, "LPV/LFT modelling and identification: Overview, synergies and a case study," IEEE International Conference on Computer-Aided Control Systems, pp. 852-857, 2008.

[79] A. Marcos and G. J. Balas, "Development of linear-parameter-varying models for aircraft," *Journal of Guidance, Control, and Dynamics*, Vol. 27, No. 2, pp. 218-228, 2004.

[80] A. Bansal and V. Sharma, "Design and analysis of robust H_∞ controller," *Control Theory and Informatics*, Vol. 3, No. 2, pp. 7-14, 2013.

[81] K. Ogata, **Modern Control Engineering**, Prentice Hall PTR, 2001.

[82] S. Boyd, L. El Ghaoui, E. Feron, V. Balakrishnan, "Linear matrix inequalities in systems and control theory," *SIAM Studies in Applied Mathematics*, Vol. 15, 1994.

[83] A. A. Siqueira and M. H. Terra, "Nonlinear and Markovian H_∞ controls of underactuated manipulators," *IEEE Transactions on Control Systems Technology*, Vol. 12, No. 6, pp. 811-826, 2004.

[84] Z. Yu, H. Chen, P. Woo, "Gain scheduled LPV H_∞ control based on LMI approach for a robotic manipulator," *Journal of Robotic Systems*, Vol. 19, No. 12, pp. 585-593, 2002.

[85] G. Hilhorst, G. Pipeleers, W. Michiels, R. Oliveira, P. Peres, J. Swevers, "Reduced-order H_2/H_∞ control of discrete-time LPV systems with experimental validation on an overhead crane test setup," American Control Conference, pp. 125-130, 2015.

[86] S. Sehgal and S. Tiwari, "LQR control for stabilizing triple link inverted pendulum system," 2nd International Conference on Power, Control and Embedded Systems, pp. 1-5, 2012.

[87] E. V. Kumar and J. Jerome, "Robust LQR controller design for stabilizing and trajectory tracking of inverted pendulum," *Procedia Engineering*, Vol. 64, pp. 169-178, 2013.

[88] P. Castillo, R. Lozano, A. Dzul, "Stabilization of a mini rotorcraft with four rotors," *IEEE Control Systems Magazine*, Vol. 25, Vol. 6, pp. 45-55, 2005.

[89] S. Arimoto, S. Kawamura, F. Miyazaki, "Bettering operation of robots by learning," *Journal of Field Robotics*, Vol. 1, No. 2, pp. 123-140, 1984.

[90] T. Y. Kuc and J. S. Lee, "An adaptive learning control of uncertain robotic systems," IEEE Conference Decision Control, pp. 1206-1211, 1991.

[91] C. Ham, Z. H. Qu, J H. Kaloust, "Nonlinear learning control for a class of nonlinear systems," *Automatica*, Vol. 37, No. 3, pp. 419-428, 2001.

[92] B. H. Park, T. Y. Kuc, J. S. Lee, "Adaptive learning control of uncertain robotic systems," *International Journal of Control*, Vol. 65, No. 5, pp. 725-744, 1996.

[93] H. S. Ahn, K. L. Moore, Y. Q. Chen, **Iterative Learning Control: Robustness and Monotonic Convergence for Interval Systems**, Springer, New York, 2007.

[94] M. X. Sun and D. W. Wang, "Higher relative degree nonlinear systems with ILC using lower-order differentiations," *Asian Journal of Control*, Vol. 4, No. 1, pp. 38-48, 2008.

[95] Y. Ye, D. W. Wang, B. Zhang, Y. Wang, "Simple LMI based learning control design," *Asian Journal of Control*, Vol. 11, No. 1, pp. 74-79, 2009.

[96] S. Hara, Y. Yamamoto, T. Omata, M. Nakano, "Repetitive control system: A new type servo system for periodic exogenous signals," *IEEE Transactions on Automatic Control*, Vol. 33, No. 7, pp. 659-668, 1988.

[97] D. H. Owens, E. Rogers, K. Galkowski, "Control theory and applications for repetitive processes," *Advances in Control*, Vol. 2, No. 3, pp. 327-333, 1999.

[98] W. Messner, R. Horowitz, W. W. Kao, M. Boals, "A new adaptive learning rule," *IEEE Transactions on Automatic Control*, Vol. 36, No. 2, pp. 188-197, 1991.

[99] W. E. Dixon, E. Zergeroglu, D. M. Dawson, B. T. Costic, "Repetitive learning control: A lyapunov-based approach," *IEEE Transactions on Systems, Man, and Cybernetics*, Vol. 32, No. 4, pp. 538-545, 2002.

[100] W. E. Dixon, A. Behal, D. M. Dawson, S. P. Nagarkatti, **Nonlinear Control of Engineering Systems: A Lyapunov-Based Approach**, Birkhauser, 2003.

[101] W. J. Cao and J. X. Xu, "Robust and almost perfect periodic tracking of nonlinear systems using repetitive VSC," American Control Conference, pp. 3830-3835, 2001.

[102] J. X. Xu and J. Xu, "Observer based learning control for a class of nonlinear systems with time-varying parametric uncertainties," *IEEE Transactions on Automatic Control*, Vol. 49, No. 2, pp. 275-281, 2004.

[103] P. R. Ouyang and W. J. Zhang, "Development of an adaptive learning PD control for robotic system applications," IEEE International Conference on Control Applications, 2004.

[104] T. Ngo, Y. Wang, T. L. Mai, J. Ge, M. H. Nguyen, S. N. Wei, "An adaptive iterative learning control for robot manipulator in task space," *International Journal of Computers, Communications and Control*, Vol. 7, No. 3, pp. 518-529, 2012.

[105] D. Del Vecchio, R. Marino, P. Tomei, "Adaptive learning control for feedback linearizable systems," *European Journal of Control*, Vol. 9, No. 5, pp. 483-496, 2003.

[106] S. Liuzzo and P. Tomei, "A global adaptive learning control for robotic manipulators," *Automatica*, Vol. 44, No. 5, pp. 1379-1384, 2008.

[107] A. Delibası, E. Zergeroglu, I. B. Kucukdemiral, G. Cansever, "Adaptive self tuning control of robot manipulators with periodic disturbance estimation," *International Journal of Robotics and Automation*, Vol. 25, No. 1, pp. 48-56, 2010.

[108] N. Sadegh and R. Horowitz, "Stability and robustness analysis of a class of adaptive controllers for robotic manipulators," *International Journal of Robotic Research*, Vol. 9, No. 3, pp. 74-92, 1990.

[109] Y. C. Wang, C. J. Chien, C. N. Chuang, "Backstepping adaptive iterative learning control for robotic systems," *Applied Mechanics and Materials*, Vol. 284-287, No.3, pp. 1759-1763, 2013.

[110] M. Benosman, "Learning-based adaptive control for nonlinear systems," European Control Conference, 2014.

[111] K. B. Ariyur and M. Krstic, **Real-Time Optimization by Extremum-Seeking Control**, Wiley-Blackwell, New Jersey, 2003.

[112] Y. C. Wang and C. J. Chien, "An observer-based adaptive iterative learning control using filtered-FNN design for robotic systems," *Advances in Mechanical Engineering*, Vol. 2014, No. 471418, 2015.

[113] J. L. Crassidis, F. L. Markley, Y. Cheng, "Survey of nonlinear attitude estimation methods," *Journal of Guidance and Control*, Vol. 30, No. 1, pp. 12-28, 2007.

[114] E. J. Lefferts, F. L. Markley, M. D. Shuster, "Kalman filtering for spacecraft attitude estimation," *Journal of Guidance, Control, and Dynamics*, Vol. 5, No. 5, pp. 417-429, 1982.

[115] S. Evren and M. Unel, "High Precision Stabilization of Pan-Tilt Systems Using Reliable Angular Acceleration Feedback from a Master-Slave Kalman Filter," *Journal of Intelligent and Robotic Systems*, DOI: 10.1007/s10846-017-0522-9, 2017.

[116] J. Diebel, "Representing attitude: Euler angles, unit quaternions, and rotation vectors," *Matrix* Vol. 58, No. 15-16, pp. 1-35, 2006.

[117] Y. B. Shalom, X. R. Li, T. Kirubarajan, **Estimation with Applications to Tracking and Navigation**, John Wiley and Sons, New York, 2001.

[118] R. P. G. Collinson, **Introduction to Avionics Systems**, Springer, New York, 2003.

[119] K. Wang and C. R. Yong Li, "Practical approaches to Kalman filtering with time-correlated measurement errors," *IEEE Transactions on Aerospace and Electronic Systems*, Vol. 48, No. 2, pp. 1669-1681, 2012.

[120] A. E. Bryson and L. J. Henrikson, "Estimation using sampled data containing sequentially correlated noise," *Journal of Spacecraft and Rockets*, Vol. 5, No. 6, pp. 662-665, 1968.

[121] M. G. Petovello, K. O'Keefe, G. Lachapelle, "Consideriation of time-correlated errors in a Kalman filter applicable to GNSS," *Journal of Geodesy*, Vol. 83, No. 1, pp. 51-56, 2009.

[122] M. G. Petovello, K. O'Keefe, G. Lachapelle, M. E. Cannon, "Erratum to: Consideriation of time-correlated errors in a Kalman filter applicable to GNSS," *Journal of Geodesy*, Vol. 85, No. 6, pp. 367-386, 2011.

[123] H. K. Khalil, L. Praly, "High-gain observers in nonlinear feedback control," *International Journal of Robust and Nonlinear Control*, Vol. 24, No. 6, pp. 993-1015, 2014.

[124] G. Tao and X. Ma, "Backlash compensation for multivariable nonlinear systems with actuator dynamics," IEEE Conference on Decision and Control, pp. 3382-3387, 1999.

[125] Y. Hori, “Disturbance suppression on an acceleration control type DC servo system,” IEEE Power Electronics Specialists Conference, pp. 222-229, 1988.

[126] F. Tian, K. Craig, M. Nagurka, “Disturbance attenuation in a magnetic levitation system with acceleration feedback,” IEEE International Conference on Industrial Technology, pp. 59-64, 2011.

[127] K. Craig, “Acceleration feedback,” https://www.multimechatronics.com.

[128] S. M. Hashemi, H. S. Abbas, H. Werner, “Low-complexity linear parameter-varying modeling and control of a robotic manipulator,” *Control Engineering Practice*, Vol. 20, No. 3, pp. 248-257, 2012.

[129] S. Evren and M. Unel, “Stabilization of a Pan-Tilt System Using a Polytopic Quasi-LPV Model and LQR Control,” 42nd Annual Conference of the IEEE Industrial Electronics Society (IECON), pp. 23-27, 2016.

[130] J. Gallier, “The schur complement and symmetric positive semidefinite (and definite) matrices,” Penn Engineering, 2010.

[131] J. Löfberg, “Yalmip: A toolbox for modeling and optimization in Matlab,” IEEE International Symposium on Computer Aided Control Systems Design, pp. 284-289, 2004.

[132] M. W. Spong, S. Hutchinson, M. Vidyasagar, **Robot Modeling and Control**, John Wiley and Sons, USA, 2006.

[133] R. A. García-García and M. Arias-Montiel, “A robust control scheme against some parametric uncertainties for the NXT ballbot,” Multibody Mechatronic Systems, pp. 249-260, 2014.

[134] J. J. Craig, P. Hsu, S. S. Sastry, “Adaptive control of mechanical manipulators,” *The International Journal of Robotics Research*, Vol. 6, No. 2, pp. 16-28, 1987.

[135] N. Sadegh, R. Horowitz, W. W. Kao, M. Tomizuka, “A unified approach to the design of adaptive and controllers for robot manipulators,” *ASME Journal of Dynamic Systems, Measurement, and Control*, Vol. 112, No. 4, pp. 618-629, 1990.

[136] J. Han, Y. He, W. Xu, “Angular acceleration estimation and feedback control: An experimental investigation,” *Mechatronics*, Vol. 17, No. 9, pp. 524-532, 2007.

[137] P. Setoodeh, A. Khayatian, E. Farjah, “Attitude estimation by separate-bias Kalman filter-based data fusion,” *The Journal of Navigation*, Vol. 57, No. 2, pp. 261-273, 2004.

[138] V. K. Madyastha, V. C. Ravindra, S. Mallikarjunan, A. Goyal A, “Extended Kalman filter vs. error state Kalman filter for aircraft attitude estimation,” AIAA Guidance, Navigation, and Control Conference, 2011.